This electronic thesis or dissertation has been downloaded from Explore Bristol Research, http://research-information.bristol.ac.uk

Author:
Scott, Aaron

Title:
Exploring the In Vivo Dynamics of Endogenous Cardiovascular Extracellular Vesicles using Zebrafish

Exploring the *In Vivo* Dynamics of Endogenous Cardiovascular Extracellular Vesicles using Zebrafish

Aaron Scott

Word count = 20565

Abstract

Maintenance of myocardial homeostasis requires a stable and harmonised contribution from various cell types. Myocardial infarction results in a sequence of repair mechanisms, including a complex coordinated cellular response, that must be appropriate to the injury severity for effective damage control and repair. Intercellular communication is integral to cellular coordination, especially in complex tissue contexts. Extracellular vesicles provide a mechanism for molecular transport across extracellular space, allowing signals to be propagated locally and systemically during homeostasis and critically in pathological scenarios. Capable of carrying a wide range of lipids, proteins and nucleic acids, EVs can convey potent 'messages' resulting in physiological changes in the recipient cell. EVs are found in most biofluid samples and have been extensively studied *ex vivo* and *in vitro*, but few assessments have been made regarding endogenously produced EVs *in vivo*, especially within vertebrate models. This project makes use of transgenic larval zebrafish as a vertebrate model system that delivers optical accessibility in combination with transgenic tractability, permitting subcellular *in vivo* live-imaging of endogenous EVs. Using a membrane-tethered fluorophore system EVs can be fluorescently labelled and tracked *in* vivo. This has allowed endothelial cell-derived EVs to be visualised in the peripheral circulation and cardiomyocyte-derived EVs to be observed in the pericardial fluid that surrounds the heart, revealing previously unseen *in vivo* distribution and behaviour. The fluorescent reporter also allows EVs to be extracted from whole larvae and assessed *ex vivo*; in this project EVs were counted via a modified flow cytometry setup, revealing subtle changes in EV numbers in response to cardiac injury. It was also demonstrated that EVs can be isolated via fluorescence activated cell sorting, which opens many opportunities for future work describing cell type specific EV cargo and how this may change during cardiac repair and regeneration.

Dedication and Acknowledgements

Firstly, I would like to acknowledge my supervisor Beck Richardson for her support, her endless enthusiasm for science is a continuous motivator and her patience is a virtue gratefully received. Working with Beck is a pleasure and I am excited for the next three years of science as we work towards a PhD. Laura Bevan plays an integral role within the Richardson Lab and her commitment to the lab has benefitted me on many occasions.

I am also thankful for the support I have benefitted from working closely with Paul Martins Group. David Gurevich always has time to discuss the ins and outs of academia, he liberally shares his experiences and I am sure I will benefit in years to come from the insight. Josie Morris, Maaike Van Den Berg, Debi Ford and Lucy MacCarthy-Morrogh have all made me feel welcome in this lab and they've each offered advice and support that have helped me to reach this point. Lab meetings with the Martin Group have been a weekly highlight over the past year and each presentation provides inspiration.

I could not have reached this point if not for the significant support my second supervisor Costanza Emanueli has generously provided and for this I am incredibly thankful. I am also grateful to my progress panel: Dr. Chrissy Hammond and Dr. Rhiannon Jenkinson, for their support in the initial stages with my project proposal and for the reassurance I gained from the knowledge that their door was always open should I need further support. The Richardson Lab also shares joint meetings with the Hammond and Martin Lab on a weekly basis to talk all things zebrafish and I am grateful for the constructive comments I have received in these meetings.

Lastly, but in many ways most importantly, the technical support I have benefited from at the University of Bristol has been invaluable. The Wolfson Bioimaging Facility provides a wealth of support and I would be amiss not to specifically mention the training I have received from Dominic Alibhai, a patient and knowledgeable teacher. The Biomedical Sciences Flow Cytometry Facility has also contributed heavily towards my project and Lorena Sueiro Ballesteros has been a pleasure to work with.

I declare that the work in this dissertation was carried out in accordance with the requirements of the University's Regulations and Code of Practice for Research Degree Programmes and that it has not been submitted for any other academic award. Except where indicated by specific reference in the text, the work is the candidate's own work. Work done in collaboration with, or with the assistance of, others, is indicated as such. Any views expressed in the dissertation are those of the author.

SIGNED: .... DATE:.........................

Table of Contents

List of Figures

List of Tables

List of Abbreviations

ARF6 – ADP-ribosylation factor 6

A5 – Annexin-V

CM – Cardiomyocyte

CA – Caudal Artery

CHT – Caudal Haematopoietic Tissue

CM-EVs – Cardiomyocyte-derived Extracellular Vesicles

CHD – Coronary Heart Disease

dpf – days post fertilisation

EC-EVs – Endothelial Cell-derived Extracellular Vesicles

EM – Electron Microscopy

ESCRT – Endosomal Sorting Complex Required for Transport

ECs – Endothelial Cells

ECM – Extracellular Matrix

EVs – Extracellular Vesicles

FC – Flow Cytometry

FACS – Fluorescence Activated Cell Sorting

FCS – Forward Scatter

FWHM – Full Width of Half Maximum

GPIbα – Glycoprotein Ibα

HSP – Heat Shock Protein

hpf – hours post fertilisation

HMECs – Human Microvascular Endothelial Cells

HUVECs – Human Umbilical Vein Endothelial Cells

ILVs – Intraluminal Vesicles

mRNA – messenger-RNA

miRNA – micro-RNA

mpi – minutes post injury

MVB – Multivesicular Body

MI – Myocardial Infarction

NTA – Nanoparticle Tracking Analysis

ox-LDL – oxidised Low-Density Lipoprotein

PF – Pericardial Fluid

PE – Phosphatidylethanolamine

PS – Phosphatidylserine

STED – Stimulated Emission Depletion

TIRF – Total Internal Reflection

Tg – Transgenic

TEM – Transmission Electron Microscopy

TNF-α – Tumour Necrosis Factor-α

UAS – Upstream Activation Sequence

Chapter 1: Background

1.1 Coronary Heart Disease

Coronary heart disease (CHD) is often highlighted by the World Health Organisation as a leading cause of morbidity and mortality throughout the world (http://www.who.int/mediacentre/factsheets/fs317/en/). CHD is characterised by the progressive narrowing of one or multiple coronary arteries, the arterial vessels that provide the ventricular myocardium of the heart with oxygenated blood. This narrowing is often caused by the build-up of fatty plaques, a process known as atherosclerosis (1). The pathogenesis of atherosclerosis is well documented (1) and involves the increased risk of plaque rupture and thrombus formation, which can result in total or partial coronary vessel occlusion restricting blood flow and limiting the oxygen supplied to the downstream myocardium (ischaemia) (2). This process can create a severe imbalance between the oxygen being supplied and the cellular demand for oxygen, which causes cell death and myocardial infarction (MI) (2, 3). Tissue repair responses to the injured myocardium lead to fibrosis and scar deposition within the ventricle wall, limiting contractility and electrical conductance of the ischaemic region and leaving the myocardium functionally compromised and susceptible to future complications, which can ultimately lead to heart failure (4). Beyond complex scar resection surgeries and complete heart transplantation, there remains no cure for end stage heart failure leading to mortality rates around the world remaining high.

For healthy myocardial function, several cell types (including cardiomyocytes (CMs), endothelial cells (ECs), fibroblasts and leukocytes) must work in concert to provide synchronous and sufficient contraction, ample perfusion, extracellular structural support and a stable immune system. Preserving the functional integrity of the heart is finely balanced and requires effective intercellular communication. When a coronary artery becomes blocked, as with the build-up or rupture of an atherosclerotic plaque, the blood flow and therefore oxygen supply to the downstream myocardium is restricted. The resulting ischaemic environment alters the physiology of the tissue, with cell death (apoptosis, necrosis and autophagy) becoming prevalent (5). The damage that ensues must be rapidly stabilised via complex repair mechanisms to maintain sufficient cardiac function. Cardiac repair processes require the concerted efforts of all constituent cell types, and therefore likely alters the intercellular communicatory landscape (6).

Secretion of soluble proteins into the extracellular space and cell-cell contact dependent signalling are well defined modes of intercellular communication, but extracellular vesicles (EVs; described below) are increasingly recognised as an exciting addition to these classic modes of intercellular communication and may prove influential in the field of cardiovascular biology (7).

1.2 Extracellular Vesicles

1.2.1 Introduction

EVs collectively describe all plasma membrane-bound vesicles produced and released by most cell types, this process is considered evolutionarily conserved having been documented in animals, bacteria and plants (8-10). An assortment of molecules, including lipids, proteins and nucleic acids can be loaded either as cytosolic cargo or as a component of the EVs membrane. The relative security of the cargo allows for molecules that might be unable or ineffectual if secreted alone, to be carried through extracellular space and remain viable within the luminal space of the EV. EVs are capable of both local and systemic trafficking and have been isolated from a wide range of biological fluids, including blood (11) and pericardial fluid (PF) (12). Surface glycans, phospholipids and proteins allow regions of extracellular matrix (ECM) (13) and recipient cells to be targeted and EVs are widely recognised to play integral roles in various communicatory pathways (14). EV based communication allows for insoluble molecules to be transferred to a recipient cell, but also potentially a cocktail of complementary molecules could be offloaded to a recipient cell to deliver a more potent or complex signal. EVs are most often considered within pathophysiological contexts, having been implicated in the progression of many diseases, including cardiovascular disease (15, 16). However, their role in maintaining homeostasis has also been considered (17). Additionally, their roles in protection, repair and regeneration present exciting possibilities to be explored (7). Understandably, EVs are rousing much enthusiasm, however the ability to reliably define the heterogeneous spectrum of EV subtypes, and further, to ascribe functional significance to that specific type, is still in its infancy. Gaps in our understanding of EV biology need to be filled to fully appreciate and realise their functional applications.

1.2.2 Classification

There are widely considered to be three classes of EV: apoptotic bodies, microvesicles and exosomes. Each class is loosely defined by size, though the more robust defining feature is their mode of biogenesis (14). The following section provides some detail on these classes, but to summarise, a table of general characteristics (**Table 1.1**) and a diagram depicting these modes of biogenesis (**Figure 1.1**) are included.

Table 1.1. Characteristics of Exosomes, Microvesicles and Apoptotic Bodies. *ND = Not Determined.*

Characteristic	Exosomes	Microvesicles	Apoptotic Bodies
Diameter	30-120 nm	100-1000 nm	>1000 nm
Density in sucrose	1.13-1.19 g/mol	ND	ND
Sedimentation	100000 g	10000 g	ND
Size/Shape	Homogenous	Heterogenous	Heterogenous
Cellular origin	Endosomal	Surface budding	Surface blebbing
Membrane	Impermeable	Impermeable	Permeable
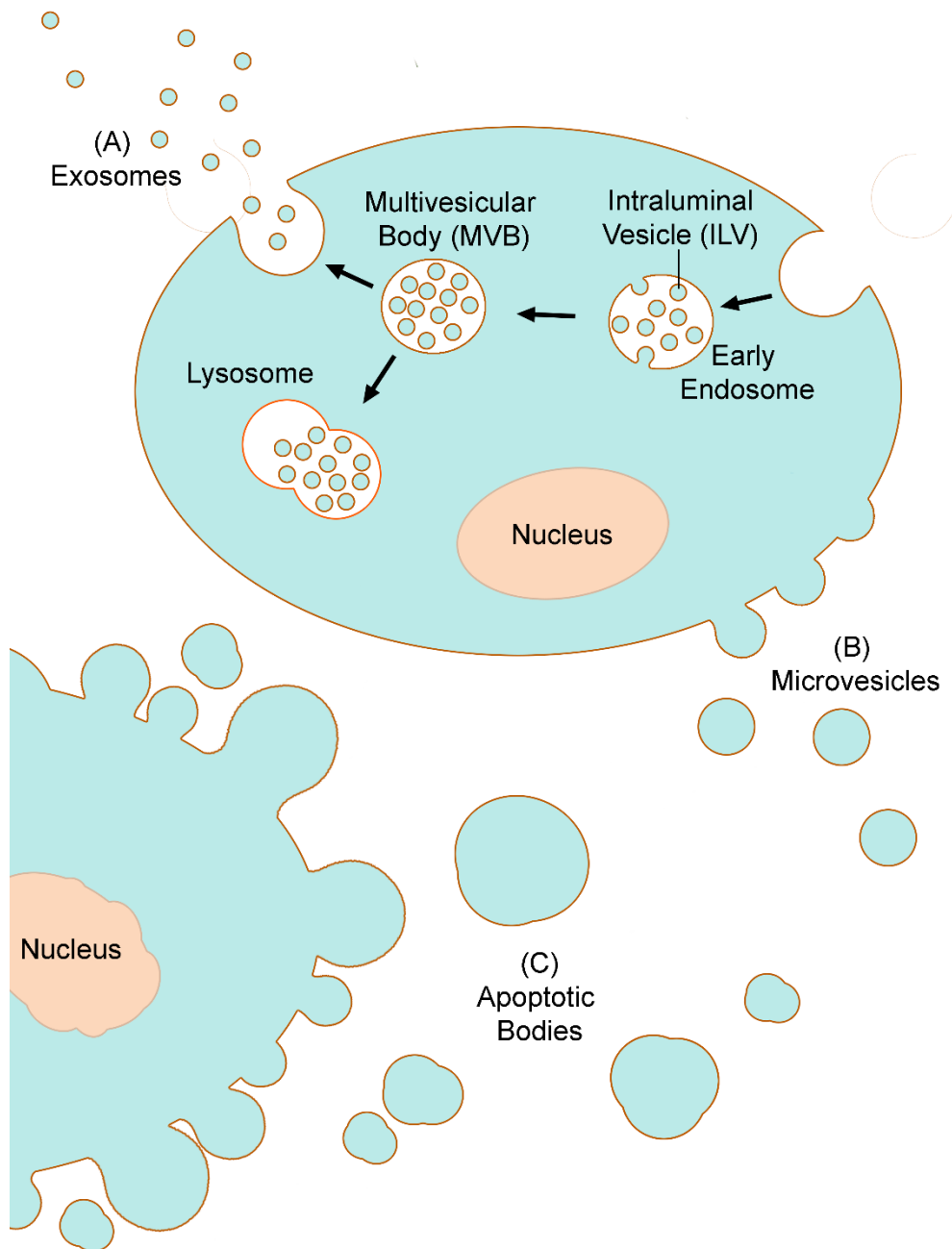
Figure 1.1. Biogenesis and Release of EVs. *EVs can be divided into three classes. (A) Exosomes are intraluminal vesicles (ILVs) that are released into extracellular space when the membrane of a multivesicular body (MVB) fuses with the cell surface membrane. MVBs can follow other pathways within the cell, such as the lysosomal degradation pathway. (B) Microvesicles bud directly from the cell surface to be released into extracellular space. (C) Apoptotic cells undergo a process known as blebbing, which releases apoptotic bodies into extracellular space as part of cellular deconstruction.*

1.2.2.1 Exosomes

Exosomes are commonly considered the smallest (30 – 120 nm in diameter) class of EV and are derived from a process of endocytic cycling (**Figure 1.1**) (18). The pathway is initiated with the invagination of the producing cells plasma membrane, incorporating surface molecules from the producing cell into the early endosome as it is formed (**Figure 1.1**). A number of separate mechanisms have been identified as driving this process of endocytosis, broadly separated as clathrin dependent and independent mechanisms (19). Clustering of molecules on the membrane, relevant as cargo or machinery for budding, initiates secondary invaginations into the lumen of these early endosomes, forming multiple ILVs (14, 20). This process can sometimes allow the cellular origin of exosomes to be inferred from membrane components shared with the producing cell (17). Although this possibility for identifying exosome origin exists, difficulties can arise from shared membrane characteristics between cell types, making certain exosome populations indistinguishable from one another (21). Relevant molecular components are also delivered from the Golgi apparatus, perhaps providing a mechanism for more specific loading of exosome cargo (18, 22).

Formed of roughly 30 proteins, the endosomal sorting complex required for transport (ESCRT) complexes (-0,-I,-II,-III) are the best characterised mechanism for ILV formation and they are considered evolutionarily conserved (23). However, small interfering RNA depletion of components essential for the formation of each of the four ESCRT complexes in mammalian cell culture studies did not prevent MVB formation, revealing the involvement of other mechanisms (24). For example, neutral sphingomyelinase hydrolyses sphingomyelin into ceramide (25) and phospholipase D2 hydrolyses phosphatidylcholine into phosphatidic acid (26) and when this occurs at the limiting membrane of the early endosome it can drive the membrane bending and budding required to form ILVs (25, 26).

As the endosome matures into a late endosome (27) with free ILVs within, it is descriptively termed a MVB (**Figure 1.1**) (23). MVB is a broad term, with their molecular components and overall function varying considerably depending on their intracellular role (23). The primary function for most MVBs is to enter a lysosomal pathway whereby fusion with a lysosome ensures degradation and recycling of vesicular components (28). MVBs are also thought to contribute to

the formation of specialised cell specific organelles, as with EC specific storage granules termed Weibel-Palade bodies (29), thought of primarily as a storage pool for von Willebrand factor (30). Azurophilic granules are another cell specific organelle that MVBs play a part in forming; these granules hold digestion enzymes within neutrophils (31). Lastly and most relevant to this project, ILVs can be released in a single secretory event, as the MVB fuses with the producing cells membrane (**Figure 1.1**) (20). Early evidence for this process was realised using immunogold labelling of the transferrin receptor in maturing reticulocytes, where images acquired using electron microscopy (EM) revealed labelled EVs being exocytosed via MVBs (32). Similar methods have since been used to confirm the same process in reticulocytes from different organisms (33, 34), but also for B lymphocytes as they secrete antigen-presenting vesicles (35). Based on these studies, MVBs destined to secrete their ILV contents are tentatively characterised by the tetraspanin CD63 and the lysosomal-associated membrane proteins LAMP1 and LAMP2 (35, 36). Upon release, the former ILVs, now in extracellular space, are termed exosomes (**Figure 1.1**A).

Rab proteins are an important group of small GTPases, well known for their diverse roles in intracellular vesicle trafficking (37). Rab proteins are also found in the proteomic analysis of isolated EVs (38) and likely play their part in the biogenesis of exosomes (14), but the extent of their involvement is not clear, leaving much of the mechanism to be inferred from their roles in the endocytic cycle. The ability of HeLa cells to produce exosomes (CD63, CD81, and MHC class II marker positive subset) decreases in response to RNAi silencing of various Rab proteins (RAB2B, RAB5A, RAB9A, RAB27A and RAB27B) (39). Silencing of each of these Rab proteins inhibited exosome production to differing degrees, with RAB27A and RAB27B appearing to be the most impactful (39). The best defined Rab proteins (including RAB5, RAB7 and RAB11) also play roles in exosomes production, with differing results depending on the cell type in question and the method used to isolate and define the exosomes.RAB5 is a marker of early/sorting endosomes and is involved in appropriating ligands at the plasma membrane, the fusion of clathrin coated vesicles to the early endosome and the motility of endosomes (40). RAB5 also marks endosomal compartments that fuse with the plasma membrane in reticulocytes and is also found in exosomes produced by these cells (41), leading the authors to infer its involvement in exosome biogenesis. A population of exosomes produced by two melanoma cell lines has also been identified and is defined in this study by the presence of

RAB5 in combination with CD63 and caveolin-1 (42). Overexpression of a dominant-negative form of RAB5 decreased the number of exosomes (syndecan, CD63, syntenin and ALIX positive subset) produced by MCF-7 cells (43). The switch in endosomal expression from predominating RAB5 to RAB7 marks the transition from early to late endosome and RAB7 aids the transport of MVBs to the lysosome (44). RAB7 knockdown via RNAi also impairs the release of the same subset of exosomes affected by overexpression of a mutated RAB5 (43). In contrast, RAB7 RNAi knockdown in the HeLa B6H4 tumour cell line appears to have no effect on exosome production (MHC class II surface receptor, HLA-DR and CD81 positive subset) (39). Further studies have begun to dissect the intracellular interactions and molecular profile of RAB7, where ubiquitination levels drive the MVB towards either a fusion event with the cell surface membrane or lysosome (45). A reduction in RAB7 ubiquitination, achieved through dominant-negative protein expression, pushed MVBs towards cell surface fusion, as shown by increased exosome production in HEK 293 cells (45). RAB11 is a marker of perinuclear recycling endosomes and is involved in trafficking from the plasma membrane to the Golgi complex (Ullrich et al., 1996). RAB11 also plays a role in exosome production in the erythroleukemia cell line K562, where dominant-negative RAB11 expression showed a decrease in the release of exosomes (transferrin receptor, tyrosine kinase Lyn and heat shock protein Hsc70 positive subset) (46). Using an RNAi screening assay in the drosophila S2 cell line, also identified Rab11 as required for exosome production (47, 48). Again, knockdown of RAB11 in the HeLa B6H4 tumour cell line did not affect exosome production (MHC class II surface receptor, HLA-DR and CD81 positive subset) (Ostrowski et al. 2010). The consistent mechanistic heterogeneity in exosome biogenesis means the driving mechanisms are not yet fully realised, though significantly more is understood when contrasted with microvesicle biogenesis.

1.2.2.2 Microvesicles

Microvesicles (typically 120 – 1000 nm in diameter) (**Table 1.1**) were previously considered to be no different to apoptotic bodies, but their biogenesis is now known to be an active process carried out by healthy cells. Relatively little is known about microvesicle biogenesis, with mechanistic evidence being intermittent, and the gaps filled by extrapolation from similar processes in exosome biogenesis and other areas of cell biology.

Initially, membrane lipids and proteins are generally thought to redistribute themselves in a non-uniform manner, forming specific microdomains on the plasma membrane of the producing cell (**Figure 1.2**A). As part of this microdomain clustering, ESCRT-I recruitment is thought to be key in generating the initial curvature or early budding of microvesicles. ESCRT-I is one of only a few protein complexes capable of generating curvature away from the cytoplasm (49) and it is also known to play a role in viral budding from the plasma membrane (50). Direct *in vivo* evidence for the involvement of ESCRT machinery in microvesicle biogenesis comes from a study that used RNA interference to screen for genes that are important in *C. elegans* morphogenesis (51). TAT-5, a conserved P4-ATPase or lipid flippase, was one of the genes identified and knockdown was found to dramatically increase the amount of phosphatidylethanolamine (PE) sequestered to the outer leaflet, leading to increased microvesicle shedding. Although this PE rearrangement is thought to develop outward curvature of the membrane, it was not thought sufficient and protein involvement had long been proposed (52). With further investigation, ESCRT-I inhibition went some way to recover the normal phenotype in TAT-5 RNAi embryos, and the GFP::MVB-12 (MVB12 is one of the proteins that forms the ESCRT-I complex) fusion construct was also used to identify increased plasma membrane localisation of ESCRT-I in TAT-5 RNAi embryos (51). Phospholipid redistribution and cytoskeletal protein contraction can also initiate the formation of a budding protrusion on the surface of the producing cell (53). Ca^{2+}-dependent enzymes such as flippases and floppases are one mechanism known to drive alterations in membrane asymmetry, resulting in, for example, the noticeable redistribution of the phospholipid phosphatidylserine (PS) from the inner to the outer leaflet. This kind of action is thought to be involved in inducing the budding process by bending the membrane and reorganising associated actin components (54-56). It is likely a combination of both lipid redistribution and protein machinery that is responsible for the primary structural formation of microvesicles.

Interlinked with the formation of microvesicles is the loading of cargo; the re-organisation that forms the early membrane lipid and protein microdomains (**Figure 1.2**A) might then initiate the necessary recruitment of cytosolic cargo (**Figure 1.2**B). For example, RNA-binding proteins are thought to be recruited as a likely mechanism for loading RNA molecules (21), but the exact mechanism for RNA loading has not been elucidated. One potential scenario has been

20

highlighted in cancer cells, where a conserved zip code RNA sequence motif in the 3' untranslated region of specific mRNAs may aid such targeting to the appropriate microdomain at the plasma membrane (57). In contrast, the mechanisms responsible for recruiting protein cargo (**Figure 1.2**B) are better understood, with membrane association and higher order oligomerisation thought to be sufficient to target proteins to sites of EV biogenesis (58). This makes membrane localisation key to the process of protein loading and palmitoylation, prenylation and myristylation tags are well known drivers of post-translational modifications that form lipid anchors and associate the protein to the inner leaflet of the plasma membrane and their potential involvement in loading proteins into EVs has been demonstrated (59, 60). The small GTPase ADP-ribosylation factor 6 (ARF6) (**Figure 1.2**C) has also been documented performing a role in the selective recruitment of protein cargo in tumour-derived microvesicles (61, 62). Additionally, small GTPase RAS-related protein RAB22A colocalises with budding microvesicles and mediates packaging and loading of cargo proteins in hypoxic breast cancer cells (63).

The final step in the formation of a microvesicle requires the scission of the budding process, enclosing the contents and releasing the microvesicle from the producing cell (**Figure 1.2**C). The formation of ILVs also depends on a scission process to allow them to be released into the lumen of the MVB and the recruitment of ESCRT-II and ESCRT-III has been implicated in the execution and completion of this step (23, 64). A similar process has been suggested as responsible for the final budding and scission of microvesicles (21). A number of ESCRT protein complexes have been found as 'cargo' inside microvesicles, further supporting the suggestion that they are responsible players in microvesicle biogenesis (14). The overall mechanistic picture for microvesicle biogenesis is the least understood of the EV classes, and many aspects remain to be elucidated (65).
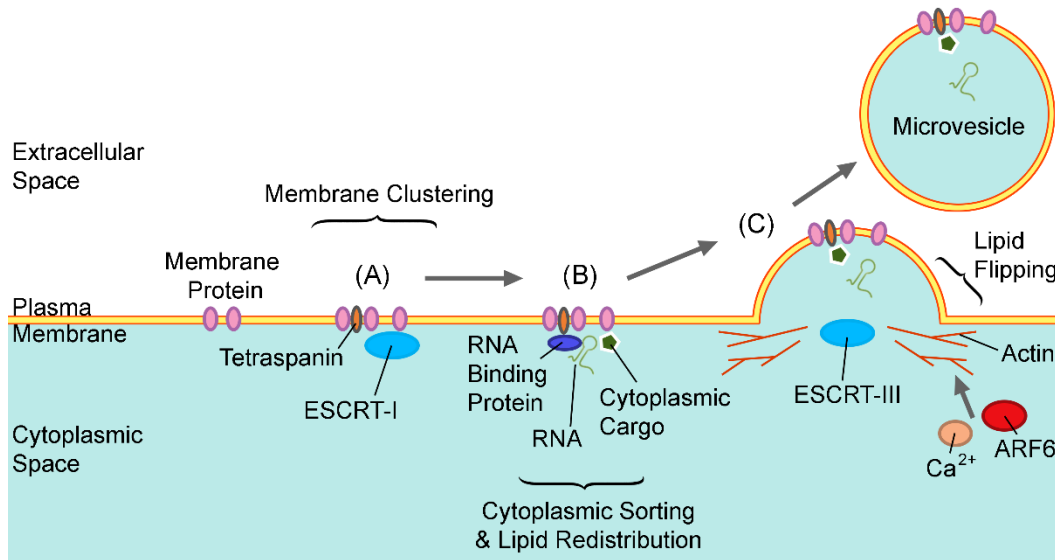
Figure 1.2. Biogenesis of Microvesicles. Sorting machineries involved in generation of microvesicles. (A) Membrane lipids and proteins are clustered into distinct domains. (B) These domains are involved in the recruitment of cytosolic proteins and RNA molecules. (C) Clustering and additional machineries promote membrane budding, followed by fission, releasing the microvesicle into extracellular space. Transmembrane proteins sorted onto microvesicles keep the same topology as on the producing cells membrane. Specific lipids are known to be flipped between leaflets of the plasma membrane upon microvesicle budding.

Alternative Release Mechanism for Exosomes and Microvesicles

EVs likely play a critical role in transporting protein cargo that is post-translationally lapidated, as this process creates a hydrophobic molecule that localises to the plasma membrane and is therefore unable to diffuse freely through extracellular space. It has been shown that membrane tethering of proteins may promote long distance signalling capabilities by way of the resulting transport mechanisms that are initiated (66). This is supported in part by the finding that cholesterol addition to Sonic Hedgehog increased the signalling distances achieved for this protein (67).This is a particularly relevant consideration for morphogen transport, as members such as Wnt and Hedgehog are post-translationally lapidated (68). These morphogens are known to be transported over considerable distances in consistently reproducible patterns or concentration gradients, particularly during development, but signalling via these ligands is also relevant in fully developed tissues (69, 70). Interestingly, it is known that cells can interact over long distances via long membrane protrusions such as the signalling-filopodia identified as cytonemes (71-73) and in the instance of Hedgehog signalling cytonemes have been demonstrated as essential for gradient establishment (74-76). In parallel, it has also been shown *in*

vitro and in Drosophila that EVs, particularly ESCRT-dependent EV production, is involved in this process where they are also capable of initiating the relevant signalling pathways within recipient cells (47, 77-80). However, although EVs appear to be relevant in this process, *in vitro* studies suggest EV transport of Wnt and Hh is not independently sufficient to activate the full complement of known target genes (77, 79). It has also been shown that wingless gradients in Drosophila can be established independent of EV mediated transport (47). This combination of evidence has led to an understanding that morphogen transport likely does not work exclusively through EV release or via cytoneme signalling, but perhaps they work in concert together with potential EV transport along cytonemes as has been shown in Drosophila (77). These joint mechanisms have primarily been dissected within the framework of early development based on morphogen transport and effects relating to cell polarity (66, 81), but their potential role in other aspects of cell-cell communication within diverse tissue contexts is open for exploration. Particularly relevant to this study would be the idea that Wnt signalling, which is known to play an important role during cardiac injury in mouse (82), could also be important in zebrafish heart regeneration and be mediated by the mechanisms described.

1.2.2.4 Apoptotic Bodies

Apoptotic bodies have long been known as large (>1000 nm in diameter) vesicles produced in the later stages of apoptosis. As the cell membrane blebs, apoptotic bodies are shed from the surface of the dying cell (83). Classically, particles less than 4 µm in diameter were considered to be cellular debris, either remnants from this apoptotic process or from shedding throughout the lifetime of the cell as a means for packaging defective/unnecessary cell components for safe disposal (84). As apoptotic bodies are produced, the integrity and typical asymmetry of the plasma membrane is lost; it becomes more permeable, and components such as PS usually sequestered on the inner leaflet become exposed on the outer surface (85). This membrane rearrangement is thought to facilitate the 'clear-up', as these newly exposed membrane components ultimately promoting macrophage phagocytosis in order to avoid intracellular components causing 'collateral damage' (86). There are similarities between apoptotic bodies and the two smaller classes of EV, but the focus for studies into intercellular communication potential has tended more towards microvesicles and exosomes and they will be the focus of this thesis.

1.2.3 Cargo

EVs can carry a diverse set of cargo, determined within the producing cell but with some factors common to most EVs. They are generally known to be enriched with various cytoskeletal proteins, molecular chaperones and signalling molecules (**Figure 1.3**). Factors associated with EV biogenesis and intracellular trafficking are also carried in some instances (21). Alongside more general components are those that are cell-type specific and selected. Specific enzymes have been highlighted as particularly relevant cargo transported by EVs (87, 88), with potential for a more immediate physiological impact to be imparted on the recipient cell. However, most attention has fallen on the transport of RNA molecules, with many studies revealing a novel messenger-RNA (mRNA) (89) or micro-RNA (miRNA) (90, 91) within their samples. Some significance has been derived from studies that identify mRNA and miRNA that is proportionally highly expressed in EVs when compared with the producing cells, an early suggestion that the loading process can be to some degree selective (92). Further, specific miRNA motifs have been shown to control their loading into EVs (93). However, the relative involvement of selective vs passive processes in RNA loading have yet to be elucidated (94).
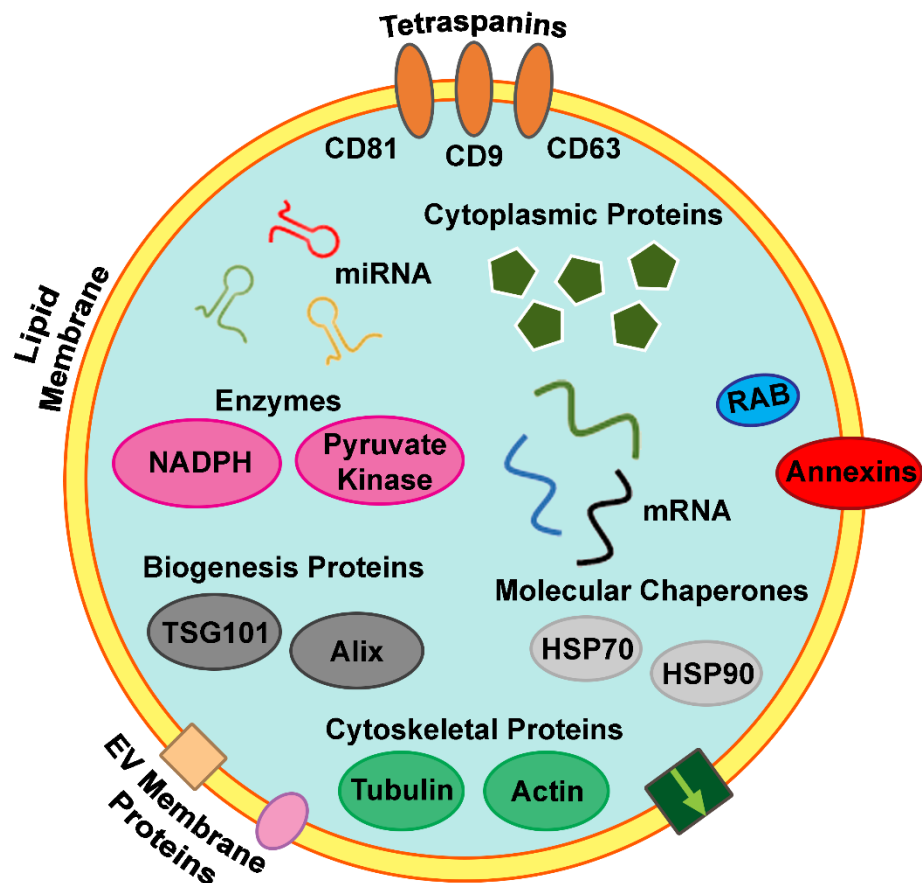
Figure 1.3. EV Composition. *EVs consist of a lipid membrane enclosing a cytosolic compartment. The lipid and protein content of the membrane can vary widely, and the composition can define specific targets and is responsible for the ways in which the EV interacts with the extracellular environment. The cargo held within the cytosol also varies widely; nucleic acids, cytosolic proteins, enzymes, molecular chaperones and components involved in EV biogenesis are all identified as EV cargos.* **Function**

1.2.4.1 Intercellular Interactions

The mechanisms by which EVs are taken up by a recipient cell are not well understood, in part because of the difficulty in visualising these small vesicles. Three main hypotheses have been proposed with the simplest suggesting that EVs act much like a secreted protein, initiating a receptor-ligand interaction to drive molecular pathways within the recipient cell (17). A second exciting possibility relies on the fusion of the two membranes, allowing the EV cargo to be deposited directly into the cytosol of the recipient cell (95). Membrane fusion (96), is likely key as a mechanism for miRNA (92) and mRNA (97) transfer.

Lastly, and most commonly documented, EVs may be endocytosed by the recipient cell and dealt with internally (98). Endocytosis is a heavily studied area and current opinions tend to group the process into either clathrin-mediated or clathrin-independent mechanisms (99-101). One of the more commonly identified uptake mechanisms is the clathrin-independent phagocytosis (98, 102), but this is very much dependent on the propensity of the cell in question (99). Another cited clathrin-independent mechanism is macropinocytosis (96, 103, 104).

Many of the cargos mentioned in the previous section have the potential to alter the physiology of a recipient cell, and this is a big driving force behind the increased interest in EVs. The potential for mRNA and miRNA transfer has sparked many people's imaginations, with the possibility of intercellular influences directly altering the transcriptional landscape of a cell. *In vitro* studies have reported the transfer or mRNA via EVs and the successful translation of protein in the recipient cell (92), with numerous studies ongoing to confirm these findings (12, 97, 105, 106).

More recent studies have begun piecing together a more complete communicatory pathway mediated by EVs. A recent example identified an important role for EV delivered NADPH oxidase 2 complexes in oxidative signalling processes within dorsal root ganglia, neurite outgrowth and regeneration of injured axons. The functional NADPH oxidase 2 complexes, initially found in the injured neurons, were retrospectively found to have originated from macrophages recruited to the injury site. The EVs delivered from the macrophages were incorporated into the axons via endocytosis and the novel downstream impacts on reactive oxygen species and their regulation of axonal regeneration were dissected (88).

1.2.4.2 Extracellular Matrix Interactions

EVs and their roles in ECM biology have not garnered the same interest and consideration as direct intercellular interactions, even though the ECM must be navigated in many instances of EV transfer. This is perhaps a direct result of the *in vitro* based foundation of our current understanding and the ECM will likely become more relevant in time. *In vitro* experiments are reductionist by design and necessity, with many ECM components and the 3-dimensional structure they provide often sacrificed in this process. *In vivo* studies present many challenges, but are by their nature more embracing of complexity, providing a native

environment where the role of ECM on EV biology must also be taken into consideration.

EVs known as matrix vesicles have long been thought to play a role in the mineralisation of cartilage and bone (107), with more recent *in vivo* studies in zebrafish contributing to this picture (108). As well as carrying ECM components, EVs themselves have been shown to aid adhesion through receptor-ligand interactions (109). Specifically, EVs have been shown to carry the ECM components laminin (110) and fibronectin (109) and these EVs can then attach to substrata and promote adhesion assembly through their cargo, promoting efficiency in cell migration. Initially, fibronectin is thought to be targeted to exosomes via interactions with cognate integrins; once released to the substrata the fibronectin is secreted from the EVs in an adhesive form thus promoting cell attachment and migration (109). These experiments were primarily conducted *in vitro*, and the role in cell adhesion assembly was demonstrated by lining culture dishes with the EVs on which migration assays with HT1080 fibrosarcoma cells were conducted, it is therefore not clear exactly which components of the substrata the EVs would initially interact with *in vivo*. EV-ECM interactions have been investigated further, with studies demonstrating that these processes can allow cancer cells to manipulate the ECM at both local and distal sites, creating a metastatic niche for later progression (111). The key findings here are that these interactions between EVs and the ECM may facilitate the remodelling of the ECM – in this specific instance by cancer cell-derived EVs. These pioneering studies are particularly relevant in cancer biology, but also show the value in assessing the role of remote site signalling in other fields and understanding these processes could aid the development of innovative preventative therapeutics.

EVs can be found in a wide range of extracellular biological fluids, which can often be characterised as or contain ECM components. Notably, the blood plasma holding blood cells in suspension is often labelled as ECM. The structural interactions of circulating EVs within the whole blood have been demonstrated to be physiologically critical, as is apparent with platelet-derived EVs and there procoagulant properties (112). The mechanisms by which EVs move through the ECM remain to be elucidated, EVs can be carried systemically by the blood flow but how they penetrate more densely packed fibrous ECM is less clear. Studies have identified EVs containing matrix metalloproteinases amongst other

proteolytic factors (113), which could aid degradation and allow EVs to pass through ECM (13).

1.2.5 Characterisation

1.2.5.1 Introduction

With the complexity and variety inherent to EV biology there are often problems in discerning one EV class from another, not least are the challenges presented in physically separating one class from another. It has been noted that mixed populations of EVs have often erroneously been identified as exosomes in the literature (14) and this has often caused confusion. The difficulties in developing a thorough characterisation of these vastly heterogenous entities has often been highlighted and the EV community are acutely aware of the need for progress in this area (**Table 1.1** highlights current consensus). Further challenges are presented when considering characterisation within living organisms.

1.2.5.2 *Ex Vivo* Characterisation

1.2.5.2.1 Isolation

To answer key questions relating to EVs there is a clear need to standardise isolation techniques (114), with the International Society of Extracellular Vesicles investing resources to meet this end (94, 115) including collaboration with researchers focussed on cardiovascular research (116). Effective and consistent isolation methods will allow for clarity in EV characterisation and the ability to more effectively compare results across laboratories. Standardised isolation and characterisation are paramount to clarify our understanding of these small vesicles, particularly with fundamental variation between EV subtypes becoming more apparent with each new study (38). EV isolation can be achieved using filtration, ultracentrifugation, immunoaffinity and microfluidic based platforms (115). Often single methods are insufficient and the current 'gold-standard' relies on a combination of differential ultracentrifugation, followed by separation of the particles based on a sucrose density gradient (117). Ultracentrifugation allows for a specific size of particle to be collected and the density gradient separation allows similar sized contaminants (e.g. protein aggregates) to be excluded from the sample. However, consideration should be given to the experiment at hand, as this will dictate the methods used.

Isolation from whole tissue is not well established and only a few methods have been tested, so far there is no standardisation of this procedure. The methods so far used include mild digestion protocols (118), mechanical separation using fine scissors (119, 120), mechanical homogenisation (121) and semi-culture conditions to allow EV release followed by standard extraction as with cell culture medium (122).

1.2.5.2.2 Labelling

The process of labelling EVs, to allow for detection and visualisation, is critical to most characterisation efforts. Many of the approaches detailed in the next sections are not unique to *ex vivo* work and are also used for *in vitro* and *in vivo* studies. The labelling technique used is often dictated by the type of experiment being performed and should be tailored to a planned approach. Non-specific labelling strategies have tended to focus on the phospholipid membrane, but efforts have also been made to label the luminal compartment of EVs. More specific approaches demand prior knowledge of EV components, but when afforded this can allow specific cargos to be labelled.

1.2.5.2.2.1 Protein Markers

There are several protein markers widely cited within the literature, none of which unambiguously identify EVs. Many of these markers are associated with the biogenesis of EVs, including some tetraspanins (CD9, CD63 and CD81), AIP1/Alix, TSG101 and CD326/EPCAM. Antibodies can be used to target these proteins and relevant labels conjugated to allow detection. Another possibility is the transgenic (Tg) modification of cells to express these marker proteins fused to a (e.g. fluorescent) labelling protein (123).

1.2.5.2.2.2 Lipid Markers

In many instances' general lipid membrane fluorescent dyes, such as PKH-67, DiL and DiR, are the most effective pan-EV labelling strategy (124-127), as they indiscriminately label a known component common to all EVs. However, this also presents a weakness, where membrane fragments as well as other contaminants might also be labelled, leaving some questions regarding specificity and consistency when using this method (128). Labelling the extracellular surface of EVs may also impact downstream applications, as this method will alter the surface properties that are integral to EV behaviour. A final consideration must be

taken to remove excess dye and avoid false positives resulting from aggregating dye.

Specific targeting of membrane components, such as the phospholipid PS has also been widely implemented for labelling EVs (114, 129). More commonly used to mark cells undergoing apoptosis, the sequestering of PS to the outer leaflet is common to EV biogenesis. Most often, labelling is achieved by way of Annexin-V (A5), a molecule which binds the reoriented PS with high affinity. This labelling method has been popular in the EV field, most likely because of early papers using flow cytometry (FC) to identify EVs labelled in this way (130, 131).

1.2.5.2.2.3 Lumen Markers

Calcein AM is an example of a membrane permeant dye that, once inside the luminal space of a cell or EV, is hydrolysed by esterase's with the resulting Calcein form being both highly fluorescent and membrane impermeable. This allows non-specific labelling of intact EVs (132, 133), but the extent to which all EVs carry esterase's remains to be fully evaluated. In contrast to membrane labelling, luminal labelling in this way will only label intact EVs, as the dye does not become fluorescent until it has been hydrolysed, this also makes excess dye less of a concern as compared with the lipid membrane dyes.

1.2.5.2.3 Detection

1.2.5.2.3.1 Electron Microscopy

EM currently offers the greatest resolution of any technique, allowing the ultrastructure of even the smallest EVs to be revealed. EM is a relatively straightforward process when regarding isolated EVs and this classic characterisation method has been refined over the years (134, 135). EM does become incredibly laborious where sections of a whole organism are required (108). In combination with standard image acquisition, antibodies conjugated to colloidal gold particles can allow specific marker proteins to be to be targeted, adding to the phenotypic information that can be acquired (35).

1.2.5.2.3.2 Super Resolution Microscopy

Super resolution microscopy allows the diffraction limits of light microscopy to be breached, this has been achieved in a number of ways, most notably in EV research is the use of stimulated emission depletion (STED) microscopy (136). The resolution gains (down to 10-30 nm) are substantial and multiple lasers allow different fluorophores to be assessed in a single sample. This allows multiple EV markers to be assessed in one sample, giving a greater perspective on the distribution of components (136), where a crude western blot for example would only indicate the presence of a protein across the whole sample. The limitations arise in relatively laborious sample preparation and the resulting lower throughput.

1.2.5.2.3.3 Total Internal Reflection Microscopy

Total internal reflection (TIRF) microscopy has been employed to great effect in imaging dynamics at the cell surface where processes such as endocytosis can be observed (137) thanks to the high signal to noise ratio permitted with this method. The process is physically limited by the evanescent field used to illuminate the sample, which must be no further than 250 nm from the cover glass. This makes it an ideal option when imaging EVs *ex vivo* for high sensitivity and the possibility to stain the EVs with luminal and membrane dyes as well as fluorescent antibodies for multiparameter assessment. This method is not currently used widely, but does significantly increase resolution and sensitivity when demonstrated (138, 139).

1.2.5.2.3.4 Nanoparticle Tracking Analysis

Nanoparticle Tracking Analysis (NTA) brings high-throughput capabilities not available with standard microscopy, and is often used in conjunction with EM to add information on the concentration of the different sized particles within a fluid sample (140). This method works by passing laser light through the sample as it is pumped at a constant pressure through a chamber, the light scattered by individual particles is received by an objective and tracked using in-built software and size can be calculated based on the Brownian motion of these particles. This method is limited in its inability to discriminate EVs from particles of a similar size, such as lipoproteins and large protein aggregates.

1.2.5.2.3.5 Flow Cytometry

FC is an established technique that is readily available in many laboratories around the world. Optimised for the assessment of multiple parameters of cells and particles, it is not possible to reliably detect EVs with a conventional setup. Detection of particles is achieved as they are passed through a laser beam, scattering light and emitting fluorescence, which can be detected and if sufficient signal is received, determined by threshold settings, then the measurement is recorded. This method imposes limitations on detection and based on light scatter alone 300-500 nm would be the size below which you could not reliably detect a particle (141). However, efforts have been made to modify commercially available machines and optimise them for EV scale detection (142). Optimising the BD Influx machine for high-resolution detection by fluorescence, for example, has presented the potential for detecting particles down to ~150 nm in diameter (142).

1.2.5.3 *In Vitro* Characterisation

EVs are produced by most cell types preventing the cellular origin from being easily ascertained when fluid samples are taken from a whole organism. Monoculture of cells *in vitro* negates this problem and this system is where much of the knowledge surrounding EVs originates. EVs isolated from cell culture medium are the primary source for much of the *ex vivo* approaches described above (see section 1.2.5.2), with most of the isolation and labelling methods described in the earlier sections focused on an *in vitro* starting point.

Cell culture experiments also allow for EVs that have been previously isolated (either from cell culture medium, or fluid samples) to be used as an exposure agent for recipient cell focussed experiments. Like the simplicity benefits derived for experiments assessing the production of EVs, cell culture studies allow for simpler readouts of cellular responses to an exogenous EV sample. In its simplest form, the readout is the ability of the specific cell type cultured to take-up the EVs used in the exposure experiment. Uptake assays are usually achieved through fluorescent labelling of EVs followed by confocal microscopy or FC based assessments (12). Uptake mechanisms can also be determined by knockdown of protein components known to be necessary for these processes, for example by use of endocytosis inhibitors (88). For EVs that are shown to be internalised, the intracellular pathway by which these EVs are processed and the

effect of their cargo is a clear point of interest. In most instances it is thought that endocytosed EVs are targeted to a MVB/lysosomal compartment, where it is assumed they are destined for degradation (143). It has been proposed, however, that there is a possibility that EVs can undergo a back-fusion step, where their membrane fuses with that of the MVB and the cargo can be released into the cytosol of the recipient cell (144-146). Understanding this process is at the leading edge of EV research and *in vitro* studies are the most direct route for greater detail to be uncovered.

Further to this, relatively standard and verified cell culture assays can be performed to assess the functional responses to EV-cell interactions. For example, angiogenic responses of human umbilical vein ECs (HUVECs) can be assessed by determining the degree of network formation after EV treatment (12). Additionally, EVs have been shown through standard assays to impact migration of ECs after exposure to cardiac progenitor cell-derived EVs (147) and enhanced survival of CMs can be seen if exposed to cardiac progenitor cell-derived EVs, through inhibition of apoptosis (148).

1.2.5.4 *In Vivo* Characterisation

A limitation of *in vivo* studies has been the inability to identify the cellular origin of EVs found in extracellular space as mixed populations from various cell types prevent precise identification (149). This limitation often restricted studies to *in vitro* experiments, where a single cell type is cultured and EVs assessed accordingly. *In vivo* studies fall into two categories, those which take exogenously prepared EVs and introduce these into an *in vivo* system and those which look to assess endogenously produced EVs with minimal interference to the system being used.

1.2.5.4.1 Labelling

EVs isolated from cell culture medium or other samples can be labelled in the same ways as described for *ex vivo* characterisations (see section 1.2.5.2.2) and then reintroduced into an *in vivo* system. A key consideration here is to avoid the EV label interfering with relevant surface molecules and thereby disrupting behaviour. Membrane dyes can allow single vesicles to be detected and to some extent allow for tracking *in vivo* (150) whereas others have used bioluminescent (151) and radioactive (152) labels to detect EVs at the global scale. These

studies have allowed EV behaviour to be understood from the angle of tissue distribution after injection into a living organism.

To allow the detection of a single EV *in vivo* a Tg approach is best pursued. Fluorophores can be expressed fused to a domain which drives lipidation of the molecule which results in tethering to the plasma membrane. This method has been used *in vivo* to label EVs derived from a tumour implanted into a mouse (153). A second Tg approach is to label EVs using fluorophores fused to EV markers, achieved in drosophila using CD63-GFP fusion protein expression (154).

1.2.5.4.2 Microscopy and Imaging

Confocal microscopy is the mainstay to most in vivo imaging efforts and has been used to image EVs in vivo (145). On initial consideration for EV tracking, confocal microscopy is limited by the diffraction limit of light, giving theoretical resolving capacities of ~250 nm. Although this is a limitation, it does not mean EVs smaller than this will not be detected, with sufficient signal from the label used and sensitivity in detection methods, EVs much smaller could be detected, but not resolved to determine if it's one or more EVs occupying close proximity to one another. Intravital multiphoton microscopy has also been used to visualise EVs in vivo, specifically to allow greater working distances needed when working with mouse (143).

1.2.5.4.2.1 Image Enhancement

Post-acquisition image representation can take some consideration, image data used for quantification efforts should essentially remain unaltered, whereas visual representations of data should not mislead the viewer but should allow for unhindered interpretation. The transfer is from quantitative to qualitative data, where a degree of subjective bias is inherent in the process. Contrast stretching, cropping and look up table changes are modifications that are widely acceptable but can have profound effects on interpretation, further manipulations tend to demand greater justification. Different scientific journals have their different rules regarding image modifications, but the key point is to make clear where any modifications have been used and make raw data readily available.

1.2.5.4.2.2 Non-linear Transformation

Unlike standard contrast-stretching which allows each value in the intensity range to be made use of by linear stretching of the intensity values to fill the full range available, non-linear transformations use a range of formulas to transform the data in a way that affects intensity values along the grey scale in an uneven way. The power-law transformation is one of the more commonly used in biology and has been used to aid EV visualisation in vivo (146). This process transforms the pixel values according to a logarithmic formula which can be used to visualise dim objects in the same image as brighter objects. If you're hoping to draw comparisons between brighter and dimer objects this process is not appropriate, and even if the brighter objects are only relevant as landmarks it is important to highlight the non-linear relationship between those objects, whilst taking care to apply the same transformation to all associated images (147).

1.2.5.4.2.3 Deconvolution

Deconvolution can greatly enhance appropriately acquired images, when carried out correctly it is perhaps more accurately described as image restoration. Deconvolution methods can increase contrast, decrease noise and recover resolution, these attributes are particularly useful when attempting to visualise EVs in cell culture studies (148) and even more so in vivo (145, 149). Confocal image acquisition is not perfect, excitation of objects outside the focal plane, imperfections in the optical detection process and mismatched refractive indices (150) result in excess noise and decreased resolution. This process can be mathematically understood by the convolution operation, understanding this operation and the contributing variables makes it possible to begin reversing some of these processes, leading some to favour the term restoration over enhancement of the image by deconvolution (151). Key to this mathematical understanding is the concept of the point spread function (PSF), where the 'point' is the source of the emitted light and the actual object dimensions are hidden by the detection of the optical spread of this light, which is noticeable axially as an elongation of the point. By taking dimensional measurements of the PSF and having dimensional measurements from your image acquisition you can theoretically reveal the dimensions of the actual object. This can be seen with the following equation:

F{recorded image(x, y, z, t)} = *F*{actual object(x, y, z, t)} x *F*{point spread function(x, y, z, t)}

Where taking a Fourier transformation of each of our three variables allows the equation to be reduced to a simple multiplication relationship between the actual object and the PSF. Which then allow the division of the Fourier transformation of the recorded image by the Fourier transformation of the point spread function to reveal the Fourier transformation of the actual object. This process is theoretically simple but there are many inconsistent variables to contend with, making this process much more complex – a complexity that is only amplified with *in vivo* contexts. Extracellular Vesicles in Coronary Heart Disease

1.3 *Extracellular Vesicles in Coronary Heart Disease*

1.3.1 Introduction

Over recent years, the study of EVs and their diverse roles within the cardiovascular system has intensified. The relevance of EVs in CHD has been suggested for many years, with changes in EV numbers and composition correlating with various stages of atherosclerosis and on to acute coronary syndromes such as MI (16). More recent efforts have focussed on the effects these EVs might impart, with roles in modulating the immune system (119), enhancing angiogenic capacity (12) and promoting cellular senescence described (155). Importantly, elucidation of EV profiles at different disease stages will strengthen their potential as diagnostic biomarkers, an idea that has progressed rapidly for some cancers (97) and shows promise for cardiovascular diseases (156). EVs also hold promise as therapeutics themselves, either synthetically loaded to deliver a desired cargo or by manipulation of the endogenous EV profile (157) to strategically promote/inhibit the release and/or uptake of EVs with known effects. The key to progress with these biomedical approaches is a greater understanding of the fundamental biology of EVs; most importantly we need to determine EV function and the true mechanisms mediating that function *in vivo*. In this way, therapeutic approaches can be made more precise, avoiding undesirable side-effects.

As is often mentioned, most if not all cell types are thought to produce EVs and the cells that form the cardiovascular system are no exception. CMs (158), ECs

(159), cardiac fibroblasts (160) and leukocytes (161) have all been shown to be capable of EV production. The EV-based interplay between these cell types and how this changes from a homeostatic to a diseased state is of great interest. For the purposes of this study, the focus is simplified to CMs and ECs, two of the major constituent cell types, but the interactions between all the relevant cell types will need to be deconstructed to make sense of a complex and nuanced picture.

1.3.2 Communication *In Vitro*

Building from the initial evidence base, numerous studies have been carried out *in vitro*, where various stimuli that might promote EV release could be tested and EVs of known cellular origin could be biochemically deconstructed, with a focus on cargo that might be relevant to disease states (see **Table 1.2**). For example, exposing primary rat CMs to hypoxic conditions in culture results in the production of EVs enriched for tumour necrosis factor-α (TNF-α) (162). Elevated levels of TNF-α have been documented in the blood serum of human patients with chronic heart failure (163), where its impact is considered detrimental as it contributes towards myocardial damage (164). These results together suggest EVs may be the mechanism by which TNF-α is transported systemically, but this remains to be shown *in vivo*. It remains unclear where these CM-derived EVs (CM-EVs), if relevant *in vivo*, are destined to end up and the response they might elicit, if any. Another cargo of CM-EVs highlighted in the literature is heat shock protein (HSP) 20. Increased levels of HSP20 have been observed in the circulation of an established cardiomyopathy hamster model (165) and later studies, using cardiac-specific overexpression in Tg mice, identified CMs as a potential origin for these elevated levels of HSP20 (166). Further to this, cell culture studies found CM-EVs to contain HSP20, highlighting a potential transfer mechanism. HSPs are widely appreciated to have cardioprotective functions (167) as shown for HSP20 following ischaemia/reperfusion injury *in vivo* (168). Consistent with these findings, the HSP20 loaded CM-EVs were found to elicit pro-angiogenic effects on cultured ECs (166). By contrast, cultured CMs isolated from a diabetic rat model produce EVs containing miR-320, which can be delivered to cardiac ECs (169) and this interaction imparts an anti-angiogenic effect by down regulating the target genes IGF-1 (170), HSP20 (171) and Ets2 (a transcription factor required for EC survival) (172). Again, *in vivo* evidence for this kind of communication is needed.

As well as being identified as putative recipients of CM-EVs, ECs have also been highlighted as producers of EVs (159, 173-176). Rat ECs, for example, have been shown to increase production of EVs that carry more HSP70 when the ECs are exposed to oxidised low-density lipoprotein (ox-LDL) (174). These EVs were then shown to be capable of activating monocytes and increasing their adhesion to ECs. Increased extracellular levels of HSP70, particularly in the blood serum of the peripheral circulation, are correlated to lower rates of progression for various vascular disorders including CHD (177). In contrast, higher levels of HSP70 have been shown to correlate with myocardial damage and progression of heart failure after acute MI (178-180). HUVECs stimulated by exposure to ox-LDL also produce EVs enriched for miR-155 (181), which appears to impart a shift in human monocytic THP1 cells from the M2 anti-inflammatory phenotype to the M1 inflammatory phenotype. These studies highlight the importance of EC/immune cell interactions, but also the impact EC-derived EVs (EC-EVs) can have on other ECs. EC-EVs isolated from the culture medium of human microvascular ECs (HMECs) have been found to carry miR-214, which was shown to impart its known effect on EC function via EV transfer to other ECs (175).The effects seen when exposing ECs to these EC-EVs included increased migration and angiogenesis in recipient cells, effects that were abrogated in cells that had been transfected with siRNA for both pre-miR-214 and mature miR-214 (175).

Table 1.2. Examples of Cardiovascular Models to Study EVs and their Cargo. *sEVs = small EVs.*

Model	Condition	Producing Cell	EV Type	Cargo	Reference
Adult Rat Primary Cells	Diabetic	CM	Microvesicles	miR-320	(169)
Adult Rat Primary Cells	Homeostatic	CM	Exosomes	HSP20	(166)
Neonatal Rat Primary Cells	Hypoxic	CM	Exosomes	TNF-α	(162)
Mouse HL-1 Cell Line	Growth Factor Treatment	CM	Exosomes	Transcriptomics Data	(182)
HMECs	Homeostatic	EC	Exosomes	miR-214	(175)
HUVECs	ox-LDL-treated	EC	Exosomes	miR-155	(181)
Mouse Blood Plasma Sample	Coronary Artery Ligation	Unknown	sEVs	miRNA-126-3p and 5p	(176)
Human PF	Aortic Valve Surgery	Unknown	Exosomes	Let-7b-5p	(12)
Human Arterial Explants	Heart Valve Surgery	Cardiac Progenitor	Exosomes	miR-210 & miR-132	(148)
Human Organ Donation	Homeostatic	Cardiosphere-Derived	Exosomes	Transcriptomics Data	(183)

1.3.3 Communication *In Vivo*

The initial studies that highlighted ultrastructural evidence for CM-EVs *in vivo* (149, 184) were based on transmission EM (TEM) analysis. TEM of cardiac progenitor cells in the mouse myocardium revealed double-membrane-bound vesicles, identified as exosomes and microvesicles based on size (184). The same study suggested these EVs were being targeted to CMs via cytoplasmic processes that appear to envelop the EVs, which were proposed as an uptake mechanism (184). Similar data were later presented identifying EVs in mouse cells as well as multivesicular bodies within human CMs (149). These studies prompted further steps to isolate EVs from relevant samples. As mentioned in section 1.2.5.2.1, isolation techniques are constantly developing rendering comparisons between different studies difficult. The eventual standardisation of techniques will make this easier in the future. However, CM-EVs and EC-EVs have been isolated successfully from various sample types including blood and PF.

1.3.3.1 Peripheral Circulation

One of the early biofluids found to contain EVs was the blood (11) and a renewed focus on these systemically present EVs has ensued (104, 185-187). EVs in the blood are known to contribute towards coagulation and inflammatory events; actions that are dictated primarily by surface molecules including PS (17, 188, 189). Importantly, increases in EV concentration within the blood have been associated with certain pathological processes and disease states (156, 176, 190-192). This puts blood plasma EVs at the centre of biomedical research efforts as our developed understanding holds potential for biomarker discovery (156) and systemic delivery for therapeutics (157). Significant effort has therefore gone into characterising blood plasma EVs (115, 193, 194), with comprehensive studies using cryo-EM with immunogold labelling to assess morphology, size, molecular phenotypes and concentration, to provide the most accurate characterisation possible with current technologies (195). EVs sampled from the blood can potentially have originated from a wide range of cell types, the majority are thought to be platelet-derived (195, 196), but erythrocytes (197), EC (198) and leukocytes (199) also contribute making characterisation efforts particularly challenging but with far reaching biomedical implications.

1.3.3.2 Pericardial Fluid

Populations of EVs have also been isolated from human PF samples (12, 200, 201) with attention on their relevance to cardiac interventions. The PF is an ultrafiltrate plasma that fills the pericardial space between the pericardium as it encloses the heart and the roots of the great vessels. This anatomical structure, as a protective sac surrounding the heart, is relevant by proximity to the heart itself. During cardiopulmonary bypass surgery bleeding from cut blood vessels is expected and will contaminate the PF, which is also breached in the process. 'Pericardial blood' samples taken from these patients is known to contain high concentrations of coagulation factors (202, 203). Further, is has been shown that EVs may mediate the transfer of signals that stimulate this clotting process (201).

Epicardial progenitor cells are thought to play a role in the repair phase following MI, where extracellular paracrine signalling would be required to elicit the necessary responses from distant cells (204-206). Gene expression studies in a mouse model of MI found the PF could initiate epicardial cell activation (206) and further, a epithelial-to-mesenchymal transition was shown to be responsible for repair in mouse (200, 207, 208). EVs isolated from human patients with acute MI were characterised by proteomic analysis revealing Clusterin expression compared to an absence in controls (200). Clusterin has been shown, by hemodynamic force assessment, to improve myocardial performance post MI in mouse (200). This improvement is suggested to be achieved through the observed activation of epicardium (including epithelial-mesenchymal-transition), arterial growth and reduced CM apoptosis (200).

EVs have also been isolated from human PF samples taken from patients that were undergoing aortic valve surgery, where the characterisation efforts focussed on small non-coding RNAs (12). The miRNAs found in the PF EVs were compared with EVs from blood plasma and they were found to have greater shared expression with the patients myocardium and vasculature (12). When the isolated PF EVs were used as an exposure agent, they were found to be capable of increasing proliferation rates, cell survival and network formation in HUVECs (12). One of the driving forces behind this proangiogenic response appeared to be the miRNA let-7b-5p acting on the target gene *TGFBR1* and decreasing its expression (12).

EVs carrying cardiovascular specific cargo appear to be abundant in the PF especially after myocardial insult and they also appear to drive relevant reparative and regenerative processes. However, there is currently limited understanding of the mechanisms driving the production of these EVs and even of the cell types responsible for their production. On top of this, there is no understanding of the spatial and temporal mechanisms dictating the pathways of these EVs through extracellular space *in vivo* and therefore no clarity on the accessibility of different cells types in which to illicit potential functional responses.

1.4 *Zebrafish*

This project aims to characterise endogenous EVs in the vertebrate model *Danio rerio* (zebrafish). Zebrafish offer an ideal model system for this study, thanks to several key attributes. Their relatively low housing and husbandry costs, both in terms of money and more directly space, allow for large numbers of individuals to be maintained within a single aquarium. Combining this with the high fecundity the species was specifically selected for, means that experiments using larval fish can be conducted on a larger scale, allowing for the experimental repetition required to derive statistical confidence in data interpretation. The accessibility of the embryonic and larval stages is also a key strength of the model system. Ex-utero development and optical transparency permit sub-cellular imaging and allow for *in vivo* observations of cellular events and interactions, using relatively non-invasive methods when compared to the methods used for intravital microscopy in mouse models. This level of unfettered optical access is essential for maximum coverage and detail to be gained from observational studies of cellular interactions *in vivo*.

The strengths so far outlined are what led to this species being developed for sophisticated genetic manipulations. Initial efforts were focussed on forward genetics approaches, with cloning (209), mutagenesis (210-213), transgenesis (214) and classic gene mapping efforts (215) driving the model forward, particularly within developmental biology as thousands of mutants were identified that directly impacted embryogenesis (216-218). This history and the genetic understanding that come with it makes the zebrafish a genetically tractable model system. Key to this study is the widespread use of genetically modified zebrafish

that express fluorescent reporters under the control of cell type specific promoters. Combining this precise fluorescent labelling with optical accessibility makes for powerful vertebrate system with unrivalled observational possibilities. As a direct result of these many attributes, zebrafish are now an established model for many human diseases (219) and their ability to repair and regenerate cardiac tissue after injury has been thoroughly investigated for its potential to reveal novel therapeutic approaches (220).

EV production and release is considered an evolutionary conserved process, however very little work has been published with regards to EV biology in zebrafish. EVs/matrix vesicles as well as MVB type structures have been identified using a combination of scanning and transmission EM on vertebral tissue sampled from adult zebrafish (108). Transient expression of HuC:CD63-GFP has been used to visualise neuronal EVs in the brain of larval zebrafish (221). Additionally, inhibition of neutral sphingomyelinase 2, often highlighted as a key component in EV budding, significantly decreased the neuronal EV numbers observed (221). Although these studies hint at the potential of the zebrafish model for EV research, they have by no means been fully characterised and their role following cardiac injury has not been determined, despite the promise for a concise *in vivo* analysis of endogenous EV dynamics. This project aims specifically to answer questions within a cardiovascular framework, but there are broader challenges in EV research that the project will address. Explicitly, the study will allow the cellular origin of released EVs to be defined and elucidate bio-distribution mechanisms by way of real-time spatial and temporal observation.

1.5 Hypothesis and Aims

The main hypotheses of this work are as follows:

Hypothesis 1: Tg zebrafish allow visualisation and isolation of endogenous CM and EC-derived EVs from a vertebrate *in vivo* model system.

Hypothesis 2: CMs and ECs show a dynamic alteration in release of EVs as a result of cardiac injury.

To address these two hypotheses, the specific aims of the project are as follows:

1) Develop live imaging techniques to visualise transgenically-labelled CM- and EC-EV dynamics, including release and uptake, in the peripheral circulation and pericardial space of larval zebrafish.
2) Develop fluorescence activated cell sorting (FACS) techniques to isolate fluorescently-labelled CM- and EC-EVs from whole zebrafish larvae.
3) Quantify the CM- and EC-EV response to cardiac injury in larval zebrafish.

Chapter 2:   Materials and Methods

2.1 Zebrafish Strains and Maintenance

Previously published Tg lines: *Tg(actin:mem-GFP)* (222),
Tg(TBP:G4m);(UAS:secA5-YFP) (223), *Tg(kdrl:mCherry-CAAX)* (224),
Tg(myl7:GFP) (225), *Tg(myl7:HRAS-mCherry)* (226) and the enhancer trap line
ET37 (227) were used in this project. All of these lines are maintained according
to standard procedures (228) and used in accordance with UK Home Office and
local University of Bristol regulations. Specifically, adult fish were maintained at a
stocking density of 1.2 fish per litre, on a 14-hour day/10-hour night light cycle.
The water was maintained at 28.5ºC, pH 7.0 and a conductivity of 450 µS.
Ammonia and nitrite were kept at 0 mg/ml and nitrate between 40 and 80 mg/ml.
Fish breeding was carried out in plastic chambers, with 3 females and two males'
setup as a breeding group the afternoon before collection. Eggs were collected
the next morning and 50 fertilised eggs were selected at the shield stage of
development at approximately 6 hours post fertilisation (hpf) (229), and
maintained in 10 cm petri dishes in 40 ml Danieau's solution (1740 mM NaCl, 21
mM KCl, 12 mM $MgSO_4.7H_2O$, 18 mM $Ca(NO_3)_2$ and 150 mM HEPES buffer)
which was changed once every two days prior to experimental procedures.

2.2 Laser Injury

For laser-induced injury, 3 days post fertilisation (dpf) zebrafish were
anaesthetised in 1.3 mM ethyl 3-aminobenzoate methanesulfonate (Tricaine/MS-
222) (Sigma: E10521). Molten 1% (weight/volume) low gelling point agarose
(Sigma: A4018) in Danieau's solution, was maintained at 40 ºC until needed. A
thin layer was added to a 35 mm glass bottom dish (Mattek: P35G-1.5-14-C)
containing the fish, which were then orientated laterally (anterior to the right, such
that the ventricle is orientated towards the objective lens) before the agarose
solidified (**Figure 2.1**A). Once the agarose was completely set, Danieau's
solution containing 1.3 mM MS-222 was then added to the dish to keep the fish
anaesthetised throughout the laser injury process (**Figure 2.1**A). A Micropoint
CO_2 laser (Spectra Physics) connected to a Zeiss Axioplan II microscope (Zeiss
Microimaging) was used for injuring as previously described (230). A 40X water

immersion objective and a double laser pulse at a wavelength of 435 nm was used to damage the surface of the apex of the ventricle (**Figure 2.1**B). The fish were then removed from the agarose and left in fresh Danieau's solution at 28 ºC until the desired timepoint post injury (**Figure 2.1**C)

2.3 Live Imaging

2-4 dpf zebrafish were anaesthetised in 1.3 mM MS-222 and mounted as described in section 2.2 (**Figure 2.1**A). Images were acquired using either a Leica SP8 confocal scanning light microscope (including a high-speed (8 KHz) resonant scanning option) (**Figure 2.1**D) or a Leica SP8X system using a white light tuneable laser with Leica's HyVolution 2 upgrade. Specific details for image acquisition are given in **Table 2.1**.
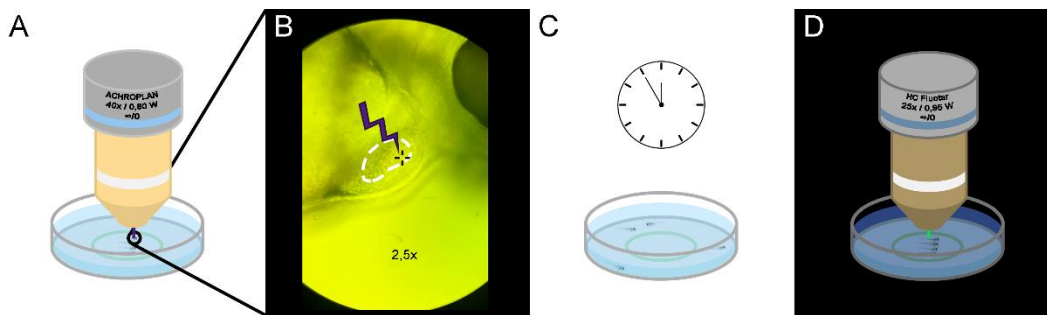
Figure 2.1. Workflow for Laser-Induced Cardiac Injury and Imaging. *(A) Larvae are anaesthetised, mounted in agarose and placed under the microscope. (B) The graticule is placed over the apex of the ventricle and the focal plane adjusted accordingly. Two pulses of laser light are used to damage the tissue. White dashed line demarks the ventricle. (C) The larvae are released from the agarose and maintained in fresh Danieau's solution until the desired timepoint post injury. (D) The larvae are anaesthetised and remounted in agarose to be imaged using fluorescent microscopy.*

Table 2.1. Examples for Image Acquisition Settings. *N/A= Not Applicable.*

	*Figure 3.3*B	*Figure 3.5*B	*Figure 3.10*B	*Figure 3.11*A-C	*Figure 3.11*A'-C'
Microscope	HyVolution2	Confocal	Confocal	Confocal	Confocal
Scanner Speed (Hz)	8000	8000	8000	400	400
Objective Lens	20x Dry	25x Water	25x Water	25x Water	25x Water
Numerical Aperture	0.75	0.95	0.95	0.95	0.95
Width, µm (pixels)	78.68 (592)	48.68 (512)	88.79 (512)	110.82 (1024)	51.91 (1024)
Height, µm (pixels)	78.68 (592)	48.68 (512)	44.40 (256)	110.82 (1024)	51.91 (1024)
Depth, µm (pixels)	N/A	N/A	N/A	50.160 (100)	20.277 (100)
Resolution, pixels/µm	7.52	10.52	5.77	9.24	19.73
Pixel Size, µm^2	0.14	0.95	0.17	0.11	0.05
Voxel Depth, µm	1	1	1	0.51	0.51
Z Slices	1	1	1	100	100
Frame Interval, sec	0.08	0.04	0.02	N/A	N/A

2.4 Post-Acquisition Adjustments

Appropriate images have been deconvolved using Huygens Professional version 16.10 (Scientific Volume Imaging, The Netherlands) using the CMLE algorithm (231-234). To achieve optimal results images were acquired at a sampling density that satisfied Nyquist-Shannon sampling theorem (235) such that all available information was captured within the constraints of the microscope settings.

Gamma adjustments were applied to images (where indicated) using the power-law transformation (γ = 0.65) to show smaller and dimmer EVs in the same image as larger and brighter cells (236, 237).

2.5 Larval Fish Dissociation and EV Isolation

16 pooled zebrafish larvae (4 dpf) were dissociated in 500 µl digestion buffer (described below) for 1 hour and 45 minutes in a Thermomixer set to 32 ºC and 800 rotations per minute. 500 µl stopping buffer (described below) was added and mixed by pipetting. Samples were then sequentially centrifuged (10 min at 300 g (2X) and 10 min at 1200 g (2X) at 4 ºC) with the supernatant transferred to a new 1.5 ml Eppendorf tube and carried to the next centrifugation step. The supernatant was then collected in a 1 ml sterile syringe and passed through a 0.8 µm sterile filter (Whatman: 1046224) to a new 1.5 ml Eppendorf tube. Samples were then centrifuged at 21000 g and 4 ºC and the supernatant discarded. The pellet containing isolated EVs was then fluorescently labelled with Calcein 450 (Violet) AM Viability Dye (eBioscience; 65-0854-39) (referred to as Calcein from this point forward) (132). The pellet was resuspended in 300 µl of 10 µM Calcein solution and incubated for 20 minutes at 37 ºC. Detergent treated negative controls were resuspended in 300 µl of 10 µM Calcein and 0.05% Triton X-100 (Sigma: T8787). Calcein negative controls were resuspended in 300 µl sterile 0.2 µm filtered PBS.

- **Perfusion Buffer** consists of 1X PBS plus 10 mM HEPES, 30 mM taurine and 5.5 mM glucose and was stored for up to three months at 4 ºC.

- **Digestion Buffer** consists of perfusion buffer plus 0.25% Trypsin, 12.5 µM $CaCl_2$ and 5 mg/ml Collagenase II and was freshly prepared on the morning of the experiment.

- **Stopping Buffer** consists of perfusion buffer plus 10% (vol/vol) FBS and 12.5 µM $CaCl_2$ and was freshly prepared on the morning of the experiment.

2.6 Flow Cytometry/Fluorescence Activated Cell Sorting

Analysis was carried out on a BD Influx flow cytometer with previously described methods considered to optimise the machine for the detection of nano-sized cell-derived vesicles (142) plus further modifications as described. High power 200 mW 488 nm laser was used for optimal excitation of small particles. In combination with the high-power, a small-particle detector allowed for high sensitivity in detecting forward scatter (FCS). Threshold triggering was based on FCS rather than fluorescence as noise generated by the flow cytometer was minimal in comparison with similar systems used by other laboratories (142), threshold triggering on a single fluorescent channel would also prevent multichannel analysis. Laser alignment and optimisation was carried out with Spherotech Rainbow calibration 8 peak beads and Biocytex Megamix beads. A 4 mm obscuration bar was used to optimally detect submicron particles. For FC a 100 µm nozzle at a pressure of 21 PSI was used, but to optimise for the FACS of nano-sized vesicles a 70 µm nozzle and 42.9 PSI was used.

2.7 Ex Vivo Imaging

EVs isolated via FACS experiments as well as from unsorted samples were used. 0.06 µm far-red labelled carboxylate-modified microspheres (Sigma: T8870) were added to the samples for a final concentration of 1:10000. For TIRF microscopy, 50 µl of sample was applied to 35 mm glass bottom dish (Mattek: P35G-1.5-14-C) and allowed to settle. For HyVolution based imaging, samples were applied to clean coverslips (Menzel-Glaser: 6776325) allowed to adhere to the slip, then Mowiol was added on top and a glass slide gently lowered onto the slip and the samples were then left in the dark for 24 hours at room temperature. Images were acquired using either a Leica AM TIRF multi-colour system attached to a Leica DMI 6000 inverted epifluorescence microscope or a Leica SP8X system

using a white light tuneable laser with Leica's HyVolution 2 upgrade. Briefly this includes automated narrowing of the confocal pinhole, with the acquired images then processed using custom deconvolution algorithms on Huygens Professional version 16.10 (Scientific Volume Imaging, The Netherlands).

Chapter 3: Characterising Extracellular Vesicle Labelling Strategies in Larval Zebrafish

3.1 Introduction

The main aim of this project is to develop strategies to allow *in vivo* imaging of endogenous cardiovascular EV dynamics. Two anatomical regions that have been described in humans and mammalian models to contain EVs of cardiovascular origin, are the peripheral circulation (156, 176) (see section 1.3.3.1) and the pericardial space (12, 156) (see section 1.3.3.2). To visualise EVs in these regions, several different Tg zebrafish lines were used corresponding to two broad approaches; global labelling of all endogenous EVs and cell-type specific labelling of EVs. Initially the global approach (see section 3.2.2 for detailed justification) was used to identify EVs in the regions of interest, test the general feasibility of the project, and assess the suitability of the approaches for labelling endogenously produced and cardiovascular relevant EVs. To do this confocal microscopy of the optically translucent larval stage zebrafish was used (**Figure 3.1**A), but without visualising EV release there was no way to discern cellular origin of those EVs identified. Larval zebrafish at 2-4 dpf have a fully functional cardiovascular system, with the ventricle and atrium of the heart already defined (238), and blood being pumped through an extensive vascular network including arteries and veins (**Figure 3.1**A) (239). Focussing on the aim to investigate the *in vivo* dynamics of cardiovascular EVs led to a second cell-type specific labelling approach, which allows EVs of CM and EC origin to be tracked in the pericardial space (**Figure 3.1**B) and peripheral circulation (**Figure 3.1**C) (see section 1.3.3.2 and 1.3.3.2 respectively) (12, 156, 176)).
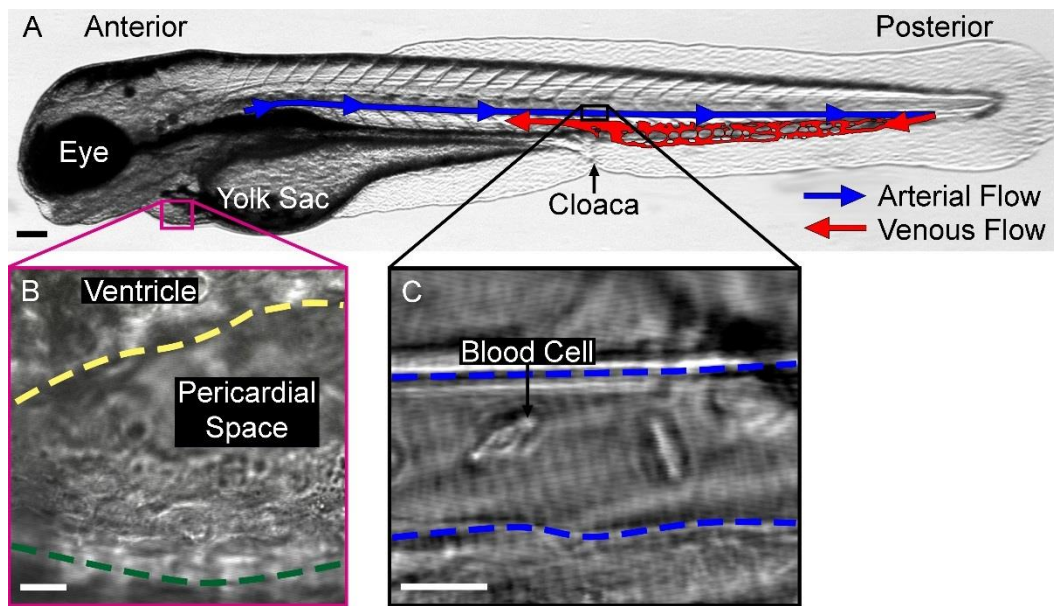
Figure 3.1. Larval Zebrafish Anatomical Regions of Interest. *(A) Orientation image of a whole larvae at 3 dpf, anterior to the left, the boxed regions highlight the regions of interest in B and C. (B) Higher magnification image of the pericardial space. Yellow dashed line demarks the ventricular myocardium and the green dashed line demarks the pericardium. (C) Higher magnification image of the dorsal aorta (DA). Blue lines demark the vessel wall. Scale bars: A = 100 µm; B,C = 10 µm.* **Extracellular Vesicles in the Peripheral Circulation**

3.2.1 Peripheral Circulation

Initially, EVs present in the peripheral circulation were investigated, as this would be the primary route by which systemic distribution would occur (156, 176, 195). The peripheral circulation provides an easily accessible region of extracellular space in the larval zebrafish, with flowing blood cells easily identifiable (**Figure 3.1**C, Movie 1) (240). The DA is a major trunk vessel that carries the blood from the aortic arches towards the posterior end of the fish; once past the cloaca, it is termed the caudal artery (CA) (241). Early investigations focused on the arterial flow of the CA, as this blood vessel is relatively uniform, symmetrical and linear in structure compared with the tortuous venous vessels of the caudal vein plexus, at the developmental stages examined. This difference in structure allowed for a representative optical slice to be acquired through the centre of the blood vessel, which is of particular importance for experimental designs that constrained acquisition to a single focal plane. The caudal section of this vessel was initially

selected as it is situated within the thinnest region of larval fish tissue, reducing optical interference and optimising detection capabilities.

3.2.2 Broad Labelling of Extracellular Vesicles

For the broader labelling approach, a near-ubiquitous (TBP) promoter was used to drive the expression of a modified Gal4 (G4m) which activates an upstream activation sequence (UAS) which in turn drives the expression of A5 which is fused to YFP and includes a short signal peptide to promote its secretion (secA5-YFP) (Tg(*TBP:G4m*);(*UAS:secA5-YFP*) (**Figure 3.2**A) (223). A5 binds PS (a relevant phospholipid in EV biogenesis and often identified as an EV membrane component – see section 1.2.5.2.2.2) with high affinity (242) thereby marking this membrane component with YFP (**Figure 3.2**B). This labelling strategy is necessarily driven by a ubiquitous promoter, aiming to achieve consistent base levels of extracellular A5-YFP throughout the fish (**Figure 3.2**C). It was designed to allow *in vivo* labelling of apoptotic cells (223) but also allows EVs (termed A5-EVs) to be visualised. Indeed, this Tg system allowed the visualisation of apoptotic cells in the peripheral circulation of Tg(*TBP:G4m*);(*UAS:secA5-YFP*) Tg fish at 3 dpf as expected (**Figure 3.2**D). This ubiquitous extracellular labelling approach, however, means it is not possible to discern the cellular origin of the EVs labelled.
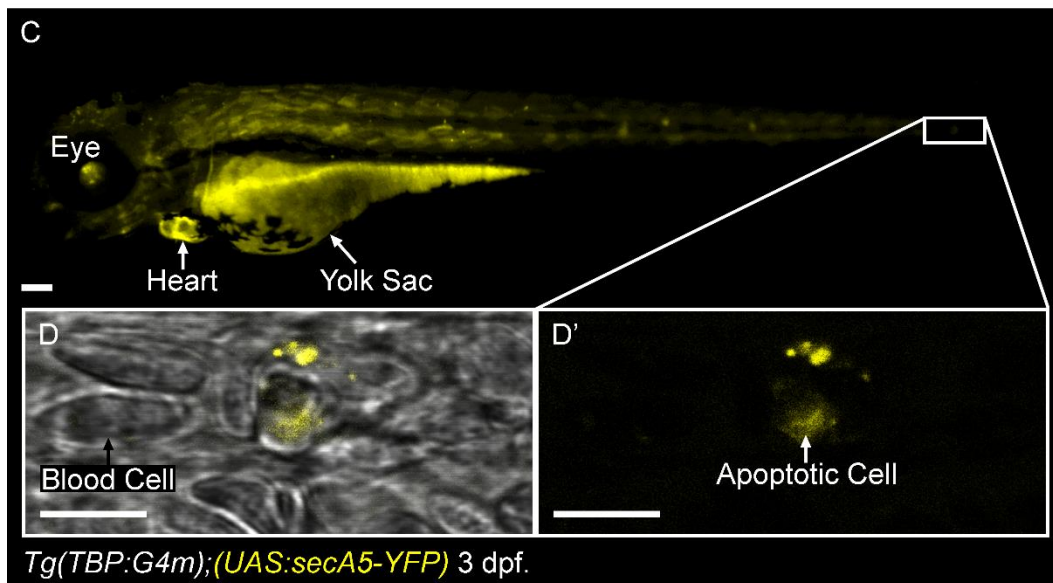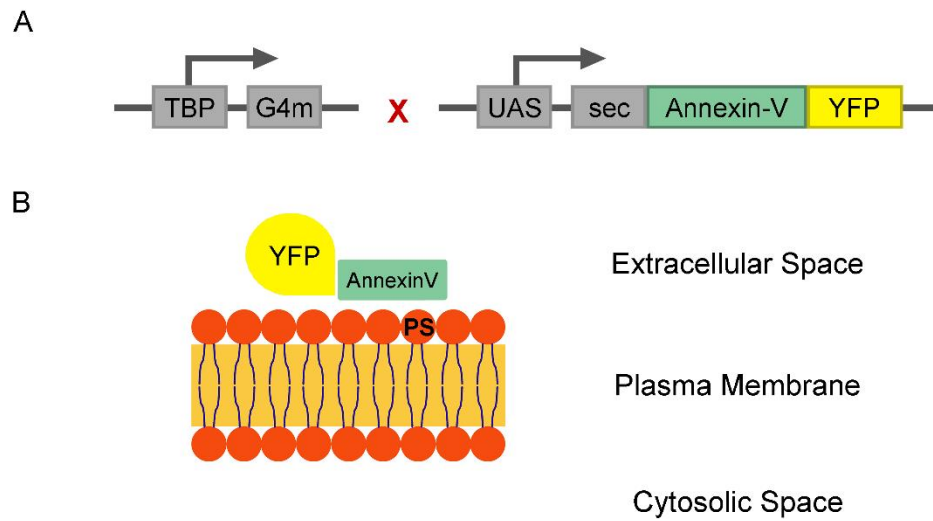
Figure 3.2. Orientation and Description of Live Imaging Approach Using A5 Labelling. *(A) Schematic of the Tg construct used to stably label externalised PS in vivo. (B) Schematic of the expressed reporter A5-YFP binding PS. Adapted from a published diagram **(153)**. (C) Fluorescent image of a 3 dpf larval Tg(TBP:G4m);(UAS:secA5-YFP) zebrafish. White box highlights the region of interest shown in D. (D) Example of a labelled apoptotic cell in the peripheral circulation. (D') The same image as in D but with only the fluorescent channel shown. Scale bars: C = 100 μm; D = 5 μm.*

3.2.3 AnnexinV-Positive Extracellular Vesicles in the Peripheral Circulation

Live imaging was carried out in 3 dpf larval zebrafish using the *Tg(TBP:G4m);(UAS:secA5-YFP)* line (**Figure 3.3**). The posterior end of the CA was targeted (**Figure 3.3**A) as this is a narrow, flat section of the fish that would allow for optical access with high resolution systems that have smaller working distances (e.g. HyVolution 63x objective lens with a 0.65 mm working distance). A5-EVs were observed in the peripheral circulation (n=4/4) using the Confocal/HyVolution2 system (see section 2.3; **Figure 3.3**B).

To assess the difference between the signal being recorded in the Tg fish and in non-Tg fish, average intensity measurements were taken for each frame of a 2-minute recording of the luminal space of the CA in *Tg(TBP:G4m);(UAS:secA5-YFP)* larval fish (n=4) and in non-Tg wildtype larval fish (n=2) (**Figure 3.3**C). Measurements were taken from the fluorescent channel within a region of interest, with an average value calculated for each frame and all frames from a time course analysed in turn and plotted on the graph (**Figure 3.3**C). Clear separation was observed between the average fluorescence intensity of the non-Tg and the Tg fish demonstrating that A5-EVs could be distinguished from background auto-fluorescent signal (**Figure 3.3**C). This analysis allowed a threshold to be set to ensure that fluorescent particles were distinguishable from background noise (**Figure 3.3**C). This analysis using a ubiquitous, extracellular labelling techniques demonstrates that EVs can be visualised *in vivo* in the peripheral circulation of Tg zebrafish.
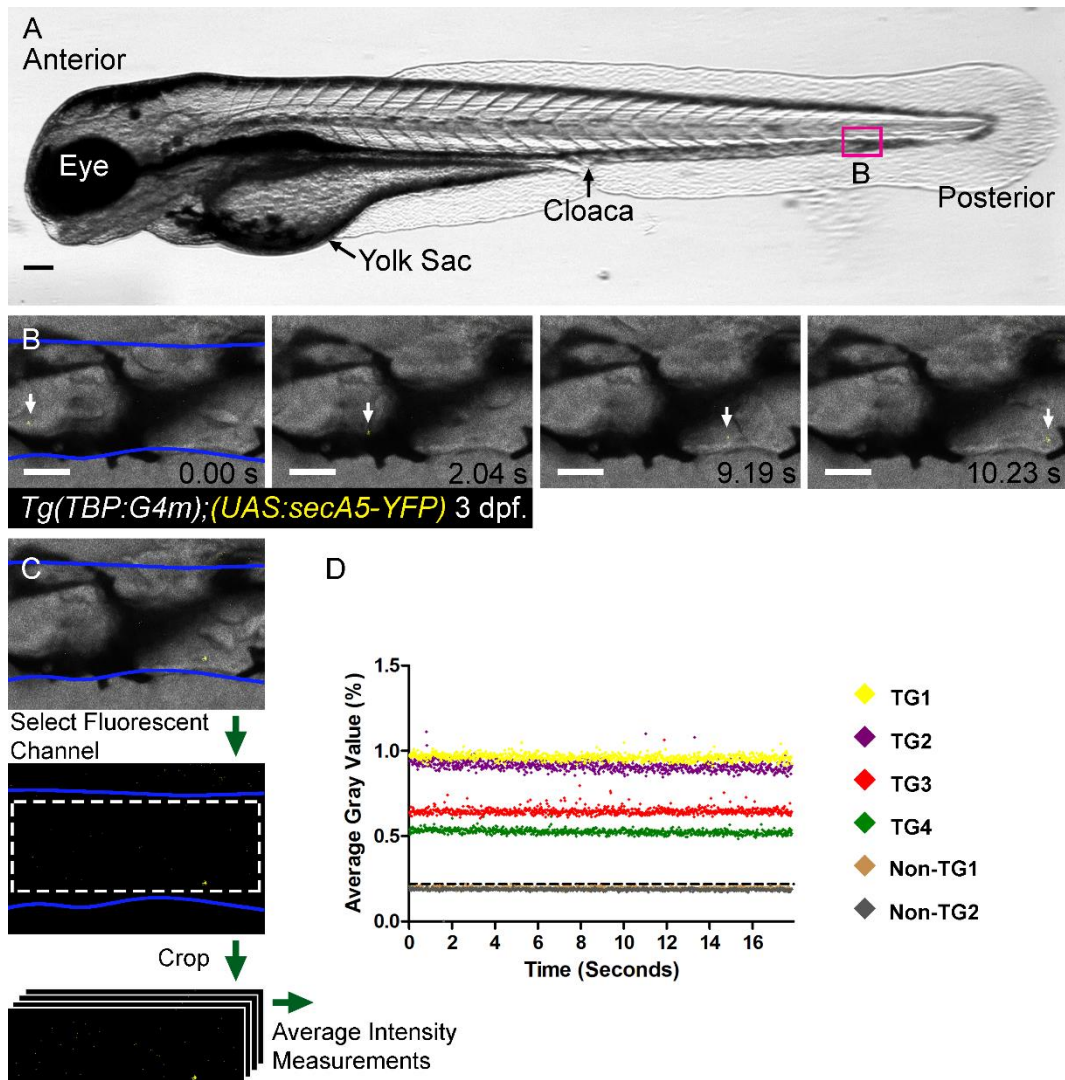
Figure 3.3. Live Imaging Sequence of A5-EVs in the Peripheral Circulation.
(A) Orientation image with magenta box highlighting the focal region for this figure at the most caudal end of the CA. (B) Image sequence of a single EV passing through the CA, white arrows highlight the EV, blue lines demark the vessel walls. (C) Schematic representation of workflow used to acquire the average intensity of each frame from a 2-minute (882 frame) recording of the peripheral circulation as it passes through the CA. (D) The average intensity of each frame from a two-minute movie of the peripheral circulation of the DA for YFP signal in four Tg(TBP:G4m);(UAS:secA5-YFP) Tg fish and two non-Tg fish are shown. The black dashed line demarks the threshold below which is non-Tg background signal. Scale bars: A = 100 μm; B = 10 μm.

3.2.4 Specific Labelling of Endothelial Cell-Derived Extracellular Vesicles

To investigate cell-type specific EVs in the peripheral circulation, the kdrl promoter driving a fluorophore fused to a CAAX box motif (*Tg(kdrl:mCherry-CAAX))* (**Figure 3.4**A) was used to specifically label the plasma membrane of ECs (**Figure 3.4**) (224). The CAAX box consists of the last 20 amino acids of c-Ha-Ras, which presents farnesylation and palmitoylation signals, along with a substrate for enzymatic action and lipidation of the molecule (243). This forces the fluorophore to tether to the inner leaflet of the plasma membrane (**Figure 3.4**B) under a cell-type specific (in this case endothelial cell) promoter (**Figure 3.4**C). EV biogenesis occurs either by an endosomal pathway, initiated by the invagination of the plasma membrane (exosomes) or ectocytosis direct from the plasma membrane of the producing cell (microvesicles). These modes of biogenesis mean that fluorophores anchored to the plasma membrane are incorporated into EVs produced by that cell. A similar method has verified this approach, where palmitoylated-fluorophore labelled tumour cells were implanted into a mouse model and fluorescent EVs released by the tumour were imaged via intravital microscopy (153).
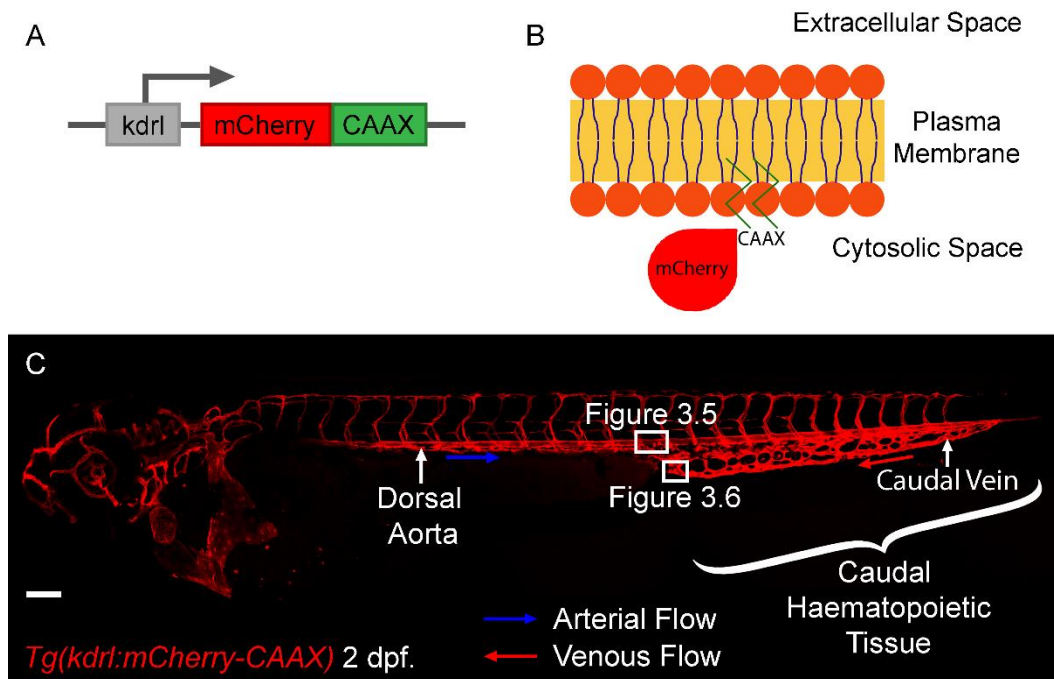
Figure 3.4. Orientation and Description of Live Imaging Approach Using EC Specific Labelling. *(A) Schematic of the Tg construct used to label the inner leaflet of EC plasma membranes. (B) Schematic of the expressed reporter mCherry-CAAX tethered to the inner leaflet of the plasma membrane. Adapted from a published diagram **(153)**. (C) Fluorescent image of a 2 dpf larval Tg(kdrl:mCherry-CAAX) zebrafish. Scale bar: C = 100 µm.* **Endothelial Cell-Derived Extracellular Vesicles in the Peripheral Circulation**

3.2.5.1 Endothelial Cell-Derived Extracellular Vesicles in the Dorsal Aorta

ECs play key roles in various cardiovascular related pathophysiological and physiological scenarios and EC-derived EVs (EC-EVs) have been highlighted as potential mediators of endothelial communications (244) (see section 1.3.2). Live imaging was carried out in 3 dpf larval zebrafish using the *Tg(kdrl:mCherry-CAAX)* line (**Figure 3.4**). After assessing the capabilities of the HyVolution system and standard confocal (**Table 2.1**) the image acquisition results were similar but the 25x 0.95NA objective on the standard system allowed for a greater working distance and therefore provided the freedom to acquire images in deeper tissues, which led to this system being chosen to acquire images of the peripheral circulation in the DA. For consistency the DA of *Tg(kdrl:mCherry-CAAX)* fish at 2 dpf was imaged at the site where it passes the cloaca as a

morphological landmark (**Figure 3.5**A). Due to high blood flow velocities the resonant scanners on the confocal setup was used to increase the acquisition rate up to 50.08 frames per second in a single plane of focus. Endogenous EC-EVs were observed in the lumen of the DA in the majority of the fish imaged (n=26/27) (**Figure 3.5**B,C; Movie 2). To assess the difference between the signal being recorded in the Tg fish and in non-Tg fish, average intensity measurements were taken for each frame of a 2-minute recording of the luminal space of the DA in *Tg(kdrl:mCherry-CAAX)* larval fish (N=4) and in non-Tg wildtype larval fish (N=2) for comparison (**Figure 3.5**D) in the same way as described above (**Figure 3.3**C). This analysis using an EC specific, intracellular labelling technique demonstrates that EC-EVs can be visualised *in vivo* in the peripheral circulation of Tg zebrafish.
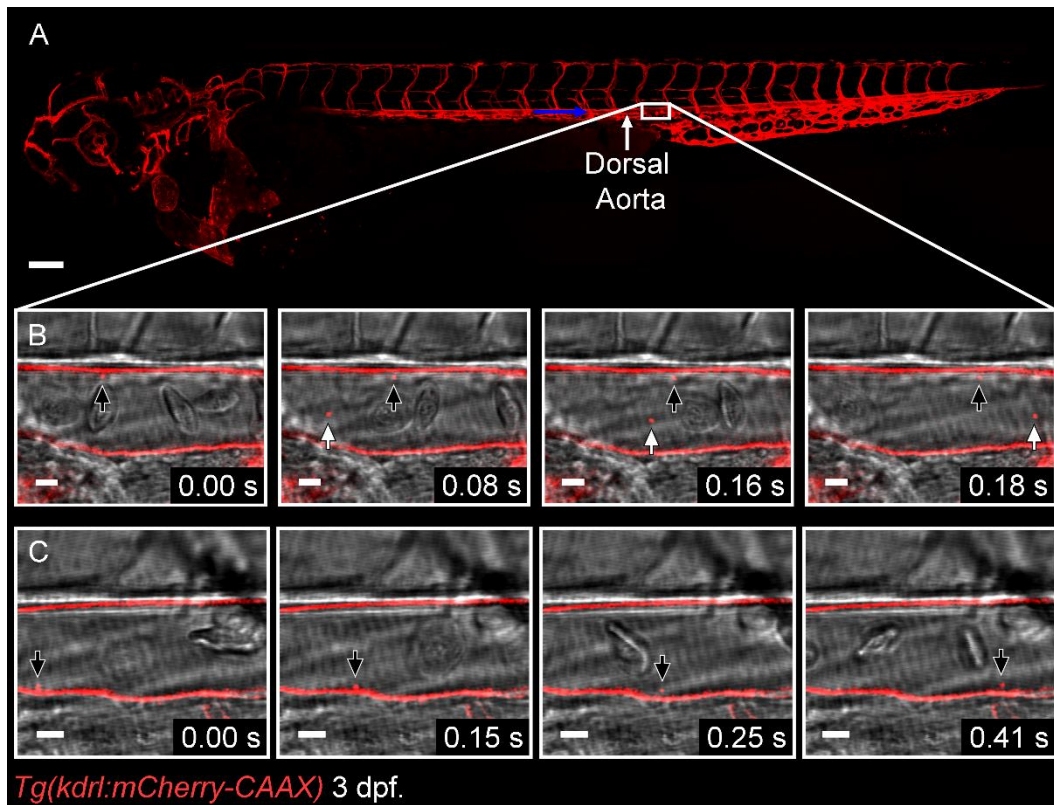
Figure 3.5. Live Imaging Sequence of EC-EVs in the Peripheral Circulation.
(A) Orientation image with white box highlighting the focal region for this figure, a section of the DA aligned with the cloaca. (B) Image sequence of two EVs passing through the DA, white arrows highlight one and the black arrows highlight the other EV. (C) Image sequence of a single EV rolling along the ECs lining the DA, black arrows highlight the EV. (D) The average intensity for mCherry signal in four Tg fish and two non-Tg fish are shown. The black dashed line demarks the threshold below which is non-Tg background signal. Scale bars: A = 100 μm; B,C = 5 μm.

3.2.5.2 Endothelial Cell-Derived Extracellular Vesicles in the Caudal Haematopoietic Tissue

To investigate endothelial-derived EVs in venous vessels as well as arterial vessels, endogenous EC-EVs were imaged in the CHT region of larval *Tg(kdrl:mCherry-CAAX)* fish at 3 dpf (**Figure 3.6**A,B). When the arterial blood flow turns 180º at the most caudal end of the larvae, it enters the caudal vein plexus, a region refered to as the caudal haematopoietic tissue (CHT) (

Figure 3.4C) (241). The vasculature of the CHT provides a highly branched and interconnected venous environment, in contrast to the arterial environment of the DA.Endogenous EC-EVs were observed in the lumen of vessels in the CHT in the majority of the fish imaged (n=20/21). In the CHT, EC-EV release into the peripheral circulation from a filopodial-like projection was also observed (n=1) (**Figure 3.6**; Movie 3). Together, these data demonstrate that this promoter driven membrane-tethered fluorophore system can be used to visualise cell-type specific EVs in vivo in the peripheral circulation.
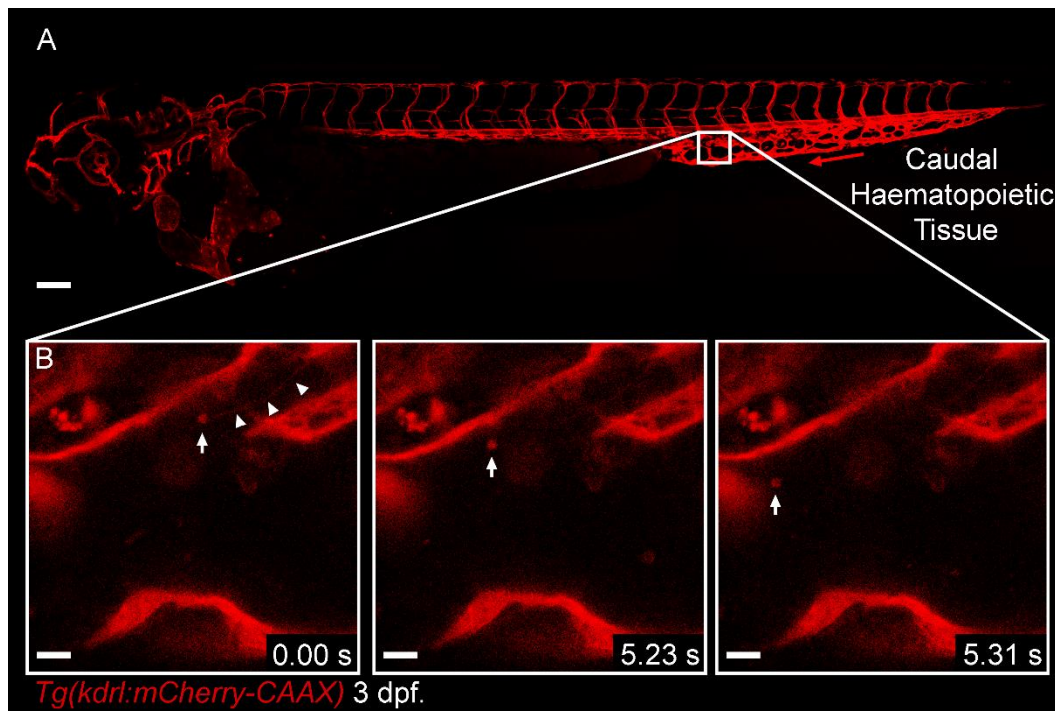
Figure 3.6. Live Imaging Sequence of EC-EV Release. *(A) Orientation image with white box highlighting the focal region for this figure, a vessel in the most anterior region of the CHT. (B) Image sequence of a single EV at the tip of a filopodial-like protrusion and then being released into the peripheral circulation. White arrows highlight the EV and white arrow heads highlight the filopodial-like protrusion. Scale bars: A = 100 µm; B = 5 µm.* **Extracellular Vesicles in the Pericardial Region**

As well as human EVs being identified in the peripheral circulation, a population of EVs has also been identified in human PF samples from patients with cardiovascular disease and, importantly, these EVs were found to mediate the transfer of proangiogenic cargo (12). However, the cellular origin of these EVs remains uncertain and nothing of their *in vivo* behaviour is known. The pericardium forms an insulating sac that encloses the heart and the roots of the great blood vessels (245, 246). The space between the pericardial wall and the epicardium of the heart is filled with an ultrafiltrate fluid, known as the PF (247) (see section 1.3.3.2). The techniques outlined in this project could allow the origin and behavioural dynamics of these pericardial space EVs to be dissected in an *in vivo* model system.

3.3.1 Pericardial Fluid/Space

The zebrafish pericardial space (**Figure 3.1**B; **Figure 3.7**A,B) is a relatively large extracellular space allowing easy initial identification and examination. However, its volumetric size combined with the movements generated by the beating heart can make imaging technically challenging. To clearly define the extent of the pericardial space in larval zebrafish at 2 dpf, dextran (molecular weight = 500,000) was microinjected through the skin into the space surrounding the heart (**Figure 3.7**B; Movie 4).
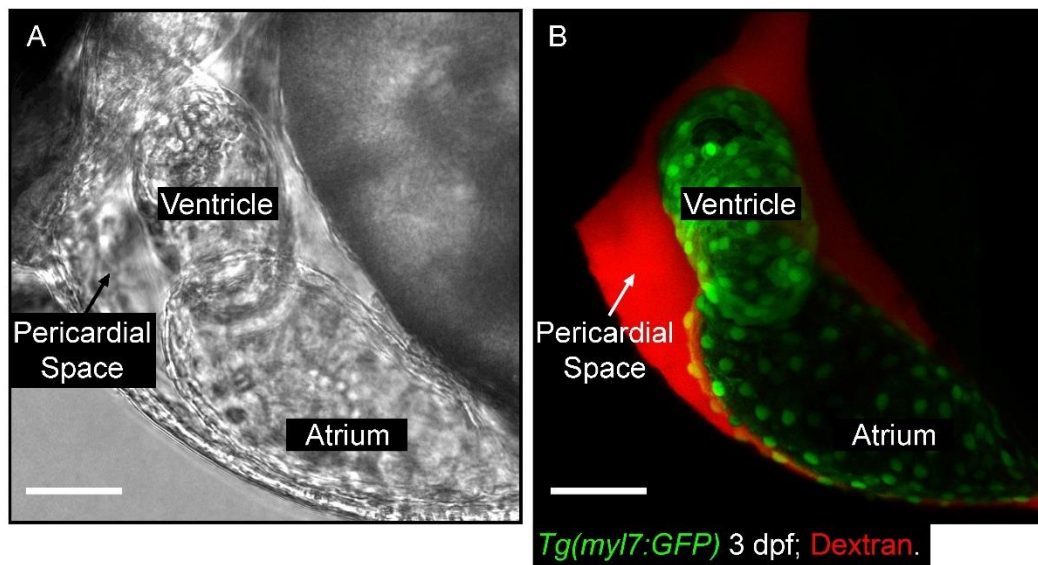
*Figure 3.7. Defining the Pericardial Space in the Larval Zebrafish. (A) Brightfield orientation image of the heart and the immediate surrounding area.(B) Fluorescent maximum intensity projection of 100 stacked images in the same XY region as in A. CMs are marked in green and the pericardial space marked by dextran in red. Scale bars: A,B = 50 µm.***AnnexinV-Positive Extracellular**

Vesicles in the Pericardial Space

To determine if EVs could be located in the zebrafish pericardial space, a broad live imaging approach was initially performed in 3 dpf larval zebrafish using the *Tg(TBP:G4m);(UAS:secA5-YFP)* line in accordance with the initial assessments made in the peripheral circulation (**Figure 3.2**) (see section 3.2.2). The working distance required to image within the pericardial space precluded the use of the Leica HyVolution2 system. The beating heart and a defined region of the pericardial space adjacent to the ventricle was imaged. A5-EVs were observed in the pericardial space (n=4/4) using the confocal system with the resonant scanner verifying that EVs can be imaged in this region using the zebrafish model (see section 2.3; **Figure 3.8**B; Movie 5).
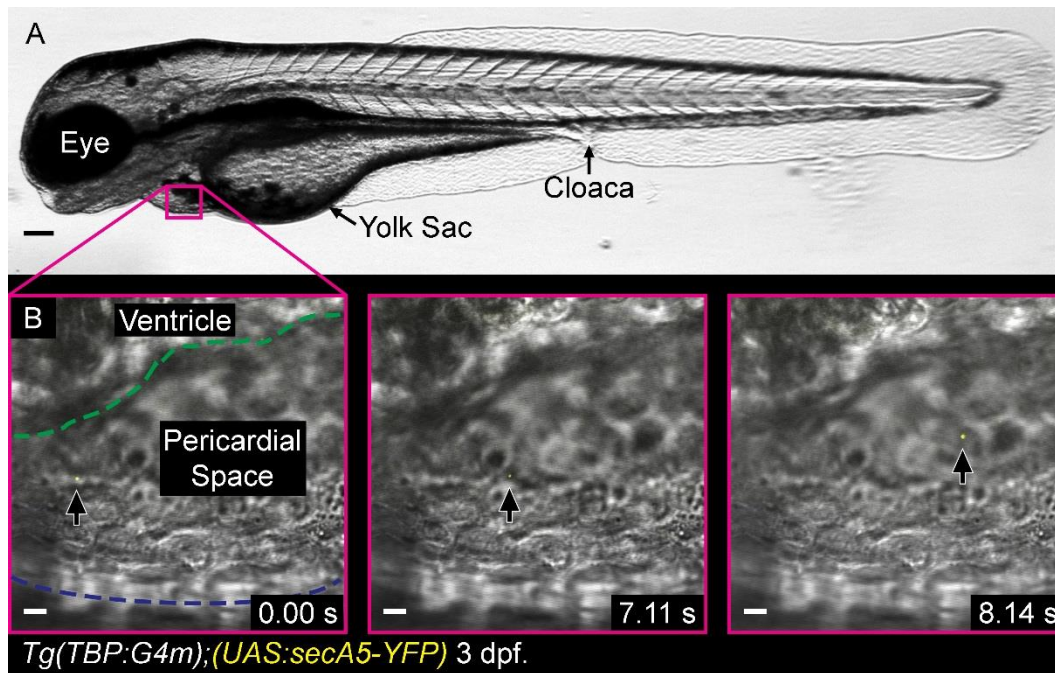
Figure 3.8. Live Imaging Sequence of A5-EVs in the Pericardial Space. (A) Orientation image with magenta box highlighting the focal region for this figure. (B) Image sequence of three EVs as they come into focus in the pericardial space, black arrows highlight the EVs. Green line demarks the ventricular myocardium and the blue dashed line demarks the pericardium. Scale bars: A = 100 µm; B = 5 µm.## Specific Labelling of Cardiomyocyte-Derived Extracellular Vesicles

To determine if CM-specific EVs could be observed in the pericardial space, a cell-type specific membrane-tethered fluorophore system was used. Similar to the method used for EC-EV labelling in the previous section, a CAAX box motif driven by the *myl7* promoter (*Tg(myl7:HRAS-mCherry)*) (**Figure 3.9**A) allows the plasma membrane (**Figure 3.9**B) of CMs to be specifically labelled (**Figure 3.9**C-D') (226). The HRAS (**Figure 3.9**A) system also includes a CAAX box motif (248) and is essentially identical to the previous system, labelling the inner leaflet of CMs (**Figure 3.9**B).
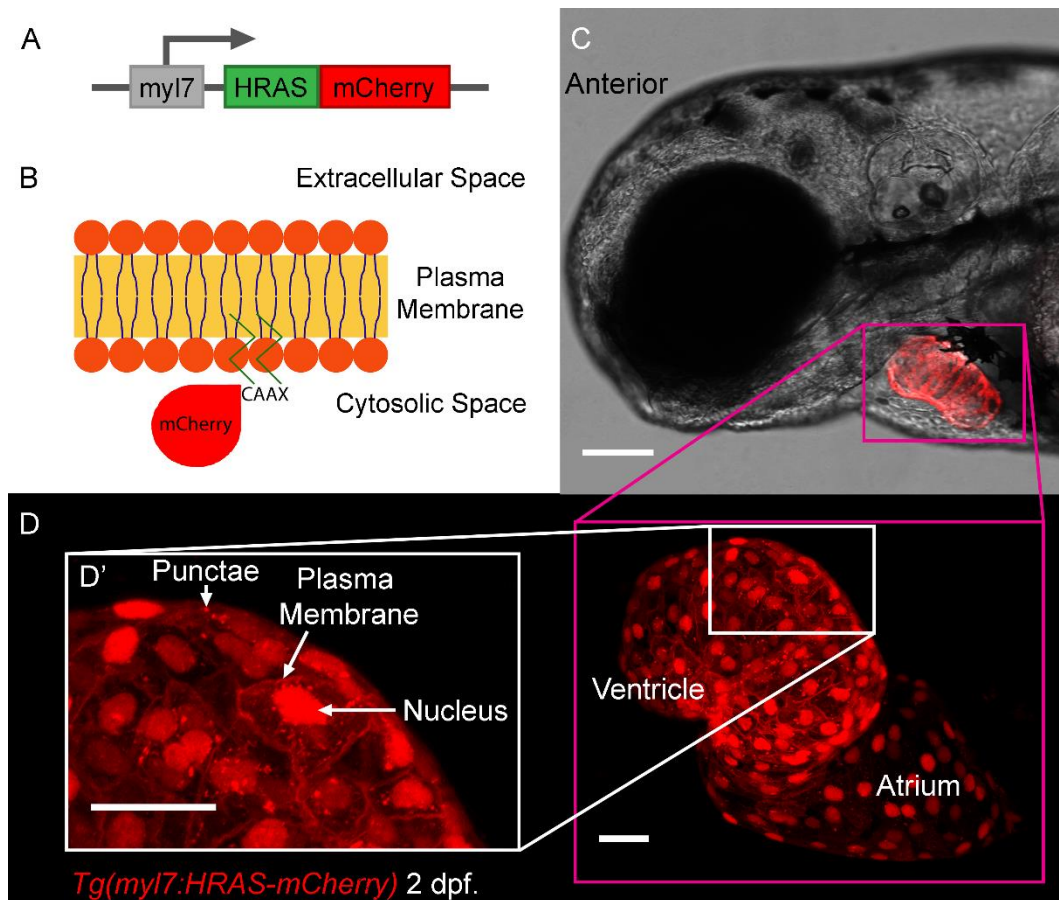
Figure 3.9. Orientation and Description of Live Imaging Approach Using CM Specific Labelling. *(A) Schematic of the Tg construct used to label the inner leaflet of the CM plasma membrane. (B) Schematic of the reporter HRAS-mCherry tethered to the inner leaflet of the plasma membrane. Adapted from a published diagram **(153)**. (C) Brightfield orientation image of the anterior end of a Tg(myl7:HRAS-mCherry) larvae at 2 dpf. The boxed region highlights the region of interest shown in D. (D) Fluorescent channel image from focal region. (D') Higher magnification of CMs allows the plasma membrane labelling to be seen clearly. Scale bars: C = 100 µm; D,D' = 25 µm.***Cardiomyocyte-Derived***

Extracellular Vesicles in the Pericardial Space

Imaging was carried out in 4 dpf larval zebrafish using the *Tg(myl7:HRAS-mCherry)* line (**Figure 3.9**; **Figure 3.10**A). To assess the difference between the signal being recorded in the Tg fish and in non-Tg fish, average intensity measurements were taken for each frame of a 2-minute recording of the luminal space of the pericardial space adjacent to the ventricular myocardium in *Tg(myl7:HRAS-mCherry)* larval fish (n=4) and in non-Tg wildtype larval fish (n=2) for comparison (**Figure 3.10**B) in the same way as described above (**Figure 3.3**C). Endogenously produced EVs in the pericardial space were then imaged

and identified moving stochastically in the pericardial space (**Figure 3.10**C; Movie 6). CM-EVs were observed in the pericardial space of all the fish assessed (n=6/6). This analysis using a CM specific, intracellular labelling technique demonstrates that CM-EVs can be visualised *in vivo* in the PF of Tg zebrafish.
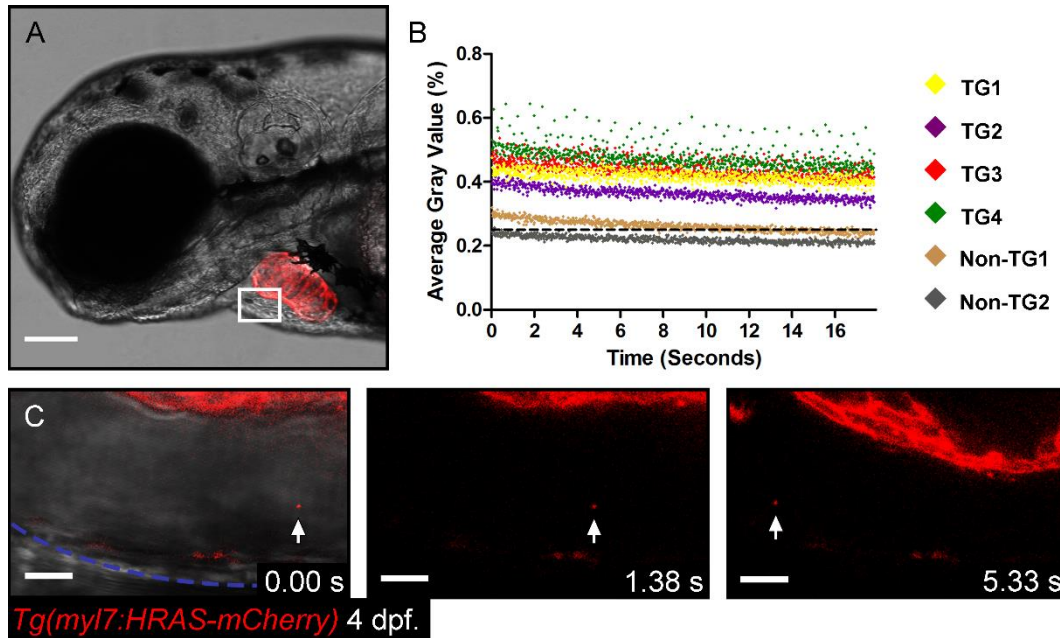
Figure 3.10. Live Imaging Sequence of CM-EVs in the Pericardial Space. (A) Brightfield orientation image of Tg(myl7:HRAS-mCherry), with CMs labelled in red. The boxed region highlights the region of interest used in analysis for B and shown in C. (B) Average intensity of each frame from a 2-minute (3000 frame) recording of the pericardial space of Tg(myl7:HRAS-mCherry) Tg and non-Tg fish. The black dashed line demarks the threshold below which is non-Tg background signal. (C) Image sequence of a CM-EV moving in the pericardial space, blue dashed line demarks the pericardium and white arrows highlight the EV. The initial frame includes the brightfield image for perspective and the subsequent two only the fluorescent image for clarity. Scale bars: A = 100 µm; C = 5 µm.

3.3.3.2 Cardiomyocyte-Derived Extracellular Vesicles Associated with the Pericardial Wall

During examinations of endogenous CM-EVs in the PF of *Tg(myl7-HRAS-mCherry); Tg(actin:mem-GFP)* fish, static mCherry positive EVs were often observed associated with the internal surface of the pericardial wall (**Figure 3.11**A-C; n=21/21). The stationary nature of these EVs allowed the use of the standard confocal microscope scanners, increasing the resolution of the acquired images (e.g. from pixel size of 0.173 μm^2 to 0.108 μm^2) and to take a z-series through the region of interest (see **Table 2.1**) (**Figure 3.11**A-C; Movie 7). Imaging in this way, sampling optimally by the Nyquist-Shannon theorem, also permitted deconvolution of the acquired data (Huygens Essentials) to restore the images (**Figure 3.11**A'-C'), allowing for an increase in the signal to noise ratio and subsequent gains in resolution, particularly in axial resolution (see section 2.4).

Convolved

Deconvolved

A

Pericardial
Wall

Ventricle

A'

B

B'

C

C'

*Tg(myl7:HRAS-mCherry);*Tg(actin:mem-GFP) 3 dpf.

D

Deconvolved
Convolved

E

***
n=18

For figure legend see next page.

Figure 3.11. Visualising CM-EVs Associating with the Pericardial Wall. (A) Low magnification convolved orientation image. CMs are marked in red and the cells of the pericardial wall are marked in grey, with the boxed region highlighting the region of interest shown in B and C. (B) Digital magnification image of the region of interest, showing CM-EVs (arrows) associating with the pericardial wall. (C) Fluorescent image of EV patch digitally magnified with a 5 µm positioning line indicated across the image. (A'-C') Corresponding deconvolved images of A-C. (D) Line graph showing the intensity values corresponding to the position along the line highlighted in C. (E) Quantification and comparison of measurements taken from convolved and deconvolved data, demonstrates the significant difference in the size of objects between the data. Matched colours represent paired observations, before and after deconvolution. For statistical analysis in E, a paired t-test was performed (n=18). The two groups differed significantly from each other with t(17) = 4.722, p = 0.0002. Scale bars: A,A' = 10 µm; B,B' = 5 µm; C,C' = 1 µm. Taking intensity measurements along a line drawn across a region of interest, in this case a cluster of static EVs on the pericardial wall, in the same place on both convolved and deconvolved data (**Figure 3.11**C,C') allows a numerical assessment of gains in resolution to be made. Graphical representation of example data shows clear gains in peak intensity values and a lessening of noise following deconvolution (**Figure 3.11**C-C'). In the intensity profile given as an example there are two resolvable peaks, where the full width of half maximum (FWHM) can be measured to give an estimate of the object size (**Figure 3.11**D). Comparing the FWHM on both convolved and deconvolved data at multiple regions of interest (n=18) clearly shows the gains achieved with this process (**Figure 3.11**E), however the actual size of the object is still unknown. This analysis as a whole, using a CM specific intracellular labelling technique, demonstrates that CM-EVs can be visualised *in vivo* associating with the pericardial wall of Tg zebrafish.
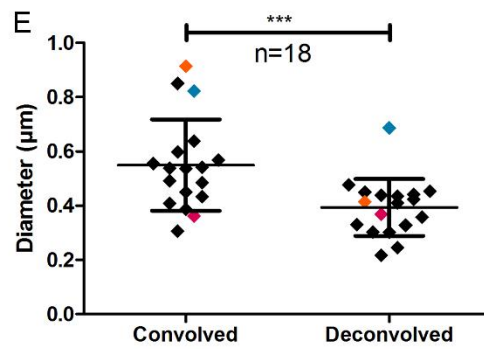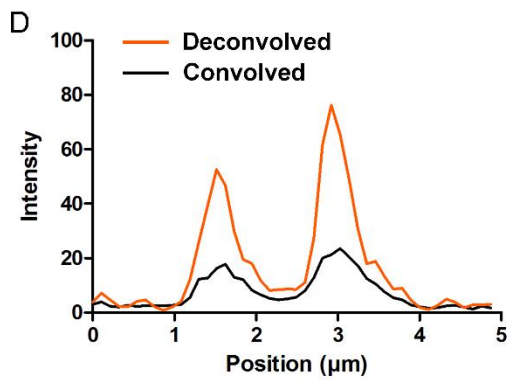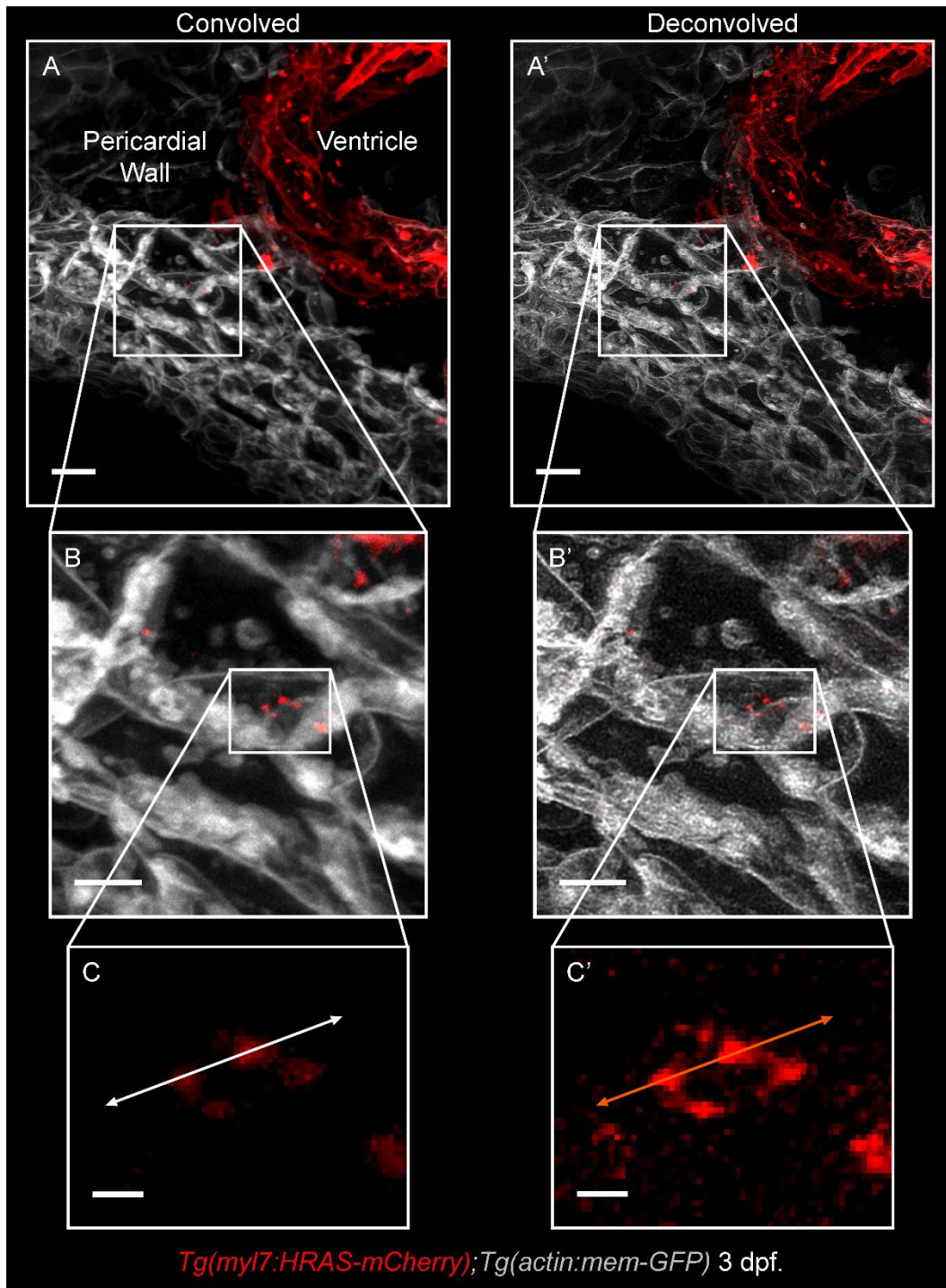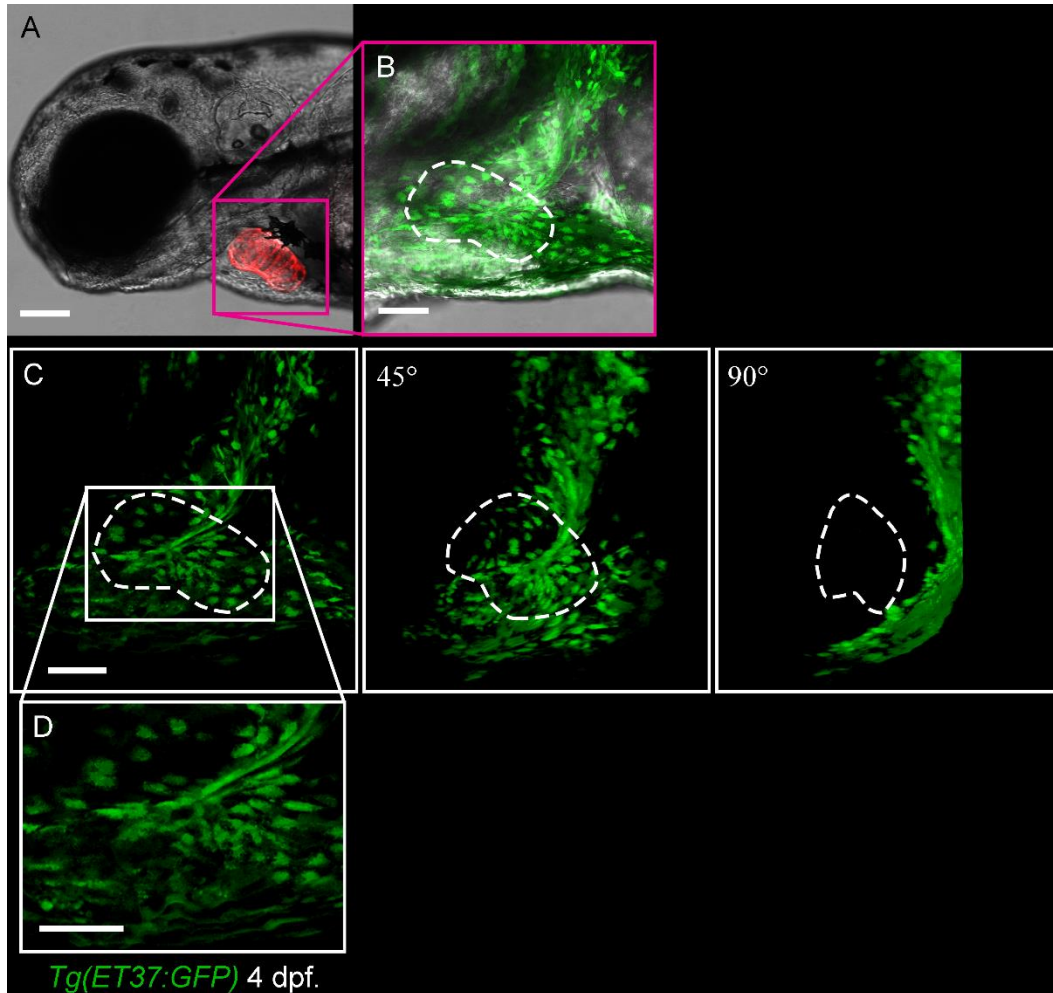
3.3.3.3 Pericardial Wall

To determine which cells these EVs are interacting with on the pericardial wall requires further investigation as little has been described for this pericardial region in zebrafish other than during the development of the epicardium (249). The pericardium is thought to be formed of a superficial fibrous pericardium composed of connective tissue and the serous pericardium formed of mesothelial cells. Therefore, a potential cell type that might be present as part of the pericardium are fibroblast-like cells although this has not been investigated in zebrafish.

To determine if fibroblasts are located in the pericardial wall, imaging was carried out in 4 dpf larval zebrafish using the *Tg(ET37:GFP)* line with similar acquisition

settings and anatomical focus to the images acquired of CM-EVs associating with the pericardium in the previous section (**Figure 3.12**A,B). Clear localisation of GFP positive fibroblasts was observed in the pericardial wall at this stage in development suggesting that the observed CM-EVs may be interacting with these cells (**Figure 3.12**C).

Figure 3.12. Defining the Pericardial Wall in Larval Zebrafish. *(A) Orientation brightfield image. CMs are marked in red.(B) Brightfield image to orientate combined with fluorescent maximum intensity projection of 134 stacks. Fibroblasts are marked in green. (C) Fluorescent 3D reconstruction of 134 stacks, 0º, 45º and 90º angles are shown for perspective. Fibroblasts are marked in green. (D) Digital magnification image of the region of interest in indicated in C. Scale bars: A = 100 µm; B-D = 50 µm.*

Chapter 4:   Extracellular Vesicle Response to Cardiac Injury in Larval Zebrafish

4.1 Introduction

The initial characterisation of total and cell-type specific EV populations outlined in the previous chapter provide a homeostatic baseline from which to explore changes in the EV profile as a response to cardiac injury. Previous studies in human patients and mammalian models have revealed increases in EV numbers in response to various pathologies, including cardiac surgery and cardiovascular disease (156, 176). This chapter describes the live imaging, quantification from imaging data and establishment of FACS techniques to quantify and extract cell-type specific EVs following a laser induced model of cardiac injury (see section 2.2) in larval zebrafish.

4.2 Endothelial Cell-Derived Extracellular Vesicles in the Peripheral Circulation

Mammalian cardiac injury models have revealed an increase in endothelium-derived circulating EVs (176) and human patients undergoing coronary artery-bypass-graft surgery show increased concentrations of blood plasma EVs although the cellular origin of these EVs is not known (156). Therefore, EC-EVs released following cardiac injury were first investigated in the peripheral circulation.

4.2.1 Endothelial Cell-Derived Extracellular Vesicles in the Dorsal Aorta

To determine if numbers of EC-EVs are altered in the DA following laser induced injury of the larval ventricle, live recording of the circulation passing through the DA was repeated at different time-points post-injury in *Tg(kdrl:mCherry-CAAX)* fish (**Figure 4.1**A,B). 25 minutes post injury (mpi) was chosen to look at the early EV number profile and 5 hpi as a later timepoint. The resulting sequence of 8-bit fluorescent images were adjusted using an iterative procedure based on the IsoData algorithm (**Figure 4.1**C) (250) and the threshold boundaries of 101-255 were applied to exclude false positive signals determined by identical acquisition

in non-Tg larval zebrafish (**Figure 4.1**D). The resulting binary image can be used to analyse particles and quantify the fluorescent EVs in the images (**Figure 4.1**C). Only objects in the size range of 0.58 µm^2 to 1.0 µm^2 were included in the analysis, with 0.58 µm^2 covering a 4-pixel object to avoid any noise being counted and 1 µm^2 being the upper limit for EV diameter and within the resolution limit of the confocal system used (see section 1.2.2.2). Initially, 25 mpi was chosen as a timepoint close to the time of injury and 5 hpi as a late timepoint, these timepoints were considered to reflect the speed with which an injury response might occur within the developing zebrafish. Quantification at 25 mpi or 5 hpi did not reveal any significant change in EC-EV numbers in the DA when compared to uninjured controls (**Figure 4.1**E).

A

Dorsal Aorta
Focal Point

Cloaca

Tg(kdrl:mCherry-CAAX) 2 dpf.

B

0.00 s 0.08 s 0.16 s 0.18 s
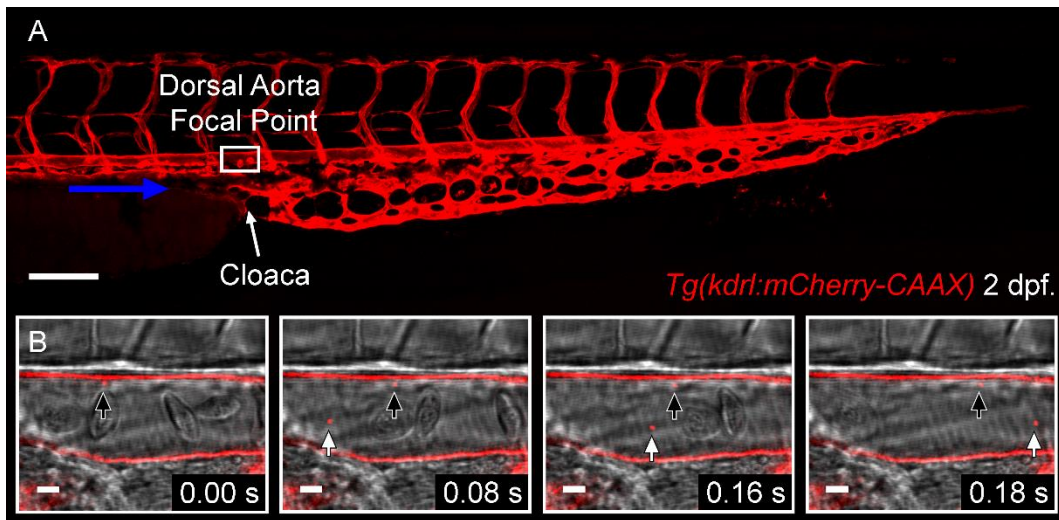
Select Fluorescent
Channel

C
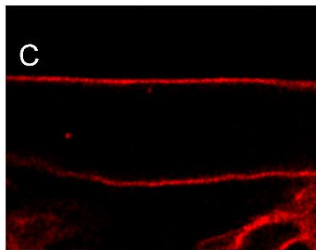
Threshold & Define
Region of Interest
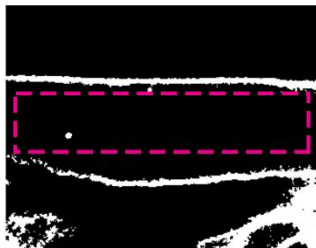
Analyse particles
over time series

D

E
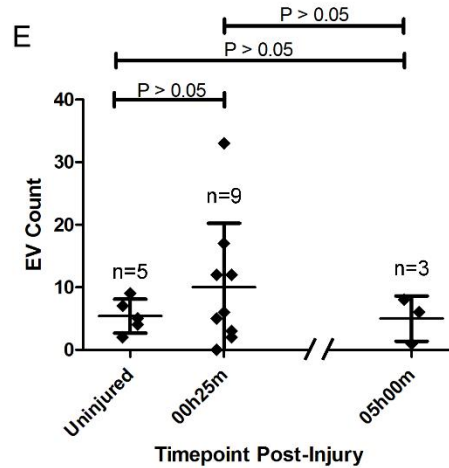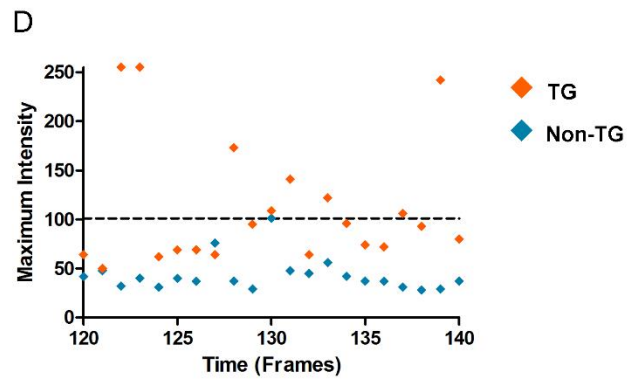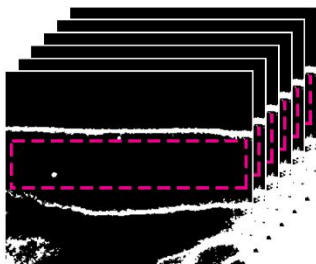
For figure legend see next page.

Figure 4.1. Quantification of EC-EVs Passing Through the DA in Response to Cardiac Injury. (A) Highlights the focal area of the DA, aligned to the cloaca. (B) 4 frames from a two-minute recording of the luminal space of the DA. (C) Schematic of the image analysis process, where the fluorescent channel is selected, a predetermined thresholding algorithm is applied, the region of interest defined and the particles within are assessed. (D) Maximum intensity value for each frame of a two-minute movie (20 selected frames shown as example), of the peripheral circulation of the DA, for 4 Tg and 2 non-Tg larval fish. Line at X (maximum intensity; = 101) demarks the threshold value used to exclude background noise based on the highest recorded value in non-Tg images. (E) Quantification of the number of EC-EVs recorded in the DA demonstrates no significant difference between timepoints. For statistical analysis in E, a one-way ANOVA test was performed, followed by Tukey's post hoc test. The three groups did not differ significantly from each other with $F = 0.750$, $p = 0.491$. Scale bars: A = 100µm, B = 5 µm.

4.2.1.1 Endothelial Cell-Derived Extracellular Vesicles in the Caudal Haematopoietic Tissue

The vessels of the CHT, in contrast to the DA, carry venous blood flow, a different tissue microenvironment in which to assess the EV profile. The 25 mpi timepoint was chosen as the highest variation was seen here in the DA and the 1h25 mpi timepoint as a closer timepoint to identify the point at which the response might return to lower variation. The same analysis methods were used to quantify EV numbers in the CHT as used in the DA and revealed similar numbers at all time-points examined (**Figure 4.2**B).
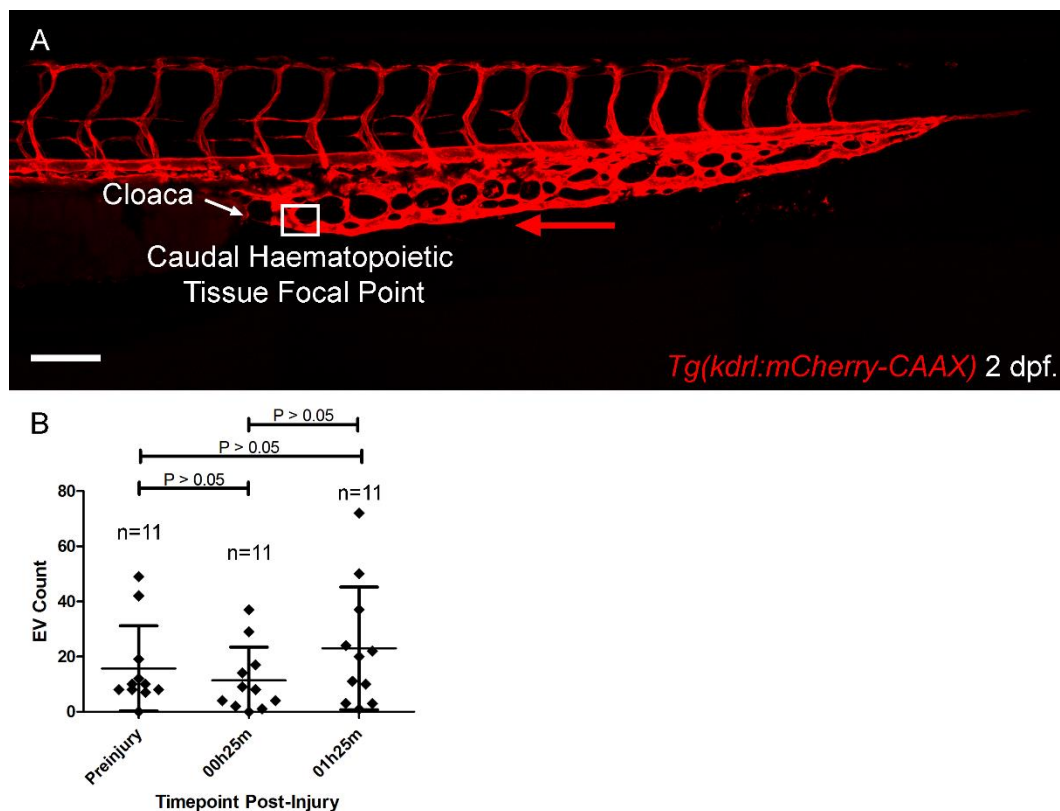
Figure 4.2. Quantification of EC-EVs Passing Through the CHT in Response to Cardiac Injury. *(A) The boxed region highlights the focal area in the CHT, close to the cloaca. (B) Each data point is the result of a two-minute recording of the peripheral circulation of the CHT. Quantification of the number of EC-EVs recorded in the CHT demonstrates no significant difference between uninjured and different injury time-points. For statistical analysis in B, a one-way ANOVA test was performed (n=11) including Bartlett's test, followed by Tukey's post hoc test. The three groups did not differ significantly from each other with F = 1.299, p = 0.287. Scale bar: A = 100µm*

Interestingly, although no significant difference in EV number was observed between uninjured controls and at different time-points post-injury, there did appear to be a difference in the total number of EVs observed in the DA compared with the CHT. Although further analysis did not reveal statistical significance between the regions, this does suggest that ECs in different anatomical sites may vary in their production of EVs and confirms the importance of analysis at different sites within the larvae (**Figure 4.3**).
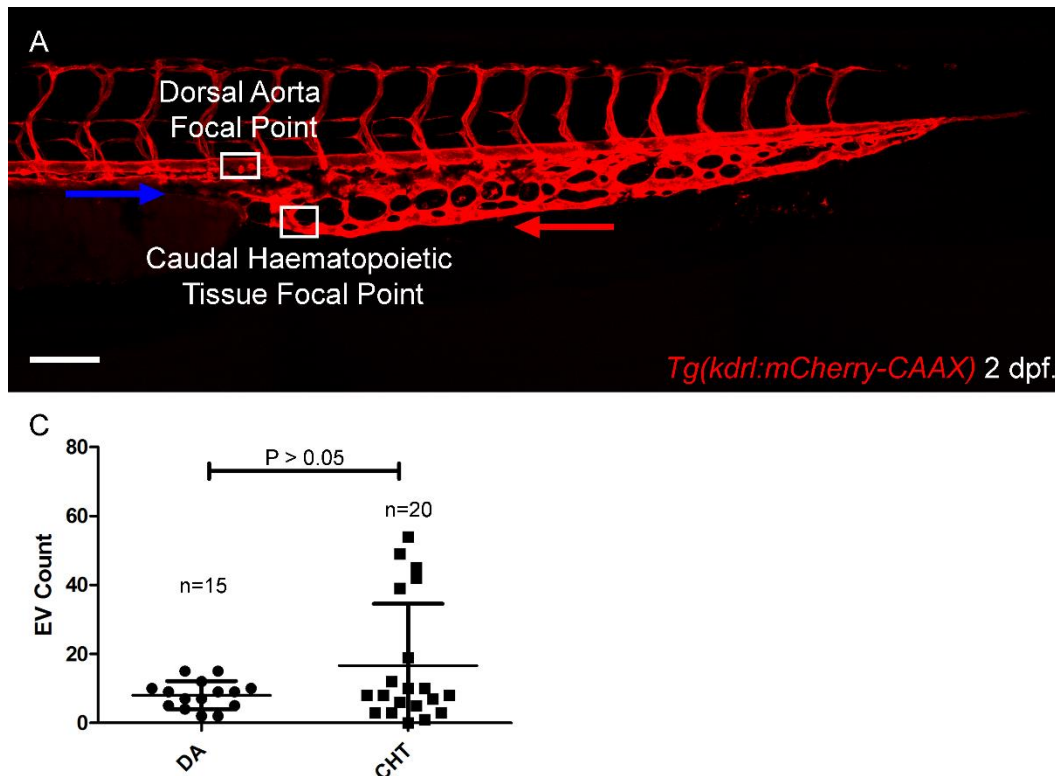
Figure 4.3. Quantification of EC-EVs Passing Through the DA Compared with the CHT. *(A) Highlights the focal areas of the DA and CHT, both aligned to the cloaca. (B) Quantification of the number of EC-EVs recorded in the DA and CHT demonstrates no significant difference between these two anatomical regions. For statistical analysis in B, a Grubbs' test was performed and significant (P < 0.05, Z: 2.29) outliers were removed, followed by an unpaired t-test (n=15-20). The two groups did not differ significantly from each other with t(33) =1.796, p= 0.082. Scale bar: A = 100µm.*

4.3 Cardiomyocyte-Derived Extracellular Vesicles in the Pericardial Space

A population of EVs from the PF, as sampled from human patients undergoing aortic valve surgery, have been characterised (12). These EVs were thought to have derived from the heart or associated vasculature but cellular origin is difficult to assess in *ex vivo* samples. Changes to cell-type specific EV profiles that might occur after cardiac injury have not yet been elucidated.

4.3.1.1 Cardiomyocyte-Derived Extracellular Vesicles in the Pericardial Fluid

To determine if numbers of CM-EVs are altered in the pericardial space following laser induced injury of the larval ventricle, live imaging was repeated at different time-points post-injury in *Tg(myl7:HRAS-mCherry)* fish (**Figure 4.4**A,B). The 5 hpi timepoint was chosen as a starting point to identify changes in EV numbers post injury. The images were analysed as described in section 4.2.1 above, with the following changes; the threshold boundaries were set as 59-255 to exclude false positive signals determined by identical acquisition in non-Tg larval zebrafish (**Figure 4.4**C) and objects in the size range of 0.69 to 1.0 μm^2 were counted. Quantification at 5 hpi did not reveal any significant change in CM-EV numbers when compared to uninjured controls although only a single time-point was analysed (**Figure 4.4**D).
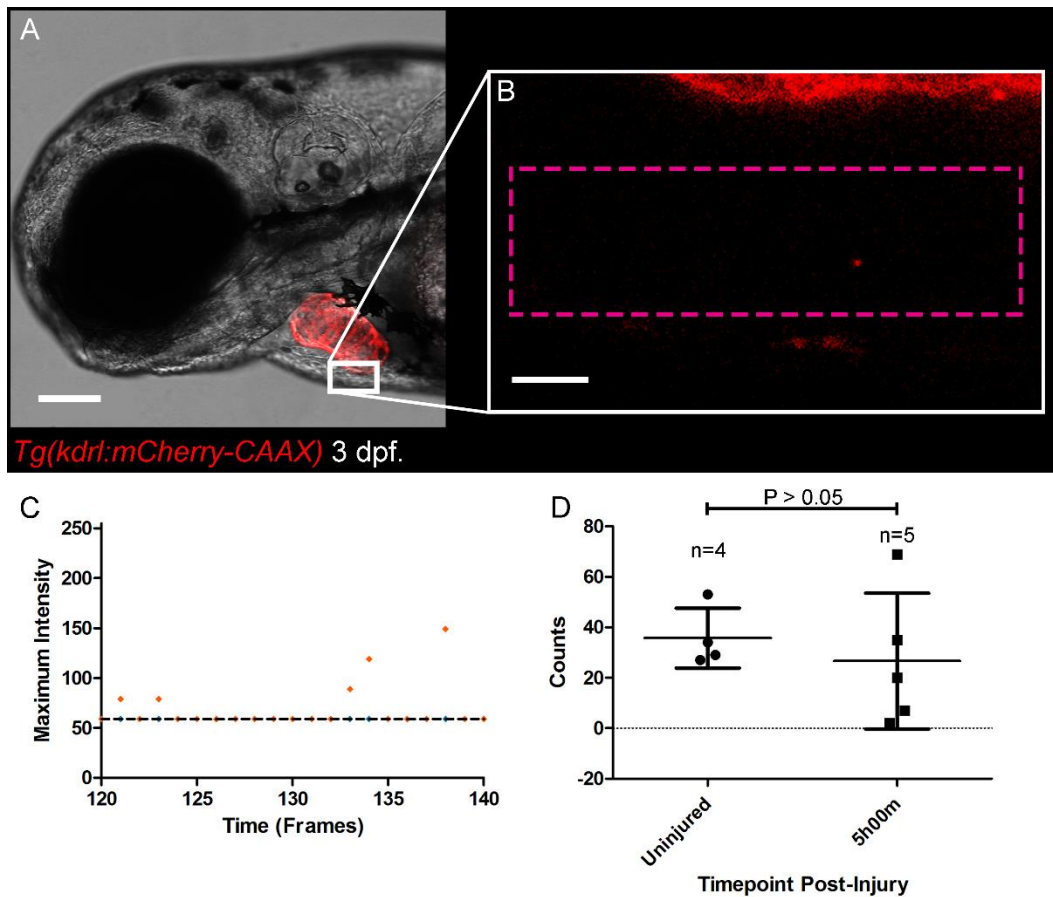
Figure 4.4. Quantification of CM-EVs in the Pericardial Space in Response to Cardiac Injury. *(A) Brightfield and fluorescent view of the head region of a Tg(myl7:mCherry-CAAX) fish at 3 dpf. The boxed region highlights the focal area of the pericardial space at the apex of the ventricle. (B) Higher magnification view of the boxed region in A showing the pericardial space immediately adjacent to the ventricle (red). The magenta box demarks the region of interest used to quantify EV numbers. (C) Maximum intensity value for each frame of a two-minute movie (20 selected frames shown as example) of the peripheral circulation of the DA, for 4 Tg and 2 non-Tg larval fish. Line at X (maximum intensity; = 59) demarks the threshold value used to exclude background noise based on the highest recorded value in non-Tg images. (D) Graph showing the number of CM-EVs counted in every frame of two-minute live recordings of the region in B in uninjured and injured Tg(myl7:HRAS-mCherry) fish at 5 hpi. Scale bar: A = 100 μm.*

4.3.1.2 Cardiomyocyte-Derived Extracellular Vesicles associated with the Pericardial Wall

To determine if numbers of CM-EVs seen associating with the pericardial wall changed in response to laser induced injury of the larval ventricle, live imaging of the pericardial wall was repeated at different time-points post-injury in *Tg(myl7:HRAS-mCherry)* fish (**Figure 4.5**A,B). The images were analysed as described in section 4.2.1 above, with the following changes; the threshold boundaries were set as 29-255 to exclude false positive signals determined by identical acquisition in non-Tg larval zebrafish (**Figure 4.4**C) and objects in the size range of 0.78 to 1.0 μm^2 were counted. Analysing a convolved dataset alongside the corresponding deconvolved dataset revealed a significant difference in the number of EVs counted (**Figure 4.5**C), leading to a cautious approach being adopted and the subsequent analysis being carried out on convolved data only. Quantification of convolved data at 3, 4, 5 and 6 hpi did not reveal a significant change in CM-EV numbers when compared to uninjured controls (**Figure 4.5**D).
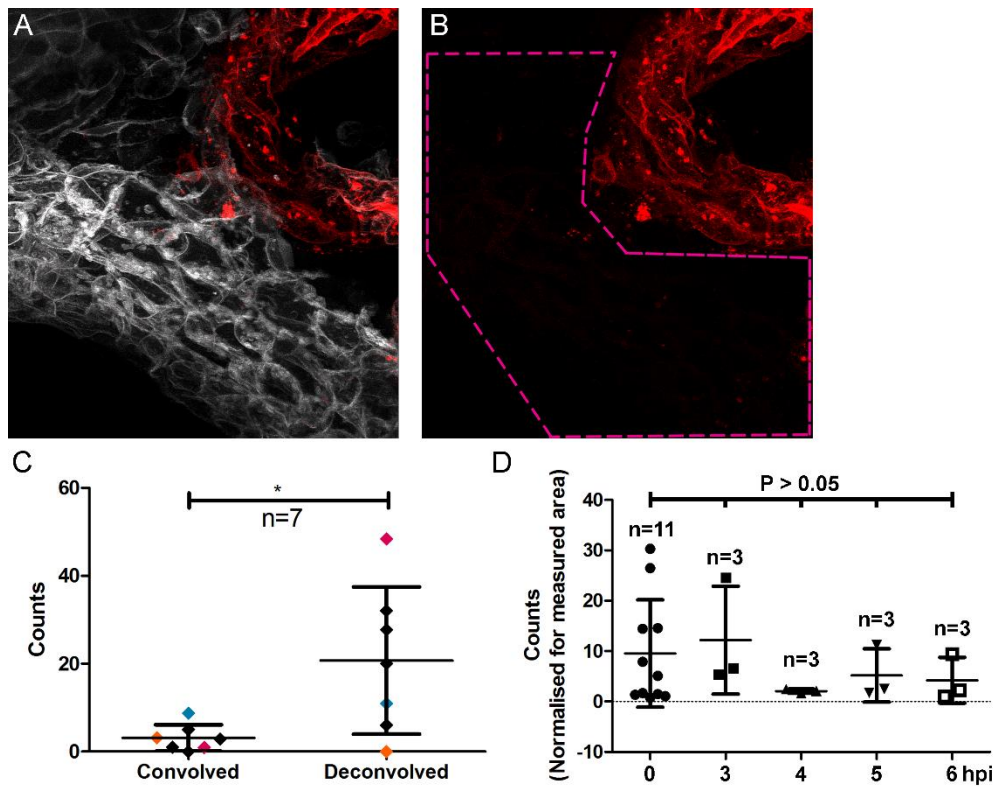
Figure 4.5. Quantification of CM-EVs Associating with the Pericardium in Response to Cardiac Injury. *(A) Maximum intensity projection image of the pericardial space of a Tg(myl7:HRAS-mCherry); Tg(actin:mem-GFP) fish at 3 dpf. The ventricle is shown in red and cells of the epidermis and pericardial wall shown in grey. (B) The magenta outline indicates the region of interest used to quantify EV numbers. (C) Graph showing the number of CM-EVs counted in maximum intensity projections of 100 z planes per data point, convolved data is shown to be significantly different to deconvolved data. Matching colours indicate the same image in its convolved and deconvolved state. (D) Graph showing the number of CM-EVs counted in maximum intensity projections of 100 z planes per data point, at different timepoints post injury, convolved data only. For statistical analysis in C, a paired t-test was performed (n=7,7). The two groups differed significantly from each other with $t(6) = 2.480$, $p = 0.048$. For statistical analysis in D, a repeated-measures ANOVA test was performed. The means across the four groups did not differ significantly from each other with $F(4,18) = 0.765$, $R^2 = 0.145$, $p = 0.562$. Scale bar: A = 100μm.*

4.4 Quantification of Total Extracellular Vesicles Ex Vivo by Flow Cytometry

With the aim to quantify larger numbers of samples and to verify the quantification from live imaging, higher-throughput FC methods to assess the EV response to cardiac injury in larval zebrafish were developed. This required a modified FC system (see section 2.6) to allow small EVs to be reliably detected, as opposed to routine cell detection. By digesting whole Tg larvae, we looked to asses global EV responses to cardiac insult. Using Calcein we were able to label intact EVs, preventing any cellular debris and/or membrane fragments from skewing the results.

4.4.1 Proof of Concept Controls

In addition to the modifications to the flow cytometer (in line with previously tested and published suggestions (142)), care was taken with appropriate controls and proposed methods for standardisation in the field (116, 251). To avoid coincidence and an underestimate of EV concentration we carried out a serial dilution of concentrated EVs from uninjured *Tg(actin:mem-GFP)*, which showed the expected linearity in relation to the event rate (**Figure 4.6**A), whilst the fluorescence intensity from the same samples stabilised at dilutions greater than 600 µl (**Figure 4.6**B). This can be seen in the scatter plot signature of the three dilutions selected (**Figure 4.6**C). This process confirms singular EVs and not aggregates are being detected at dilutions of more than 600 µl.
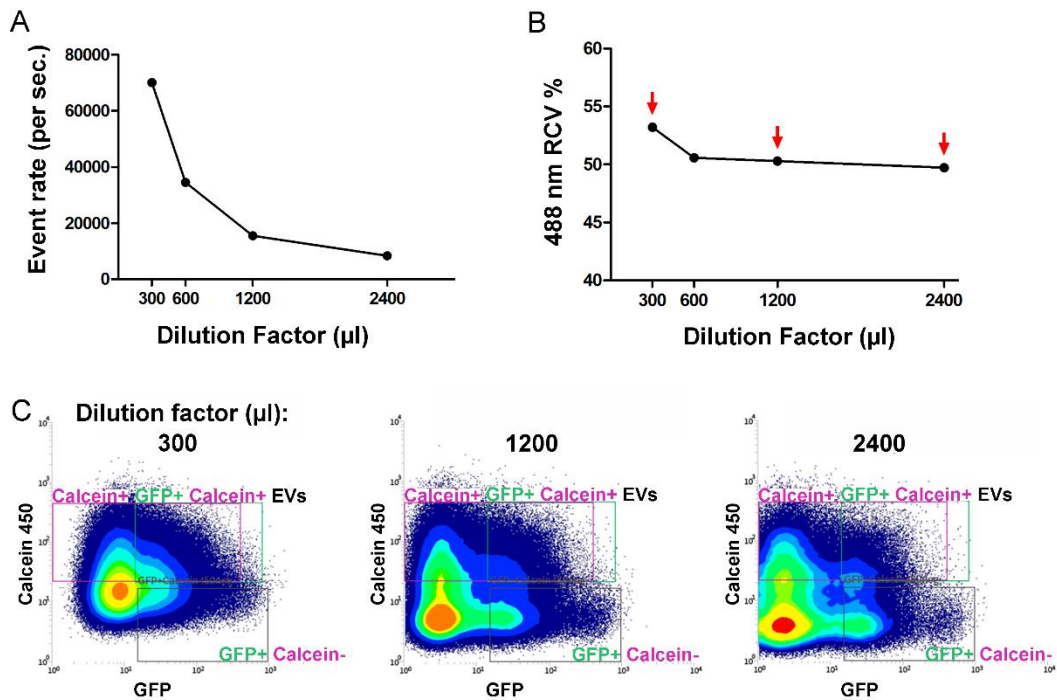
Figure 4.6. EV Detection by Modified FC: Serial Dilution Assessment. *16 pooled whole uninjured Tg(actin:mem-GFP) larval zebrafish (4 dpf) were digested and EVs isolated by centrifugation and filtration (see section 2.5). (A) Analysis of event rate over serial dilutions of EV sample. (B) Analysis of fluorescent intensity over serial dilutions of EV sample. (C) Scatter plots (GFP vs Calcein) of EV samples at different dilutions as indicated by arrows in B.*Several control

experiments were performed to allow gates for positive events to be set more

reliably. Firstly, samples without larval zebrafish were processed as normal

including Calcein labelling (**Figure 4.7**A), this revealed noise inherent in sample

preparations, revealing the thresholds above which positive signals can be gated

for. EVs isolated from non-Tg fish and labelled with Calcein (**Figure 4.7**B)

showed a clear signature, allowing the Tg fluorophore gates to be more reliably

set to an area on the scatterplot that does not overlap with this non-Tg Calcein

labelled sample. EVs isolated from Tg fish but without Calcein labelling revealed

a clear signature (**Figure 4.7**C) allowing the Calcein positive gates to be more

reliably set beyond the threshold of the Tg fluorescent signal (**Figure

4.7**C).These controls allowed specific gates to be set to capture Calcein+, GFP+

and mCherry+ events from uninjured Tg(kdrl:mCherry-CAAX); Tg(actin:mem-GFP) larvae (**Figure 4.7**D).

A No fish + Calcein AM
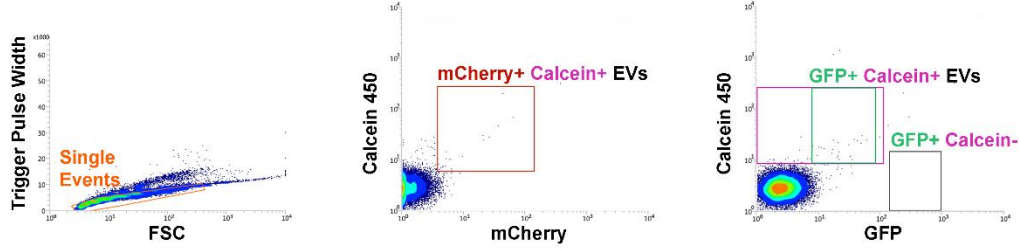
B Non-transgenic + Calcein AM
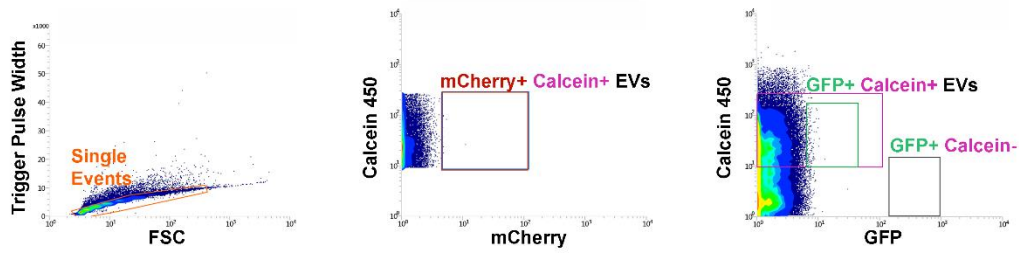
C Transgenic - Calcein AM
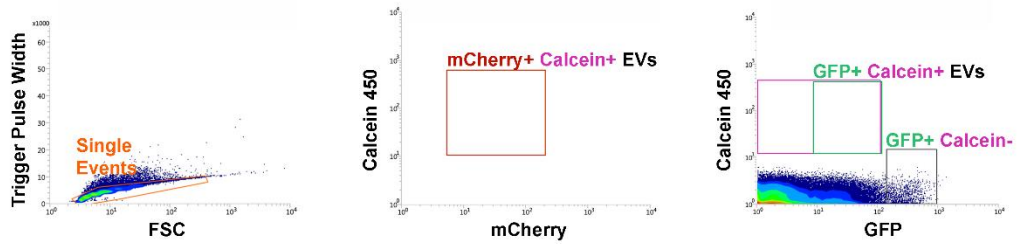
D Transgenic + Calcein AM
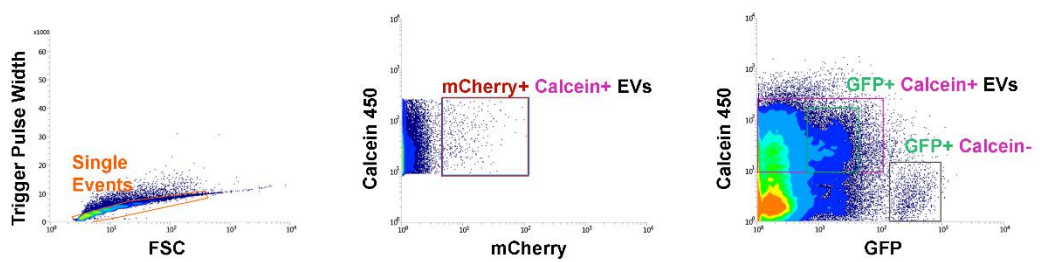
For figure legend see next page.

Figure 4.7. EV Detection by Modified FC – Control experiments for Tg and Calcein Labelling of EVs. *The scatter plots of Trigger Pulse Width against FSC on the left-side are where an initial gate is created to count only singular events. The scatter plots of Calcein intensity vs mCherry intensity in the middle, are where mCherry+ and Calcein+ EVs can be gated for. The scatter plots of Calcein intensity against GFP intensity on the right-side are where GFP+ and Calcein+ EVs can be gated for (gate for GFP+ and Calcein- is also shown, as a distinct population could be detected in the Tg + Calcein samples). (A) Scatter plot representation of sample without EVs from larvae (No Fish) and labelled using Calcein. (B) Scatter plot representation of EVs sampled from non-Tg larvae and labelled using Calcein. (C) Scatter plot representation of EVs sampled from Tg(kdrl:mCherry-CAAX); Tg(actin:mem-GFP) larvae and labelled using Calcein. (D) Scatter plot representation of EVs sampled from Tg(kdrl:mCherry-CAAX); Tg(actin:mem-GFP) larvae without Calcein labelling.*

Finally, a sample was prepared that included EVs isolated from Tg fish which were dyed with Calcein and treated with detergent. The initial steps of this process give positive signals in the predetermined gates for Calcein, mCherry and GFP (**Figure 4.8**A). However, the additional detergent treatment then degrades any lipid structures including membrane bound vesicles (**Figure 4.8**B). The scatterplot for the detergent treated sample still demonstrates events that trigger below the thresholds set, essentially leaving nothing but noise, with a similar scatterplot signature to the previous sample with no larval zebrafish included, only buffers and Calcein (**Figure 4.7**A).
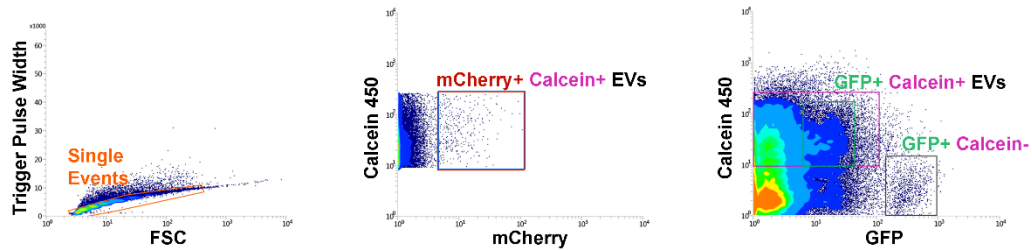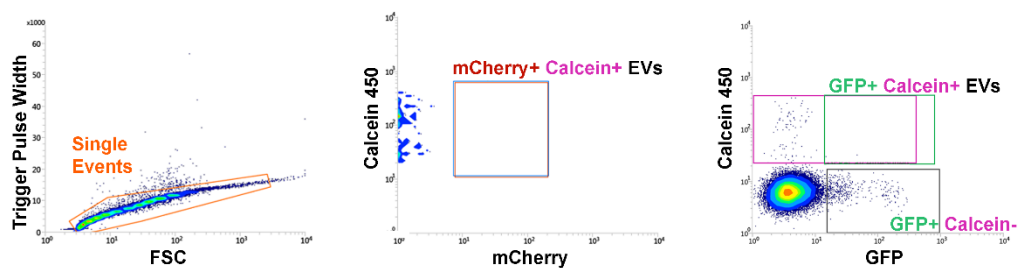
Figure 4.8. EV Detection by Modified FC - Detergent Treatment. (A) Scatter plot representation of EVs sampled from Tg(kdrl:mCherry-CAAX); Tg(actin:mem-GFP) larvae and labelled using Calcein. (B) Scatter plot representation of EVs sampled from Tg(kdrl:mCherry-CAAX); Tg(actin:mem-GFP) larvae and labelled using Calcein followed by detergent treatment.

4.4.2 Results

Once we had confidence in the system, we were able to begin assessing EV injury responses. With relevant literature in mammalian systems highlighting 24 hours as a timepoint where EV concentration peaks in the peripheral circulation post experimental MI (176), we focused on 6, 12, 18 and 24 hpi as our initial timepoints to investigate EV number (**Figure 4.9**). Our *in vivo* imaging data was acquired with the assumption that an EV-based response would occur within shorter timescales in the developing zebrafish when compared to mammalian models, but the insignificant results obtain prompted later timepoints to be considered. The results revealed a significant difference in means and a significant difference specifically between 18 and 24 hpi.
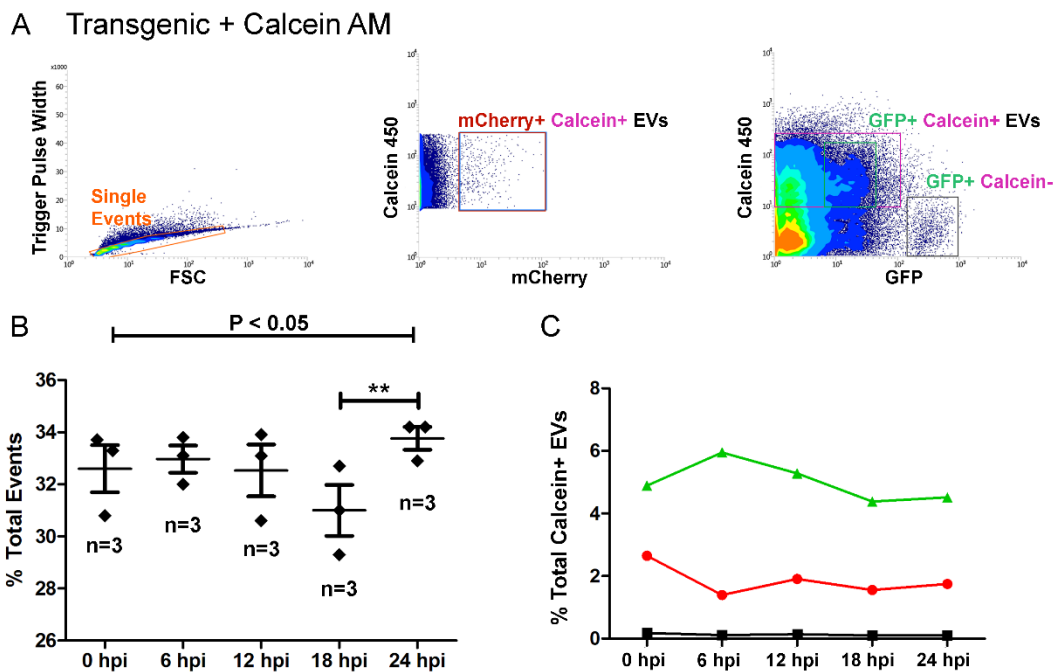
Figure 4.9. FC Assessment of EV Numbers Resulting from Cardiac Injury in Larval Zebrafish. (A) Final gates set for Calcein+/mCherry+ EVs and Calcein+/GFP+ EVs. (B) Total number of EVs determined by Calcein+ labelling over timepoints post-cardiac injury, each data point consists of EVs prepared from 16 pooled larvae. (C) EVs derived from actin+ cells (green), EC-EVs (red) and double positive EVs (black) are shown as a percentage of total calcein+ EVs. For statistical analysis in B, a repeated-measures ANOVA test was performed, followed by Bonferroni's Multiple Comparisons test. The means across the five groups differed significantly from each other with $F(4,2) = 6.87$, $R^2 = 0.775$, $p = 0.011$. Multiple comparisons revealed a significant difference between 18 and 24 hpi with $p < 0.01$, the difference was insignificant for all other comparisons.

Being able to assess EV numbers by FC presents the opportunity to isolate specific EV populations by FACS methods. Initially EVs isolated by size and density where imaged using the HyVolution system as an initial assessment, this method revealed labelled EVs to be scarce in a raw preparation but using 60 nm fluorescent beads gave some perspective on relative sizes (**Figure 4.10**A). Trialling FACS provided a more concentrated example and some EVs remained intact after FACS, as assessed by TIRF microscopy (**Figure 4.10**B) (see section 2.7).
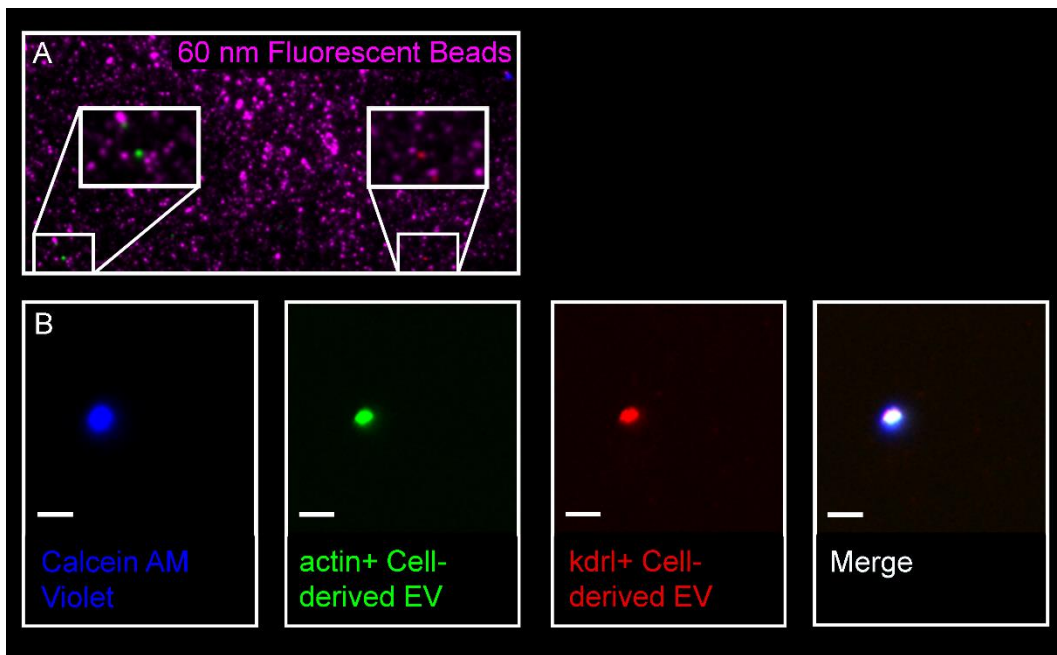
Figure 4.10 TIRF Imaging of FACS Isolated EV. *(A) EVs isolated by density and size not by fluorescence, including 60 nm fluorescent beads for comparison. (B) FACS for Calcein+, GFP+ and mCherry+ EVs allows for the isolation of intact EVs derived from actin+ cells and ECs. Scale bar = 5 µm*

Discussion

EVs represent a novel intercellular communication mechanism that offer huge potential as disease biomarkers and therapeutic delivery systems. However, in order to realise their full potential, further *in vivo* data on EV dynamics is required. During this project, endogenous EVs of known cellular origin were observed *in vivo* using Tg larval zebrafish. Firstly, populations of EC-EVs were observed in the peripheral circulation passing through the dorsal aorta and caudal vein of the CHT (**Figure 3.5**, **Figure 4.1** and **Figure 4.2**). Novel *in vivo* behaviours were observed, such as the EVs seen loosely interacting with the vascular endothelium , showing a 'rolling' like motion across the surface of ECs lining the vessel (**Figure 3.5**; Movie 2). Secondly, CM-EVs were detected in the PF surrounding the heart and filling the pericardial space (**Figure 3.10**; Movie 6). These EVs were often observed moving stochastically, but this could easily be an artefact of imaging a single optical slice through a large volume, sometimes they appeared to be influenced, as would be expected, by the hemodynamic 'streams' generated by the beating heart. CM-EVs were also observed interacting with the pericardial wall (**Figure 3.11**; Movie 7), either with the cells themselves or associated ECM. Thirdly, techniques were established to extract and isolate EVs from whole Tg larval zebrafish and enumerated by a modified FC setup (**Figure 4.9**). This presents the potential for EVs to be assessed for dynamics *in vivo* using fluorescence microscopy and then with this Tg system the same EV populations can be more systematically characterised *ex vivo* using FC. Finally, the number of cardiovascular EVs were assessed at different time-points post laser induced cardiac injury in larval zebrafish (see Chapter 4:). The initial assessment of the EV response did not reveal significant changes in cell-type specific EVs following injury, although there appeared to be a significant increase in total EV numbers between 18 hpi and 24 hpi (**Figure 4.9**), which warrants further investigation.

EV based intercellular communication and its importance in physiological/pathophysiological processes is becoming well established; this is true across systems but also specifically within cardiovascular biology. This evidence is predominantly the result of cell culture-based studies, with limited results from *in vivo* experiments. The subcellular size of EVs is the primary concern for *in vivo* studies, tracking EVs within disparate tissue and extracellular settings is particularly challenging and demands certain standards are met.

Effective labelling of EVs is a perquisite for visualisation and needs to be both specific and capable of providing sufficient signal to allow for their detection. The prenylated-fluorophore reporter systems used in this study not only meets this standard but also allows for quantification of these EVs *in vivo* and *ex vivo*.

An often-cited challenge in EV research is the difficulty in defining the cellular origin of EVs and their cargo. The system characterised here provides a new standard, where the origin of EVs is clearly marked and can be immediately assessed *in vivo* and *ex vivo*. Demonstrating the feasibility of this system for the stated purpose opens many potential avenues for future study, where theoretically any cell type can be labelled with the methods described and the EV production and behaviour assessed.

5.1 In Vivo Imaging of Extracellular Vesicle Behaviours

The real strength of the translucent larval zebrafish model system is the ability to carry out live cellular and sub-cellular level time-lapse imaging of EV dynamics *in vivo*. Nuances in behaviour can be assessed in detail and behaviours observed that might be unlikely or unable to occur *in vitro*. Characterising release, uptake and function (see section 1.2.4) *in vivo* proved a real challenge in the timescale of this study, but the imaging experiments presented highlight the feasibility of meeting this challenge in the future.

5.1.1 Endothelial Cell-Derived Extracellular Vesicles Rolling Interactions with Endothelial Cells

One *in vivo* behaviour identified during the characterisation of endothelial cell-derived EVs during this study was the observation that EC-EVs were often seen 'rolling' along, and potentially interacting with, the ECs lining the blood vessels (**Figure 3.5**). This process was visually akin to the well characterised process of leukocyte rolling prior to extravasation out of the vessel into the surrounding tissue (252, 253), in fact this rolling process is a key step for leukocytes exiting the circulation and crossing the vascular endothelium (85, 254). It has been shown that leukocytes require the selectin family of adhesion molecules for this rolling behaviour to be initiated (255, 256), with specific sequential interactions with P- and L-selectin key to rolling and arrest *in vivo* (257). Activation through chemokine signalling and integrins on the surface of the leukocyte is then thought

to be responsible for stabilising the connection for complete arrest (258). Other aspects such as the hemodynamic forces in play and the shear stress the leukocyte is exposed to are also thought to play key roles, in concert with signalling and receptor based interactions (253, 259). Future work will be required to determine if EVs utilise similar mechanisms to interact with ECs and the functional consequences of these interactions.

Additionally, platelets also use surface receptors to interact with the vascular endothelium and other platelets when forming aggregations (260). The von Willebrand factor receptor (261, 262), glycoprotein Ibα (GPIbα) (263), and a signalling collagen receptor, GPVI (264), are involved in the adhesion of platelets. Initiating contact to exposed subendothelial collagen requires the binding of GPIbα on the membrane surface of platelets to immobilised von Willebrand factor (265), this interaction results in a rolling effect along the endothelium. The decrease in velocity allows GPVI to bind collagen (266). This is particularly interesting, as plasma EVs isolated from patients following MI were also found with increased expression of GPIbα (267). Other studies using proteomics approaches combined with gene ontology methods have revealed EVs to contain proteins involved broadly in the binding and rolling process across cell types (268, 269). This study is the first documented observation of this potentially important EV behaviour *in vivo*.

5.1.2 Endothelial Cell-Derived Extracellular Vesicles Released via Filopodial-Like Protrusion

When using the Tg(*kdrl:mCherry-CAAX*) endothelial Tg reporter system, potential EV release from the tip of a filopodial-like projection was observed in the CHT venous region of a 3 dpf larval fish (**Figure 3.6**). Similar processes have previously been documented transporting EVs in drosophila (77) and aiding uptake of EVs by human primary fibroblasts (270). Revealing this dynamic behaviour *in vivo* may begin to reinforce a novel mechanism for EV release beyond direct shedding from the plasma membrane and exocytosis. Further documentation and attempts to inhibit the process by targeting specific molecular components, could allow the functional relevance of this process to be fully elucidated.

5.1.3 Cardiomyocyte-Derived Extracellular Vesicles Interactions with the Pericardium

The pericardium is exposed to rhythmic changes in flow and pressure forces generated through the PF, as a result of the beating heart as well as longer term changes through developmental stages (271). These processes have been shown to play a role in epicardial development in zebrafish, with proepicardial cell clusters that originate on the pericardium identified as the origin for this cell layer, with flow dynamics dictating the attachment sites for these proepicardial cells as they are released into the pericardial space (271). As these are the only studies so far focussed on the pericardial space and the currents generated within the PF, aspects from this study may help to dissect the role hydrodynamic forces play in EV release and how they will influence behaviour and eventual arrest sites. It would also be interesting to use Tg zebrafish with the epicardial cells fluorescently labelled, in combination with *Tg(ET37:GFP)* labelled fibroblasts, to determine the recipient cells for these CM-EVs. To really understand the interactions presented here and visualised by light microscopy, the next essential step would be to assess the ultrastructural picture by EM (see section 1.2.5.2.3.1). The strengths of optical imaging in the zebrafish can be combined most effectively with EM when the fully integrated methods of correlative light electron microscopy are used (Hosseini et al., 2014). This would allow putative EVs associating with the pericardial wall to be identified by fluorescent signal, the larval zebrafish could then be fixed as rapidly as possible and the region identified by light microscopy can then be investigated by EM (Hosseini et al., 2014).

5.1.4 Complementary Transgenic Approaches

Identifying the cells that CMs and ECs might be communicating with could also be approached using the Cre/Lox system (236, 272). This system allows the fate of EVs to be determined by colour switching in recipient cells with the switch mediated by Cre mRNA overexpression in the producing cell and this mRNA packaged by an unknown mechanism into the EVs produced by that cell. These EVs are then thought to travel to their endogenous targets and the mRNA is translated within any recipient cells, the Cre can then cut at LoxP sites in a ubiquitously expressed floxed colour switch transgene, which removes the first fluorophore and a stop codon sequence and allows the sequential fluorophore to be expressed, switching the colour of the recipient cell. Initially this system was

demonstrated to assess tumour-derived EVs in mouse (236), but has since been used to assess what the authors determined to be contact-dependent cytoplasmic transfer between macrophages and tumour cells in zebrafish (273). Some caution would be necessary if adopting this system, firstly it gives a readout of mRNA transfer only, as the authors do not find the effects observed to be the result of protein transfer, as Cre protein levels were beyond detection (236). mRNA is one of many possible cargoes that can impact the physiology of a recipient cell, so the system is limited in this sense. It is also true that the mechanisms responsible for Cre mRNA transfer or indeed loading are unknown and that the Cre/LoxP system is considered 'leaky' in various applications (273, 274), making well thought-out control experiments an imperative as well as careful selection of appropriate promoters. The benefits and obstacles presented in using this system to assess functional transfer of EV cargo are thoroughly explored in an International Society of Extracellular Vesicles position paper (94).

To further explore the nature of the EVs being detected *in vivo* the presented approaches in this study could be combined with markers that might reveal intracellular origin and suggest something of the mechanism for their biogenesis. For example, there are three published Tg zebrafish lines that directly label Rab5, Rab7 and Rab11 by way of GFP-fusion expression. Presence of Rab5, Rab7 or Rab11 -GFP fluorescent signal colocalised with the EVs as identified in this study, would suggest early endosomal, late endosomal or recycling endosomal origins respectively. Each of these Rab proteins have been highlighted in the literature as being components within EV isolates and have been implicated in EV biogenesis (see section 1.2.2.1), but their mechanistic involvement *in vivo* has yet to be elucidated. For each of the Rab proteins there is also a constitutive active and a dominant-negative Tg line that can be controlled via cell-type specific promoters to potentially allow *in vivo* function of these EVs to be probed (Clark et al., 2011). This would contribute towards a comprehensive picture *in vivo*, where an understanding of intracellular and cellular origin can be gained by using stable transgenic fluorescent labelling of endogenous EVs, allowing a depth of knowledge to be obtained whilst observing native EV dynamics.

5.2 Ex Vivo Assessments

During this project EVs isolated from whole larval zebrafish were assessed using a modified FC setup (**Figure 4.9**). The results recorded at different timepoints post cardiac injury revealed large amounts of variability within groups, which meant there was no significant differences observed across most timepoints (**Figure 4.9**). Aside from increasing experimental replicates, a few technical matters may be influential in obfuscating the data. Firstly, the modified FC setup is still only capable of recording a larger subset of EVs, there are further modifications that could be made if the machine was dedicated to EV experiments (142) and improvements on the technology are continuously being made available (275-277). Another important aspect is the labelling approach, although it appears effective, we cannot be sure of the labelling efficiencies nor can we be sure of the consistency with which EVs are being labelled. This issue could possibly be circumvented to some degree, by being sure of the number of insertions of the Tg construct into the genome and using only heterozygous Tg fish to introduce more consistency in potential labelling. Lastly, there will be inherent variability in the laser-induced cardiac injury method, because of user inexperience. Inconsistency in the amount of damaged tissue would likely lead to variability in EV numbers. This issue could be addressed in a few ways, including the use of more controlled laser injuries, as with the use of more sophisticated confocal setups and methods used to photoconvert single cells, but with higher laser power needed to induce cell death.

5.2.1 Assessment of Extracellular Vesicle-Based Cardiac Injury Response in Adult Zebrafish

Using FC to assess changes in EV profile resulting from cardiac injury was successfully demonstrated using larval zebrafish (**Figure 4.9**). Samples were necessarily pooled to collect sufficient numbers of EVs for analysis and this was especially necessary for the EC-EVs, which were much fewer in number compared with Calcein+ EVs or total EV numbers. In fact, CM-EVs were indistinguishable from background noise when extracted from larval zebrafish and assessed by FC. A future step that would avoid some of the issues encountered in this study, would be to carry out similar experiments using adult zebrafish. This should also allow EV profile changes to be assessed in individuals, where specific changes will not be lost in the mean result given with

pooled samples. Further, individual organs/tissues could be sampled from the adult zebrafish to reveal specific differences pertinent to that sample (e.g. in the heart following cardiac injury) and perhaps highlight signalling events to remote sites such as the spleen (176). Working with adult zebrafish would also allow regenerative processes to be probed, as separated from often indistinguishable developmental processes in larval zebrafish. The cryoinjury method would be used for cardiac injury (278), a much more relevant disease model system, where *ex vivo* assessments could be aligned with defined phases of repair and regeneration in an attempt to reveal associations that may highlight functional significance and warrant further investigation.

5.2.2 Ultrastructural Assessment Using Electron Microscopy

The absolute size of the EVs characterised in this study are obscured by the light-based detection methods employed for *in vivo* imaging, to appreciate the ultrastructure of these EVs would require the use of EM (see section 1.2.5.2.3.1). To achieve this, the most straightforward approach would be to extract and isolate EVs using the methods described previously (section 2.5), once isolated different whole mount preparations would allow for either TEM (Théry et al., 2006) or cryo-electron microscopy (Brisson et al., 2017). EM could also be used in combination with immunogold labelling for EV markers such as CD63 (see section 1.2.5.2.2.1) to highlight specific EV characteristics and reveal details of intracellular origins (Brisson et al., 2017). Combining the model system presented in this study with EM analysis would allow us to further assess EVs from a known cellular origin, a challenge that is often difficult to overcome.

5.3 Summary

During this study, using a transgenically expressed ubiquitous extracellular labelling approach it was possible to label and live-image endogenously produced EVs *in vivo*. Further, endogenously produced CM-EVs were live-imaged *in vivo* within the pericardial space. CM-EVs were seen moving within the pericardial fluid and associating statically with the pericardial wall, either with a so far unidentified cell type or associated extracellular matrix. Live-imaging of endogenously produced EC-EVs being transported by the peripheral circulation *in vivo* was also performed, with interesting interactions between EC-EVs and EC filopodial-like projections which perhaps hint at a novel release mechanism. EVs

were extracted globally from whole larvae and then isolated using a non-specific method based on size and density and the EV sample was then quantitatively analysed *ex vivo* based on fluorescence using FC. Finally, FACS can be used to isolate specific populations of EV based on their fluorescence and therefore cellular origin presenting opportunities for cardiovascular EV cargo analyses in the future.

Appendix

Figure Legends for Movies (supplied on USB memory stick)

Movie 1. Live Imaging Sequence of Larval Zebrafish Peripheral Circulation.
Brightfield image sequence (1000 frames = 39.96 seconds) through the centre of the DA of a 3 dpf larval zebrafish, showing blood cells passing through the vessel. Taken from the 2-minute movies used for data analysis. Scale bar = 10 µm.

Movie 2. Live Imaging Sequence of EC-EVs in the Peripheral Circulation.
Image sequence (64 frames = 1.26 seconds) of a single EV rolling along the ECs lining the DA of a 3 dpf Tg(kdrl:mCherry-CAAX) larval zebrafish. The fluorescent channel and brightfield combined are shown alongside the fluorescent channel alone. Scale bar = 10 µm.

Movie 3. Live Imaging Sequence of EC-EV Release into the CV. *Image sequence (121 frames = 4.8 seconds) of a single EV at the tip of a filopodial-like protrusion and then being released into the peripheral circulation of a 3 dpf Tg(kdrl:mCherry-CAAX) larval zebrafish. Gamma adjustments made as described in section 2.4. Scale bar = 5 µm.*

Movie 4. Defining the Pericardial Space in the Larval Zebrafish. *Fluorescent 3-D reconstruction (Imaris) of 100 stacked images through the pericardial region of a 3 dpf Tg(myl7:GFP) larval zebrafish. The pericardial space marked by dextran is in grey. Scale bar = defined in movie and changes with digital zoom.*

Movie 5. Live Imaging Sequence of A5-EVs in the Pericardial Space. *Image sequence of three EVs as they come into focus in the pericardial space of a 3 dpf Tg(TBP:G4m);(UAS:secA5-YFP) larval zebrafish. Scale bar = 5 µm.*

Movie 6. Live Imaging Sequence of CM-EVs in the Pericardial Space. *Image sequence (441 frames = 8.8 seconds) of a CM-EV moving in the pericardial space of a 4 dpf Tg(myl7:HRAS-mCherry) larval zebrafish. The fluorescent channel and brightfield combined are shown alongside the fluorescent channel alone. Gamma adjustments made as described in section 2.4. Scale bar = 10 µm.*

Movie 7. Visualising CM-EVs Associating with the Pericardial Wall.
Fluorescent 3-D reconstruction (Imaris) of 100 stacked images through the pericardial region of a 3dpf Tg(myl7:HRAS-mCherry);Tg(actin:mem-GFP) larval zebrafish. The near-ubiquitous expression of the actin expressing cells are pseudo-coloured grey. Scale bar = defined in movie and changes with digital zoom.

Bibliography

1.   Ross R. The pathogenesis of atherosclerosis: a perspective for the 1990s. Nature. 1993;362(6423):801.
2.   Davies MJ, Thomas AC. Plaque fissuring--the cause of acute myocardial infarction, sudden ischaemic death, and crescendo angina. British heart journal. 1985;53(4):363.
3.   Ambrose JA, Singh M. Pathophysiology of coronary artery disease leading to acute coronary syndromes. F1000prime reports. 2015;7.
4.   Kannel WB, Cupples LA, D'Agostino RB. Sudden death risk in overt coronary heart disease: the Framingham Study. American heart journal. 1987;113(3):799-804.
5.   Whelan RS, Kaplinskiy V, Kitsis RN. Cell death in the pathogenesis of heart disease: mechanisms and significance. Annual review of physiology. 2010;72:19-44.
6.   Zhang Y, Kanter EM, Yamada KA. Remodeling of cardiac fibroblasts following myocardial infarction results in increased gap junction intercellular communication. Cardiovascular Pathology. 2010;19(6):e233-e40.
7.   Emanueli C, Shearn AI, Angelini GD, Sahoo S. Exosomes and exosomal miRNAs in cardiovascular protection and repair. Vascular pharmacology. 2015;71:24-30.
8.   Schorey JS, Cheng Y, Singh PP, Smith VL. Exosomes and other extracellular vesicles in host–pathogen interactions. EMBO reports. 2015;16(1):24-43.
9.   Deatherage BL, Cookson BT. Membrane vesicle release in bacteria, eukaryotes, and archaea: a conserved yet underappreciated aspect of microbial life. Infection and immunity. 2012;80(6):1948-57.
10.   Robinson DG, Ding Y, Jiang L. Unconventional protein secretion in plants: a critical assessment. Protoplasma. 2016;253(1):31-43.
11.   Crawford N. The Presence of Contractile Proteins in Platelet Microparticles Isolated from Human and Animal Platelet-free Plasma. British journal of haematology. 1971;21(1):53-69.
12.   Beltrami C, Besnier M, Shantikumar S, Shearn AI, Rajakaruna C, Laftah A, et al. Human pericardial fluid contains exosomes enriched with cardiovascular-expressed microRNAs and promotes therapeutic angiogenesis. Molecular Therapy. 2017;25(3):679-93.
13.   Rilla K, Mustonen A-M, Arasu UT, Härkönen K, Matilainen J, Nieminen P. Extracellular vesicles are integral and functional components of the extracellular matrix. Matrix Biology. 2017.
14.   Colombo M, Raposo G, Théry C. Biogenesis, secretion, and intercellular interactions of exosomes and other extracellular vesicles. Annual review of cell and developmental biology. 2014;30:255-89.
15.   Das S, Halushka MK. Extracellular vesicle microRNA transfer in cardiovascular disease. Cardiovascular pathology. 2015;24(4):199-206.
16.   Boulanger CM, Loyer X, Rautou P-E, Amabile N. Extracellular vesicles in coronary artery disease. Nature Reviews Cardiology. 2017.
17.   Yáñez-Mó M, Siljander PR-M, Andreu Z, Zavec AB, Borràs FE, Buzas EI, et al. Biological properties of extracellular vesicles and their physiological functions. Journal of extracellular vesicles. 2015;4.
18.   Klumperman J, Raposo G. The complex ultrastructure of the endolysosomal system. Cold Spring Harbor perspectives in biology. 2014;6(10):a016857.
19.   Doherty GJ, McMahon HT. Mechanisms of endocytosis. Annual review of biochemistry. 2009;78:857-902.

20.   Denzer K, Kleijmeer MJ, Heijnen H, Stoorvogel W, Geuze HJ. Exosome: from internal vesicle of the multivesicular body to intercellular signaling device. Journal of cell science. 2000;113(19):3365-74.

21.   van Niel G, D'Angelo G, Raposo G. Shedding light on the cell biology of extracellular vesicles. Nature Reviews Molecular Cell Biology. 2018.

22.   Rojas R, van Vlijmen T, Mardones GA, Prabhu Y, Rojas AL, Mohammed S, et al. Regulation of retromer recruitment to endosomes by sequential action of Rab5 and Rab7. The Journal of cell biology. 2008;183(3):513-26.

23.   Hanson PI, Cashikar A. Multivesicular body morphogenesis. Annual review of cell and developmental biology. 2012;28:337-62.

24.   Stuffers S, Sem Wegner C, Stenmark H, Brech A. Multivesicular endosome biogenesis in the absence of ESCRTs. Traffic. 2009;10(7):925-37.

25.   Trajkovic K, Hsu C, Chiantia S, Rajendran L, Wenzel D, Wieland F, et al. Ceramide triggers budding of exosome vesicles into multivesicular endosomes. Science. 2008;319(5867):1244-7.

26.   Ghossoub R, Lembo F, Rubio A, Gaillard CB, Bouchet J, Vitale N, et al. Syntenin-ALIX exosome biogenesis and budding into multivesicular bodies are controlled by ARF6 and PLD2. Nature communications. 2014;5:3477.

27.   Stoorvogel W, Strous GJ, Geuze HJ, Oorschot V, Schwartzt AL. Late endosomes derive from early endosomes by maturation. Cell. 1991;65(3):417-27.

28.   Luzio JP, Pryor PR, Bright NA. Lysosomes: fusion and function. Nature reviews Molecular cell biology. 2007;8(8):622-32.

29.   Hannah MJ, Williams R, Kaur J, Hewlett LJ, Cutler DF, editors. Biogenesis of Weibel–Palade bodies. Seminars in cell & developmental biology; 2002: Elsevier.

30.   Rondaij MG, Bierings R, Kragt A, van Mourik JA, Voorberg J. Dynamics and plasticity of Weibel-Palade bodies in endothelial cells. Arteriosclerosis, thrombosis, and vascular biology. 2006;26(5):1002-7.

31.   Cieutat A-M, Lobel P, August J, Kjeldsen L, Sengeløv H, Borregaard N, et al. Azurophilic granules of human neutrophilic leukocytes are deficient in lysosome-associated membrane proteins but retain the mannose 6-phosphate recognition marker. Blood. 1998;91(3):1044-58.

32.   Pan B-T, Teng K, Wu C, Adam M, Johnstone RM. Electron microscopic evidence for externalization of the transferrin receptor in vesicular form in sheep reticulocytes. The Journal of cell biology. 1985;101(3):942-8.

33.   Johnstone RM, Adam M, Hammond J, Orr L, Turbide C. Vesicle formation during reticulocyte maturation. Association of plasma membrane activities with released vesicles (exosomes). Journal of Biological Chemistry. 1987;262(19):9412-20.

34.   Vidal M, Sainte-Marie J, Philippot JR, Bienvenue A. Asymmetric distribution of phospholipids in the membrane of vesicles released during in vitro maturation of guinea pig reticulocytes: evidence precluding a role for "aminophospholipid translocase". Journal of cellular physiology. 1989;140(3):455-62.

35.   Raposo G, Nijman HW, Stoorvogel W, Liejendekker R, Harding CV, Melief CJ, et al. B lymphocytes secrete antigen-presenting vesicles. Journal of Experimental Medicine. 1996;183(3):1161-72.

36.   Jaiswal JK, Andrews NW, Simon SM. Membrane proximal lysosomes are the major vesicles responsible for calcium-dependent exocytosis in nonsecretory cells. J Cell Biol. 2002;159(4):625-35.

37.   Zerial M, Stenmark HJCoicb. Rab GTPases in vesicular transport. 1993;5(4):613-20.

38.   Théry C, Boussac M, Véron P, Ricciardi-Castagnoli P, Raposo G, Garin J, et al. Proteomic analysis of dendritic cell-derived exosomes: a secreted

subcellular compartment distinct from apoptotic vesicles. The Journal of Immunology. 2001;166(12):7309-18.

39. Ostrowski M, Carmo NB, Krumeich S, Fanget I, Raposo G, Savina A, et al. Rab27a and Rab27b control different steps of the exosome secretion pathway. 2010;12(1):19.

40. Zerial M, McBride HJNrMcb. Rab proteins as membrane organizers. 2001;2(2):107.

41. Vidal M, Stahl PJEjocb. The small GTP-binding proteins Rab4 and ARF are associated with released exosomes during reticulocyte maturation. 1993;60(2):261-7.

42. Logozzi M, De Milito A, Lugini L, Borghi M, Calabro L, Spada M, et al. High levels of exosomes expressing CD63 and caveolin-1 in plasma of melanoma patients. 2009;4(4):e5219.

43. Baietti MF, Zhang Z, Mortier E, Melchior A, Degeest G, Geeraerts A, et al. Syndecan–syntenin–ALIX regulates the biogenesis of exosomes. 2012;14(7):677.

44. Chavrier P, Parton RG, Hauri HP, Simons K, Zerial MJC. Localization of low molecular weight GTP binding proteins to exocytic and endocytic compartments. 1990;62(2):317-29.

45. Song P, Trajkovic K, Tsunemi T, Krainc DJJoN. Parkin modulates endosomal organization and function of the endo-lysosomal pathway. 2016;36(8):2425-37.

46. Savina A, Vidal M, Colombo MIJJocs. The exosome pathway in K562 cells is regulated by Rab11. 2002;115(12):2505-15.

47. Beckett K, Monier S, Palmer L, Alexandre C, Green H, Bonneil E, et al. Drosophila S2 cells secrete wingless on exosome-like vesicles but the wingless gradient forms independently of exosomes. Traffic. 2013;14(1):82-96.

48. Koles K, Nunnari J, Korkut C, Barria R, Brewer C, Li Y, et al. Mechanism of evenness interrupted (Evi)-exosome release at synaptic boutons. 2012;287(20):16820-34.

49. Hurley JH. ESCRTs are everywhere. The EMBO journal. 2015:e201592484.

50. Henne WM, Buchkovich NJ, Emr SD. The ESCRT pathway. Developmental cell. 2011;21(1):77-91.

51. Wehman AM, Poggioli C, Schweinsberg P, Grant BD, Nance J. The P4-ATPase TAT-5 inhibits the budding of extracellular vesicles in C. elegans embryos. Current Biology. 2011;21(23):1951-9.

52. Morris RJ. Ionic control of the metastable inner leaflet of the plasma membrane: Fusions natural and artefactual. FEBS letters. 2010;584(9):1665-9.

53. Akers JC, Gonda D, Kim R, Carter BS, Chen CC. Biogenesis of extracellular vesicles (EV): exosomes, microvesicles, retrovirus-like vesicles, and apoptotic bodies. Journal of neuro-oncology. 2013;113(1):1.

54. Hugel B, Martínez MC, Kunzelmann C, Freyssinet J-M. Membrane microparticles: two sides of the coin. Physiology. 2005;20(1):22-7.

55. Al-Nedawi K, Meehan B, Micallef J, Lhotak V, May L, Guha A, et al. Intercellular transfer of the oncogenic receptor EGFRvIII by microvesicles derived from tumour cells. Nature cell biology. 2008;10(5):619.

56. Piccin A, Murphy WG, Smith OP. Circulating microparticles: pathophysiology and clinical implications. Blood reviews. 2007;21(3):157-71.

57. Bolukbasi MF, Mizrak A, Ozdener GB, Madlener S, Ströbel T, Erkan EP, et al. miR-1289 and "Zipcode"-like sequence enrich mRNAs in microvesicles. Molecular Therapy-Nucleic Acids. 2012;1.

58. Fang Y, Wu N, Gan X, Yan W, Morrell JC, Gould SJ. Higher-order oligomerization targets plasma membrane proteins and HIV gag to exosomes. PLoS biology. 2007;5(6):e158.

59.	Shen B, Fang Y, Wu N, Gould SJ. Biogenesis of the posterior pole is mediated by the exosome/microvesicle protein-sorting pathway. Journal of Biological Chemistry. 2011;286(51):44162-76.

60.	Yang J-M, Gould SJ. The cis-acting signals that target proteins to exosomes and microvesicles. Portland Press Limited; 2013.

61.	D'Souza-Schorey C, Chavrier P. ARF proteins: roles in membrane traffic and beyond. Nature reviews Molecular cell biology. 2006;7(5):347.

62.	Muralidharan-Chari V, Clancy J, Plou C, Romao M, Chavrier P, Raposo G, et al. ARF6-regulated shedding of tumor cell-derived plasma membrane microvesicles. Current Biology. 2009;19(22):1875-85.

63.	Wang T, Gilkes DM, Takano N, Xiang L, Luo W, Bishop CJ, et al. Hypoxia-inducible factors and RAB22A mediate formation of microvesicles that stimulate breast cancer invasion and metastasis. Proceedings of the National Academy of Sciences. 2014;111(31):E3234-E42.

64.	Tamai K, Tanaka N, Nakano T, Kakazu E, Kondo Y, Inoue J, et al. Exosome secretion of dendritic cells is regulated by Hrs, an ESCRT-0 protein. Biochemical and biophysical research communications. 2010;399(3):384-90.

65.	Cocucci E, Racchetti G, Meldolesi J. Shedding microvesicles: artefacts no more. Trends in cell biology. 2009;19(2):43-51.

66.	Gradilla A-C, Sanchez-Hernandez D, Brunt L, Scholpp S. From top to bottom: Cell polarity in Hedgehog and Wnt trafficking. BMC biology. 2018;16(1):37.

67.	Lewis PM, Dunn MP, McMahon JA, Logan M, Martin JF, St-Jacques B, et al. Cholesterol modification of sonic hedgehog is required for long-range signaling activity and effective modulation of signaling by Ptc1. Cell. 2001;105(5):599-612.

68.	Steinhauer J, Treisman JE. Lipid-modified morphogens: functions of fats. Current opinion in genetics & development. 2009;19(4):308-14.

69.	Willert K, Nusse R. Wnt proteins. Cold Spring Harbor perspectives in biology. 2012;4(9):a007864.

70.	Port F, Basler K. Wnt trafficking: new insights into Wnt maturation, secretion and spreading. Traffic. 2010;11(10):1265-71.

71.	Ramírez-Weber F-A, Kornberg TB. Cytonemes: cellular processes that project to the principal signaling center in Drosophila imaginal discs. Cell. 1999;97(5):599-607.

72.	Kornberg TB, Roy S. Cytonemes as specialized signaling filopodia. Development. 2014;141(4):729-36.

73.	Stanganello E, Hagemann AI, Mattes B, Sinner C, Meyen D, Weber S, et al. Filopodia-based Wnt transport during vertebrate tissue patterning. Nature communications. 2015;6:5846.

74.	Bischoff M, Gradilla A-C, Seijo I, Andrés G, Rodríguez-Navas C, González-Méndez L, et al. Cytonemes are required for the establishment of a normal Hedgehog morphogen gradient in Drosophila epithelia. Nature cell biology. 2013;15(11):1269.

75.	Chen W, Huang H, Hatori R, Kornberg TB. Essential basal cytonemes take up Hedgehog in the Drosophila wing imaginal disc. Development. 2017;144(17):3134-44.

76.	González-Méndez L, Seijo-Barandiarán I, Guerrero I. Cytoneme-mediated cell-cell contacts for Hedgehog reception. eLife. 2017;6.

77.	Gradilla A-C, González E, Seijo I, Andrés G, Bischoff M, González-Mendez L, et al. Exosomes as Hedgehog carriers in cytoneme-mediated transport and secretion. Nature communications. 2014;5:5649.

78.	Menck K, Klemm F, Gross JC, Pukrop T, Wenzel D, Binder C. Induction and transport of Wnt 5a during macrophage-induced malignant invasion is mediated by two types of extracellular vesicles. Oncotarget. 2013;4(11):2057.

79. Gross JC, Chaudhary V, Bartscherer K, Boutros M. Active Wnt proteins are secreted on exosomes. Nature cell biology. 2012;14(10):1036.

80. Korkut C, Ataman B, Ramachandran P, Ashley J, Barria R, Gherbesi N, et al. Trans-synaptic transmission of vesicular Wnt signals through Evi/Wntless. Cell. 2009;139(2):393-404.

81. Gradilla A-C, Simon E, Aguilar G, Guerrero I. From intra-to extracellular vesicles: extracellular vesicles in developmental signalling. Essays in biochemistry. 2018;62(2):215-23.

82. Ozhan G, Weidinger G. Wnt/β-catenin signaling in heart regeneration. Cell regeneration. 2015;4(1):3.

83. Kerr JF, Wyllie AH, Currie AR. Apoptosis: a basic biological phenomenon with wide-ranging implications in tissue kinetics. British journal of cancer. 1972;26(4):239.

84. Elmore S. Apoptosis: a review of programmed cell death. Toxicologic pathology. 2007;35(4):495-516.

85. Bratton DL, Fadok VA, Richter DA, Kailey JM, Guthrie LA, Henson PM. Appearance of phosphatidylserine on apoptotic cells requires calcium-mediated nonspecific flip-flop and is enhanced by loss of the aminophospholipid translocase. Journal of Biological Chemistry. 1997;272(42):26159-65.

86. Hanayama R, Tanaka M, Miwa K, Shinohara A, Iwamatsu A, Nagata S. Identification of a factor that links apoptotic cells to phagocytes. Nature. 2002;417(6885):182-7.

87. Arslan F, Lai RC, Smeets MB, Akeroyd L, Choo A, Aguor EN, et al. Mesenchymal stem cell-derived exosomes increase ATP levels, decrease oxidative stress and activate PI3K/Akt pathway to enhance myocardial viability and prevent adverse remodeling after myocardial ischemia/reperfusion injury. Stem cell research. 2013;10(3):301-12.

88. Hervera A, De Virgiliis F, Palmisano I, Zhou L, Tantardini E, Kong G, et al. Reactive oxygen species regulate axonal regeneration through the release of exosomal NADPH oxidase 2 complexes into injured axons. Nature cell biology. 2018:1.

89. Baj-Krzyworzeka M, Szatanek R, Węglarczyk K, Baran J, Urbanowicz B, Brański P, et al. Tumour-derived microvesicles carry several surface determinants and mRNA of tumour cells and transfer some of these determinants to monocytes. Cancer Immunology, Immunotherapy. 2006;55(7):808-18.

90. Pigati L, Yaddanapudi SC, Iyengar R, Kim D-J, Hearn SA, Danforth D, et al. Selective release of microRNA species from normal and malignant mammary epithelial cells. PloS one. 2010;5(10):e13515.

91. Mittelbrunn M, Gutiérrez-Vázquez C, Villarroya-Beltri C, González S, Sánchez-Cabo F, González MÁ, et al. Unidirectional transfer of microRNA-loaded exosomes from T cells to antigen-presenting cells. Nature communications. 2011;2:282.

92. Valadi H, Ekström K, Bossios A, Sjöstrand M, Lee JJ, Lötvall JO. Exosome-mediated transfer of mRNAs and microRNAs is a novel mechanism of genetic exchange between cells. Nature cell biology. 2007;9(6):654.

93. Villarroya-Beltri C, Gutiérrez-Vázquez C, Sánchez-Cabo F, Pérez-Hernández D, Vázquez J, Martin-Cofreces N, et al. Sumoylated hnRNPA2B1 controls the sorting of miRNAs into exosomes through binding to specific motifs. Nature communications. 2013;4:2980.

94. Mateescu B, Kowal EJ, van Balkom BW, Bartel S, Bhattacharyya SN, Buzás EI, et al. Obstacles and opportunities in the functional analysis of extracellular vesicle RNA–an ISEV position paper. Journal of extracellular vesicles. 2017;6(1):1286095.

95. Montecalvo A, Larregina AT, Shufesky WJ, Stolz DB, Sullivan ML, Karlsson JM, et al. Mechanism of transfer of functional microRNAs between mouse dendritic cells via exosomes. Blood. 2012;119(3):756-66.

96. Parolini I, Federici C, Raggi C, Lugini L, Palleschi S, De Milito A, et al. Microenvironmental pH is a key factor for exosome traffic in tumor cells. Journal of Biological Chemistry. 2009;284(49):34211-22.

97. Skog J, Würdinger T, Van Rijn S, Meijer DH, Gainche L, Curry Jr WT, et al. Glioblastoma microvesicles transport RNA and proteins that promote tumour growth and provide diagnostic biomarkers. Nature cell biology. 2008;10(12):1470.

98. Morelli AE, Larregina AT, Shufesky WJ, Sullivan ML, Stolz DB, Papworth GD, et al. Endocytosis, intracellular sorting, and processing of exosomes by dendritic cells. Blood. 2004;104(10):3257-66.

99. Feng D, Zhao WL, Ye YY, Bai XC, Liu RQ, Chang LF, et al. Cellular internalization of exosomes occurs through phagocytosis. Traffic. 2010;11(5):675-87.

100. Nakase I, Kobayashi NB, Takatani-Nakase T, Yoshida T. Active macropinocytosis induction by stimulation of epidermal growth factor receptor and oncogenic Ras expression potentiates cellular uptake efficacy of exosomes. Scientific reports. 2015;5:10300.

101. Tian T, Zhu Y-L, Zhou Y-Y, Liang G-F, Wang Y-Y, Hu F-H, et al. Exosome uptake through clathrin-mediated endocytosis and macropinocytosis and mediating miR-21 delivery. Journal of Biological Chemistry. 2014;289(32):22258-67.

102. Christianson HC, Svensson KJ, van Kuppevelt TH, Li J-P, Belting M. Cancer cell exosomes depend on cell-surface heparan sulfate proteoglycans for their internalization and functional activity. Proceedings of the National Academy of Sciences. 2013;110(43):17380-5.

103. Fitzner D, Schnaars M, van Rossum D, Krishnamoorthy G, Dibaj P, Bakhti M, et al. Selective transfer of exosomes from oligodendrocytes to microglia by macropinocytosis. J Cell Sci. 2011;124(3):447-58.

104. Théry C, Ostrowski M, Segura E. Membrane vesicles as conveyors of immune responses. Nature reviews immunology. 2009;9(8):581-93.

105. Tominaga N, Kosaka N, Ono M, Katsuda T, Yoshioka Y, Tamura K, et al. Brain metastatic cancer cells release microRNA-181c-containing extracellular vesicles capable of destructing blood–brain barrier. Nature communications. 2015;6:6716.

106. Bao L, You B, Shi S, Shan Y, Zhang Q, Yue H, et al. Metastasis-associated miR-23a from nasopharyngeal carcinoma-derived exosomes mediates angiogenesis by repressing a novel target gene TSGA10. Oncogene. 2018:1.

107. Anderson HC, Reynolds JJ. Pyrophosphate stimulation of calcium uptake into cultured embryonic bones. Fine structure of matrix vesicles and their role in calcification. Developmental biology. 1973;34(2):211-27.

108. Yang L, Zhang Y, Cui F. Two types of mineral-related matrix vesicles in the bone mineralization of zebrafish. Biomedical materials. 2007;2(1):21.

109. Sung BH, Ketova T, Hoshino D, Zijlstra A, Weaver AM. Directional cell movement through tissues is controlled by exosome secretion. Nature communications. 2015;6:7164.

110. Mu W, Rana S, Zöller M. Host matrix modulation by tumor exosomes promotes motility and invasiveness. Neoplasia. 2013;15(8):875-IN4.

111. Peinado H, Zhang H, Matei IR, Costa-Silva B, Hoshino A, Rodrigues G, et al. Pre-metastatic niches: organ-specific homes for metastases. Nature Reviews Cancer. 2017;17(5):302.

112.   Ridger VC, Boulanger CM, Angelillo-Scherrer A, Badimon L, Blanc-Brude O, Bochaton-Piallat M-L, et al. Microvesicles in vascular homeostasis and diseases. Thrombosis and haemostasis. 2017;117(7):1296-316.
113.   Shimoda M, Khokha R. Proteolytic factors in exosomes. Proteomics. 2013;13(10-11):1624-36.
114.   Théry C, Amigorena S, Raposo G, Clayton A. Isolation and characterization of exosomes from cell culture supernatants and biological fluids. Current protocols in cell biology. 2006:3.22. 1-3.. 9.
115.   Witwer KW, Buzas EI, Bemis LT, Bora A, Lässer C, Lötvall J, et al. Standardization of sample collection, isolation and analysis methods in extracellular vesicle research. Journal of extracellular vesicles. 2013;2(1):20360.
116.   Coumans FA, Brisson AR, Buzas EI, Dignat-George F, Drees EE, El-Andaloussi S, et al. Methodological Guidelines to Study Extracellular Vesicles. Circulation research. 2017;120(10):1632-48.
117.   Aalberts M, van Dissel-Emiliani FM, van Adrichem NP, van Wijnen M, Wauben MH, Stout TA, et al. Identification of distinct populations of prostasomes that differentially express prostate stem cell antigen, annexin A1, and GLIPR2 in humans. Biology of reproduction. 2012;86(3).
118.   Perez-Gonzalez R, Gauthier SA, Kumar A, Levy E. The exosome secretory pathway transports amyloid precursor protein carboxyl-terminal fragments from the cell into the brain extracellular space. Journal of Biological Chemistry. 2012;287(51):43108-15.
119.   Loyer X, Zlatanova I, Devue C, Yin M, Howangyin K-Y, Klaihmon P, et al. Intra-Cardiac Release of Extracellular Vesicles Shapes Inflammation Following Myocardial Infarction. Circulation research. 2018:CIRCRESAHA. 117.311326.
120.   Leroyer AS, Ebrahimian TG, Cochain C, Récalde A, Blanc-Brude O, Mees B, et al. Microparticles from ischemic muscle promotes postnatal vasculogenesis. Circulation. 2009;119(21):2808-17.
121.   Wang G-J, Liu Y, Qin A, Shah SV, Deng Z-b, Xiang X, et al. Thymus exosomes-like particles induce regulatory T cells. The Journal of Immunology. 2008;181(8):5242-8.
122.   Deng Z-b, Poliakov A, Hardy RW, Clements R, Liu C, Liu Y, et al. Adipose tissue exosome-like vesicles mediate activation of macrophage-induced insulin resistance. Diabetes. 2009;58(11):2498-505.
123.   Verweij FJ, Bebelman MP, Jimenez CR, Garcia-Vallejo JJ, Janssen H, Neefjes J, et al. Quantifying exosome secretion from single cells reveals a modulatory role for GPCR signaling. J Cell Biol. 2018:jcb. 201703206.
124.   Hoshino A, Costa-Silva B, Shen T-L, Rodrigues G, Hashimoto A, Mark MT, et al. Tumour exosome integrins determine organotropic metastasis. Nature. 2015;527(7578):329-35.
125.   Takahashi Y, Nishikawa M, Shinotsuka H, Matsui Y, Ohara S, Imai T, et al. Visualization and in vivo tracking of the exosomes of murine melanoma B16-BL6 cells in mice after intravenous injection. Journal of biotechnology. 2013;165(2):77-84.
126.   Niu C, Wang X, Zhao M, Cai T, Liu P, Li J, et al. Macrophage foam cell–derived extracellular vesicles promote vascular smooth muscle cell migration and adhesion. Journal of the American Heart Association. 2016;5(10):e004099.
127.   Wiklander OP, Nordin JZ, O'Loughlin A, Gustafsson Y, Corso G, Mäger I, et al. Extracellular vesicle in vivo biodistribution is determined by cell source, route of administration and targeting. Journal of extracellular vesicles. 2015;4(1):26316.
128.   Takov K, Yellon DM, Davidson SM. Confounding factors in vesicle uptake studies using fluorescent lipophilic membrane dyes. Journal of extracellular vesicles. 2017;6(1):1388731.

129.	Jansen F, Nickenig G, Werner N. Extracellular vesicles in cardiovascular disease: potential applications in diagnosis, prognosis, and epidemiology. Circulation research. 2017;120(10):1649-57.

130.	Dachary-Prigent J, Freyssinet J-M, Pasquet J-M, Carron J-C, Nurden AT. Annexin V as a probe of aminophospholipid exposure and platelet membrane vesiculation: a flow cytometry study showing a role for free sulfhydryl groups. Blood. 1993;81(10):2554-65.

131.	Pasquet J-M, Toti F, Nurden AT, Dachary-Prigent J. Procoagulant activity and active calpain in platelet-derived microparticles. Thrombosis research. 1996;82(6):509-22.

132.	Gray WD, Mitchell AJ, Searles CD. An accurate, precise method for general labeling of extracellular vesicles. MethodsX. 2015;2:360-7.

133.	Faille D, El-Assaad F, Mitchell AJ, Alessi MC, Chimini G, Fusai T, et al. Endocytosis and intracellular processing of platelet microparticles by brain endothelial cells. Journal of cellular and molecular medicine. 2012;16(8):1731-8.

134.	Février B, Raposo G. Exosomes: endosomal-derived vesicles shipping extracellular messages. Current opinion in cell biology. 2004;16(4):415-21.

135.	van Weering JR, Brown E, Sharp TH, Mantell J, Cullen PJ, Verkade P. Intracellular membrane traffic at high resolution. Methods in cell biology. 2010;96:619.

136.	Koliha N, Wiencek Y, Heider U, Jüngst C, Kladt N, Krauthäuser S, et al. A novel multiplex bead-based platform highlights the diversity of extracellular vesicles. Journal of extracellular vesicles. 2016;5(1):29975.

137.	Cocucci E, Aguet F, Boulant S, Kirchhausen T. The first five seconds in the life of a clathrin-coated pit. Cell. 2012;150(3):495-507.

138.	Ter-Ovanesyan D, Kowal EJ, Regev A, Church GM, Cocucci E. Imaging of Isolated Extracellular Vesicles Using Fluorescence Microscopy. Extracellular Vesicles: Springer; 2017. p. 233-41.

139.	Nordin JZ, Lee Y, Vader P, Mäger I, Johansson HJ, Heusermann W, et al. Ultrafiltration with size-exclusion liquid chromatography for high yield isolation of extracellular vesicles preserving intact biophysical and functional properties. Nanomedicine: Nanotechnology, Biology and Medicine. 2015;11(4):879-83.

140.	Dragovic RA, Gardiner C, Brooks AS, Tannetta DS, Ferguson DJ, Hole P, et al. Sizing and phenotyping of cellular vesicles using Nanoparticle Tracking Analysis. Nanomedicine: Nanotechnology, Biology and Medicine. 2011;7(6):780-8.

141.	Orozco AF, Lewis DE. Flow cytometric analysis of circulating microparticles in plasma. Cytometry Part A. 2010;77(6):502-14.

142.	Van Der Vlist EJ, Nolte EN, Stoorvogel W, Arkesteijn GJ, Wauben MH. Fluorescent labeling of nano-sized vesicles released by cells and subsequent quantitative and qualitative analysis by high-resolution flow cytometry. Nature protocols. 2012;7(7):1311-26.

143.	Tian T, Wang Y, Wang H, Zhu Z, Xiao Z. Visualizing of the cellular uptake and intracellular trafficking of exosomes by live-cell microscopy. Journal of cellular biochemistry. 2010;111(2):488-96.

144.	Kleijmeer MJ, Stoorvogel W, Griffith JM, Yoshie O, Geuze HJ. Selective enrichment of tetraspan proteins on the internal vesicles of multivesicular endosomes and on exosomes secreted by human B-lymphocytes. Journal of Biological Chemistry. 1998;273(32):20121-7.

145.	Kobayashi T, Stang E, Fang KS, de Moerloose P, Parton RG, Gruenberg J. A lipid associated with the antiphospholipid syndrome regulates endosome structure and function. Nature. 1998;392(6672):193.

146.	Kobayashi T, Vischer UM, Rosnoblet C, Lebrand C, Lindsay M, Parton RG, et al. The tetraspanin CD63/lamp3 cycles between endocytic and secretory

compartments in human endothelial cells. Molecular biology of the cell. 2000;11(5):1829-43.

147.   Vrijsen K, Sluijter J, Schuchardt M, Van Balkom B, Noort W, Chamuleau S, et al. Cardiomyocyte progenitor cell-derived exosomes stimulate migration of endothelial cells. Journal of cellular and molecular medicine. 2010;14(5):1064-70.

148.   Barile L, Lionetti V, Cervio E, Matteucci M, Gherghiceanu M, Popescu LM, et al. Extracellular vesicles from human cardiac progenitor cells inhibit cardiomyocyte apoptosis and improve cardiac function after myocardial infarction. Cardiovascular research. 2014;103(4):530-41.

149.   Sahoo S, Losordo DW. Exosomes and cardiac repair after myocardial infarction. Circulation research. 2014;114(2):333-44.

150.   Hyenne V, Lefebvre O, Goetz JG. Going live with tumor exosomes and microvesicles. Cell adhesion & migration. 2017;11(2):173-86.

151.   Kanada M, Bachmann MH, Hardy JW, Frimannson DO, Bronsart L, Wang A, et al. Differential fates of biomolecules delivered to target cells via extracellular vesicles. Proceedings of the National Academy of Sciences. 2015;112(12):E1433-E42.

152.   Morishita M, Takahashi Y, Nishikawa M, Sano K, Kato K, Yamashita T, et al. Quantitative analysis of tissue distribution of the B16BL6-derived exosomes using a streptavidin-lactadherin fusion protein and iodine-125-labeled biotin derivative after intravenous injection in mice. Journal of pharmaceutical sciences. 2015;104(2):705-13.

153.   Lai CP, Kim EY, Badr CE, Weissleder R, Mempel TR, Tannous BA, et al. Visualization and tracking of tumour extracellular vesicle delivery and RNA translation using multiplexed reporters. Nature communications. 2015;6.

154.   Panáková D, Sprong H, Marois E, Thiele C, Eaton S. Lipoprotein particles are required for Hedgehog and Wingless signalling. Nature. 2005;435(7038):58.

155.   Abbas M, Jesel L, Auger C, Amoura L, Messas N, Manin G, et al. Endothelial Microparticles From Acute Coronary Syndrome Patients Induce Premature Coronary Artery Endothelial Cell Aging and ThrombogenicityClinical Perspective: Role of the Ang II/AT1 Receptor/NADPH Oxidase-Mediated Activation of MAPKs and PI3-Kinase Pathways. Circulation. 2017;135(3):280-96.

156.   Emanueli C, Shearn AI, Laftah A, Fiorentino F, Reeves BC, Beltrami C, et al. Coronary Artery-Bypass-Graft Surgery Increases the Plasma Concentration of Exosomes Carrying a Cargo of Cardiac MicroRNAs: An Example of Exosome Trafficking Out of the Human Heart with Potential for Cardiac Biomarker Discovery. PloS one. 2016;11(4):e0154274.

157.   Andaloussi SE, Mäger I, Breakefield XO, Wood MJ. Extracellular vesicles: biology and emerging therapeutic opportunities. Nature reviews Drug discovery. 2013;12(5):347-57.

158.   Waldenström A, Gennebäck N, Hellman U, Ronquist G. Cardiomyocyte microvesicles contain DNA/RNA and convey biological messages to target cells. PloS one. 2012;7(4):e34653.

159.   Hergenreider E, Heydt S, Tréguer K, Boettger T, Horrevoets AJ, Zeiher AM, et al. Atheroprotective communication between endothelial cells and smooth muscle cells through miRNAs. Nature cell biology. 2012;14(3):249.

160.   Bang C, Batkai S, Dangwal S, Gupta SK, Foinquinos A, Holzmann A, et al. Cardiac fibroblast–derived microRNA passenger strand-enriched exosomes mediate cardiomyocyte hypertrophy. The Journal of clinical investigation. 2014;124(5):2136-46.

161.   Mesri M, Altieri DC. Endothelial cell activation by leukocyte microparticles. The Journal of Immunology. 1998;161(8):4382-7.

162.   Yu X, Deng L, Wang D, Li N, Chen X, Cheng X, et al. Mechanism of TNF-α autocrine effects in hypoxic cardiomyocytes: initiated by hypoxia inducible

factor 1α, presented by exosomes. Journal of molecular and cellular cardiology. 2012;53(6):848-57.

163.   Levine B, Kalman J, Mayer L, Fillit HM, Packer M. Elevated circulating levels of tumor necrosis factor in severe chronic heart failure. New England Journal of Medicine. 1990;323(4):236-41.

164.   Li D, Zhao L, Liu M, Du X, Ding W, Zhang J, et al. Kinetics of tumor necrosis factor α in plasma and the cardioprotective effect of a monoclonal antibody to tumor necrosis factor α in acute myocardial infarction. American heart journal. 1999;137(6):1145-52.

165.   Kozawa O, Matsuno H, Niwa M, Hatakeyama D, Oiso Y, Kato K, et al. HSP20, low-molecular-weight heat shock-related protein, acts extracellularly as a regulator of platelet functions: a novel defense mechanism. Life sciences. 2002;72(2):113-24.

166.   Zhang X, Wang X, Zhu H, Kranias EG, Tang Y, Peng T, et al. Hsp20 functions as a novel cardiokine in promoting angiogenesis via activation of VEGFR2. PloS one. 2012;7(3):e32765.

167.   Radford NB, Fina M, Benjamin IJ, Moreadith RW, Graves KH, Zhao P, et al. Cardioprotective effects of 70-kDa heat shock protein in transgenic mice. Proceedings of the National Academy of Sciences. 1996;93(6):2339-42.

168.   Fan G-C, Ren X, Qian J, Yuan Q, Nicolaou P, Wang Y, et al. Novel cardioprotective role of a small heat-shock protein, Hsp20, against ischemia/reperfusion injury. Circulation. 2005;111(14):1792-9.

169.   Wang X, Huang W, Liu G, Cai W, Millard RW, Wang Y, et al. Cardiomyocytes mediate anti-angiogenesis in type 2 diabetic rats through the exosomal transfer of miR-320 into endothelial cells. Journal of molecular and cellular cardiology. 2014;74:139-50.

170.   Wang X, Qian R, Zhang W, Chen S, Jin H, Hu R. MicroRNA-320 expression in myocardial microvascular endothelial cells and its relationship with insulin-like growth factor-1 in type 2 diabetic rats. Clinical and Experimental Pharmacology and Physiology. 2009;36(2):181-8.

171.   Ren X-P, Wu J, Wang X, Sartor MA, Qian J, Jones K, et al. MicroRNA-320 is involved in the regulation of cardiac ischemia/reperfusion injury by targeting heat-shock protein 20. Circulation. 2009;119(17):2357-66.

172.   Bronisz A, Godlewski J, Wallace J, Merchant AS, Nowicki MO, Mathsyaraja H, et al. Reprogramming of the tumour microenvironment by stromal PTEN-regulated miR-320. Nature cell biology. 2012;14(2):159.

173.   Walker JD, Maier CL, Pober JS. Cytomegalovirus-infected human endothelial cells can stimulate allogeneic CD4+ memory T cells by releasing antigenic exosomes. The Journal of Immunology. 2009;182(3):1548-59.

174.   Zhan R, Leng X, Liu X, Wang X, Gong J, Yan L, et al. Heat shock protein 70 is secreted from endothelial cells by a non-classical pathway involving exosomes. Biochemical and biophysical research communications. 2009;387(2):229-33.

175.   van Balkom BW, De Jong OG, Smits M, Brummelman J, den Ouden K, de Bree PM, et al. Endothelial cells require miR-214 to secrete exosomes that suppress senescence and induce angiogenesis in human and mouse endothelial cells. Blood. 2013;121(19):3997-4006.

176.   Akbar N, Digby JE, Cahill TJ, Tavare AN, Corbin AL, Saluja S, et al. Endothelium-derived extracellular vesicles promote splenic monocyte mobilization in myocardial infarction. JCI insight. 2017;2(17).

177.   Zhu J, Quyyumi AA, Wu H, Csako G, Rott D, Zalles-Ganley A, et al. Increased serum levels of heat shock protein 70 are associated with low risk of coronary artery disease. Arteriosclerosis, thrombosis, and vascular biology. 2003;23(6):1055-9.

178.   Pizon M, Gburek T, Pizon M, Sztefko K. Kinetics of plasma heat shock protein HSP-70 release in coronary artery surgery: on-pump versus off-pump. Minerva chirurgica. 2006;61(6):483-91.

179.   Dybdahl B, Slørdahl S, Waage A, Kierulf P, Espevik T, Sundan A. Myocardial ischaemia and the inflammatory response: release of heat shock protein 70 after myocardial infarction. Heart. 2005;91(3):299-304.

180.   Satoh M, Shimoda Y, Akatsu T, Ishikawa Y, Minami Y, Nakamura M. Elevated circulating levels of heat shock protein 70 are related to systemic inflammatory reaction through monocyte Toll signal in patients with heart failure after acute myocardial infarction. European journal of heart failure. 2006;8(8):810-5.

181.   He S, Wu C, Xiao J, Li D, Sun Z, Li M. Endothelial extracellular vesicles modulate the macrophage phenotype: Potential implications in atherosclerosis. Scandinavian journal of immunology. 2018;87(4):e12648.

182.   Gennebäck N, Hellman U, Malm L, Larsson G, Ronquist G, Waldenström A, et al. Growth factor stimulation of cardiomyocytes induces changes in the transcriptional contents of secreted exosomes. Journal of extracellular vesicles. 2013;2(1):20167.

183.   Ibrahim AG-E, Cheng K, Marbán E. Exosomes as critical agents of cardiac regeneration triggered by cell therapy. Stem cell reports. 2014;2(5):606-19.

184.   Barile L, Gherghiceanu M, Popescu LM, Moccetti T, Vassalli G. Ultrastructural evidence of exosome secretion by progenitor cells in adult mouse myocardium and adult human cardiospheres. BioMed Research International. 2012;2012.

185.   György B, Szabó TG, Pásztói M, Pál Z, Misják P, Aradi B, et al. Membrane vesicles, current state-of-the-art: emerging role of extracellular vesicles. Cellular and molecular life sciences. 2011;68(16):2667-88.

186.   van der Pol E, Böing AN, Harrison P, Sturk A, Nieuwland R. Classification, functions, and clinical relevance of extracellular vesicles. Pharmacological reviews. 2012;64(3):676-705.

187.   Raposo G, Stoorvogel W. Extracellular vesicles: exosomes, microvesicles, and friends. J Cell Biol. 2013;200(4):373-83.

188.   Morel O, Toti F, Hugel B, Freyssinet J-M. Cellular microparticles: a disseminated storage pool of bioactive vascular effectors. Current opinion in hematology. 2004;11(3):156-64.

189.   Zwicker JI, Trenor CC, Furie BC, Furie B. Tissue factor–bearing microparticles and thrombus formation. Arteriosclerosis, thrombosis, and vascular biology. 2011;31(4):728-33.

190.   Horstman LL, Ahn YS. Platelet microparticles: a wide-angle perspective1. Critical reviews in oncology/hematology. 1999;30(2):111-42.

191.   VanWijk MJ, VanBavel E, Sturk A, Nieuwland R. Microparticles in cardiovascular diseases. Cardiovascular research. 2003;59(2):277-87.

192.   Morel O, Toti F, Hugel B, Bakouboula B, Camoin-Jau L, Dignat-George F, et al. Procoagulant microparticles: disrupting the vascular homeostasis equation? Arteriosclerosis, thrombosis, and vascular biology. 2006;26(12):2594-604.

193.   Van Der Pol E, Hoekstra A, Sturk A, Otto C, Van Leeuwen T, Nieuwland R. Optical and non-optical methods for detection and characterization of microparticles and exosomes. Journal of Thrombosis and Haemostasis. 2010;8(12):2596-607.

194.   György B, Módos K, Pállinger É, Pálóczi K, Pásztói M, Misják P, et al. Detection and isolation of cell-derived microparticles are compromised by protein complexes resulting from shared biophysical parameters. Blood. 2011;117(4):e39-e48.

195.   Arraud N, Linares R, Tan S, Gounou C, Pasquet JM, Mornet S, et al. Extracellular vesicles from blood plasma: determination of their morphology, size, phenotype and concentration. Journal of Thrombosis and Haemostasis. 2014;12(5):614-27.
196.   Aatonen MT, Öhman T, Nyman TA, Laitinen S, Grönholm M, Siljander PR-M. Isolation and characterization of platelet-derived extracellular vesicles. Journal of extracellular vesicles. 2014;3(1):24692.
197.   Diamant M, Tushuizen ME, Sturk A, Nieuwland R. Cellular microparticles: new players in the field of vascular disease? European journal of clinical investigation. 2004;34(6):392-401.
198.   Hussein A, Meesters EW, Osmanovic N, Romijn F, Nieuwland R, Sturk A. Antigenic characterization of endothelial cell-derived microparticles and their detection ex vivo. Journal of Thrombosis and Haemostasis. 2003;1(11):2434-43.
199.   Gutiérrez-Vázquez C, Villarroya-Beltri C, Mittelbrunn M, Sánchez-Madrid F. Transfer of extracellular vesicles during immune cell-cell interactions. Immunological reviews. 2013;251(1):125-42.
200.   Foglio E, Puddighinu G, Fasanaro P, D'Arcangelo D, Perrone GA, Mocini D, et al. Exosomal clusterin, identified in the pericardial fluid, improves myocardial performance following MI through epicardial activation, enhanced arteriogenesis and reduced apoptosis. International journal of cardiology. 2015;197:333-47.
201.   Nieuwland R, Berckmans RJ, Rotteveel-Eijkman RC, Maquelin KN, Roozendaal KJ, Jansen PG, et al. Cell-derived microparticles generated in patients during cardiopulmonary bypass are highly procoagulant. Circulation. 1997;96(10):3534-41.
202.   Tabuchi N, Boonstra P. Activation of fibrinolysis in the pericardial cavity during cardiopulmonary bypass. The Journal of thoracic and cardiovascular surgery. 1993;106(5):828-33.
203.   Chung JH, Gikakis N, Rao AK, Drake TA, Colman RW, Edmunds LH. Pericardial blood activates the extrinsic coagulation pathway during clinical cardiopulmonary bypass. Circulation. 1996;93(11):2014-8.
204.   Limana F, Capogrossi MC, Germani A. The epicardium in cardiac repair: from the stem cell view. Pharmacology & therapeutics. 2011;129(1):82-96.
205.   Limana F, Zacheo A, Mocini D, Mangoni A, Borsellino G, Diamantini A, et al. Identification of myocardial and vascular precursor cells in human and mouse epicardium. Circulation research. 2007;101(12):1255-65.
206.   Limana F, Bertolami C, Mangoni A, Di Carlo A, Avitabile D, Mocini D, et al. Myocardial infarction induces embryonic reprogramming of epicardial c-kit+ cells: Role of the pericardial fluid. Journal of molecular and cellular cardiology. 2010;48(4):609-18.
207.   Zhou B, Honor LB, He H, Ma Q, Oh J-H, Butterfield C, et al. Adult mouse epicardium modulates myocardial injury by secreting paracrine factors. The Journal of clinical investigation. 2011;121(5):1894-904.
208.   van Wijk B, Gunst QD, Moorman AF, Van den Hoff MJ. Cardiac regeneration from activated epicardium. PloS one. 2012;7(9):e44692.
209.   Streisinger G, Walker C, Dower N, Knauber D, Singer F. Production of clones of homozygous diploid zebra fish (Brachydanio rerio). Nature. 1981;291(5813):293.
210.   Chakrabarti S, Streisinger G, Singer F, Walker C. Frequency of γ-ray induced specific locus and recessive lethal mutations in mature germ cells of the zebrafish, Brachydanio rerio. Genetics. 1983;103(1):109-23.
211.   Walker C, Streisinger G. Induction of mutations by γ-rays in pregonial germ cells of zebrafish embryos. Genetics. 1983;103(1):125-36.

212.   Grunwald DJ, Streisinger G. Induction of recessive lethal and specific locus mutations in the zebrafish with ethyl nitrosourea. Genetics Research. 1992;59(2):103-16.

213.   Solnica-Krezel L, Schier AF, Driever W. Efficient recovery of ENU-induced mutations from the zebrafish germline. Genetics. 1994;136(4):1401-20.

214.   Stuart GW, McMURRAY JV, Westerfield M. Replication, integration and stable germ-line transmission of foreign sequences injected into early zebrafish embryos. Development. 1988;103(2):403-12.

215.   Streisinger G, Singer F, Walker C, Knauber D, Dower N. Segregation analyses and gene-centromere distances in zebrafish. Genetics. 1986;112(2):311-9.

216.   Driever W, Solnica-Krezel L, Schier A, Neuhauss S, Malicki J, Stemple D, et al. A genetic screen for mutations affecting embryogenesis in zebrafish. Development. 1996;123(1):37-46.

217.   Haffter P, Granato M, Brand M, Mullins MC, Hammerschmidt M, Kane DA, et al. The identification of genes with unique and essential functions in the development of the zebrafish, Danio rerio. Development. 1996;123(1):1-36.

218.   Amsterdam A, Burgess S, Golling G, Chen W, Sun Z, Townsend K, et al. A large-scale insertional mutagenesis screen in zebrafish. Genes & development. 1999;13(20):2713-24.

219.   Lieschke GJ, Currie PD. Animal models of human disease: zebrafish swim into view. Nature Reviews Genetics. 2007;8(5):353-67.

220.   Jopling C, Sleep E, Raya M, Martí M, Raya A, Belmonte JCI. Zebrafish heart regeneration occurs by cardiomyocyte dedifferentiation and proliferation. Nature. 2010;464(7288):606-9.

221.   Xu B, Zhang Y, Du X-F, Li J, Zi H-X, Bu J-W, et al. Neurons secrete miR-132-containing exosomes to regulate brain vascular integrity. Cell research. 2017;27(7):882.

222.   Cooper MS, Szeto DP, Sommers-Herivel G, Topczewski J, Solnica-Krezel L, Kang HC, et al. Visualizing morphogenesis in transgenic zebrafish embryos using BODIPY TR methyl ester dye as a vital counterstain for GFP. Developmental Dynamics. 2005;232(2):359-68.

223.   van Ham TJ, Mapes J, Kokel D, Peterson RT. Live imaging of apoptotic cells in zebrafish. The FASEB Journal. 2010;24(11):4336-42.

224.   Fujita M, Cha YR, Pham VN, Sakurai A, Roman BL, Gutkind JS, et al. Assembly and patterning of the vascular network of the vertebrate hindbrain. Development. 2011;138(9):1705-15.

225.   Lepilina A, Coon AN, Kikuchi K, Holdway JE, Roberts RW, Burns CG, et al. A dynamic epicardial injury response supports progenitor cell activity during zebrafish heart regeneration. Cell. 2006;127(3):607-19.

226.   Yoruk B, Gillers BS, Chi NC, Scott IC. Ccm3 functions in a manner distinct from Ccm1 and Ccm2 in a zebrafish model of CCM vascular disease. Developmental biology. 2012;362(2):121-31.

227.   Choo BG, Kondrichin I, Parinov S, Emelyanov A, Go W, Toh W-c, et al. Zebrafish transgenic Enhancer TRAP line database (ZETRAP). BMC developmental biology. 2006;6(1):5.

228.   Westerfield M. The zebrafish book: a guide for the laboratory use of zebrafish. http://zfin org/zf_info/zfbook/zfbk html. 2000.

229.   Kimmel CB, Ballard WW, Kimmel SR, Ullmann B, Schilling TF. Stages of embryonic development of the zebrafish. Developmental dynamics. 1995;203(3):253-310.

230.   Otten C, Abdelilah-Seyfried S. Laser-inflicted injury of zebrafish embryonic skeletal muscle. Journal of visualized experiments: JoVE. 2013(71).

231.   McNamara RP, Costantini LM, Myers TA, Schouest B, Maness NJ, Griffith JD, et al. Nef Secretion into Extracellular Vesicles or Exosomes Is Conserved

across Human and Simian Immunodeficiency Viruses. mBio. 2018;9(1):e02344-17.

232. Sibarita J-B. Deconvolution microscopy. Microscopy Techniques: Springer; 2005. p. 201-43.

233. Bobrie A, Colombo M, Krumeich S, Raposo G, Théry C. Diverse subpopulations of vesicles secreted by different intracellular mechanisms are present in exosome preparations obtained by differential ultracentrifugation. Journal of extracellular vesicles. 2012;1(1):18397.

234. Nicola AM, Frases S, Casadevall A. Lipophilic dye staining of Cryptococcus neoformans extracellular vesicles and capsule. Eukaryotic cell. 2009;8(9):1373-80.

235. Shannon CE. Communication in the presence of noise. Proceedings of the IRE. 1949;37(1):10-21.

236. Zomer A, Maynard C, Verweij FJ, Kamermans A, Schäfer R, Beerling E, et al. In vivo imaging reveals extracellular vesicle-mediated phenocopying of metastatic behavior. Cell. 2015;161(5):1046-57.

237. Johnson J. Not seeing is not believing: improving the visibility of your fluorescence images. Molecular biology of the cell. 2012;23(5):754-7.

238. Stainier D, Lee RK, Fishman MC. Cardiovascular development in the zebrafish. I. Myocardial fate map and heart tube formation. Development. 1993;119(1):31-40.

239. Lawson ND, Weinstein BM. Arteries and veins: making a difference with zebrafish. Nature Reviews Genetics. 2002;3(9):674.

240. Chan PK, Lin CC, Cheng SH. Noninvasive technique for measurement of heartbeat regularity in zebrafish (Danio rerio) embryos. BMC biotechnology. 2009;9(1):11.

241. Isogai S, Horiguchi M, Weinstein BM. The vascular anatomy of the developing zebrafish: an atlas of embryonic and early larval development. Developmental biology. 2001;230(2):278-301.

242. Koopman G, Reutelingsperger C, Kuijten G, Keehnen R, Pals S, Van Oers M. Annexin V for flow cytometric detection of phosphatidylserine expression on B cells undergoing apoptosis. Blood. 1994;84(5):1415-20.

243. Houseknecht JB, Temple JS, Bateman Jr RC. Analysis of cell-cycle profiles in transfected cells using a membrane-targeted GFP. Biotechniques. 1998;24:348-54.

244. Sheldon H, Heikamp E, Turley H, Dragovic R, Thomas P, Oon CE, et al. New mechanism for Notch signaling to endothelium at a distance by Delta-like 4 incorporation into exosomes. Blood. 2010;116(13):2385-94.

245. Shabetai R. The pericardium: Springer Science & Business Media; 2012.

246. Chinchoy E, Ujhelyi MR, Hill AJ, Skadsberg ND, Iaizzo PA. The pericardium. Handbook of Cardiac Anatomy, Physiology, and Devices: Springer; 2005. p. 101-10.

247. Ben-Horin S, Shinfeld A, Kachel E, Chetrit A, Livneh A. The composition of normal pericardial fluid and its implications for diagnosing pericardial effusions. The American journal of medicine. 2005;118(6):636-40.

248. Rotblat B, Prior IA, Muncke C, Parton RG, Kloog Y, Henis YI, et al. Three separable domains regulate GTP-dependent association of H-ras with the plasma membrane. Molecular and cellular biology. 2004;24(15):6799-810.

249. Andrés-Delgado L, Mercader N. Interplay between cardiac function and heart development. Biochimica et Biophysica Acta (BBA)-Molecular Cell Research. 2016;1863(7):1707-16.

250. Ridler T, Calvard S. Picture thresholding using an iterative selection method. IEEE trans syst Man Cybern. 1978;8(8):630-2.

251.   Welsh JA, Holloway JA, Wilkinson JS, Englyst NA. Extracellular Vesicle Flow Cytometry Analysis and Standardization. Frontiers in cell and developmental biology. 2017;5:78.

252.   King MR, Hammer DA. Multiparticle adhesive dynamics: hydrodynamic recruitment of rolling leukocytes. Proceedings of the National Academy of Sciences. 2001;98(26):14919-24.

253.   Ley K, Laudanna C, Cybulsky MI, Nourshargh S. Getting to the site of inflammation: the leukocyte adhesion cascade updated. Nature Reviews Immunology. 2007;7(9):678.

254.   Vestweber D. How leukocytes cross the vascular endothelium. Nature Reviews Immunology. 2015;15(11):692.

255.   Mayadas TN, Johnson RC, Rayburn H, Hynes RO, Wagner DD. Leukocyte rolling and extravasation are severely compromised in P selectin-deficient mice. Cell. 1993;74(3):541-54.

256.   Arbonés ML, Ord DC, Ley K, Ratech H, Maynard-Curry C, Otten G, et al. Lymphocyte homing and leukocyte rolling and migration are impaired in L-selectin-deficient mice. Immunity. 1994;1(4):247-60.

257.   Ley K, Bullard DC, Arbonés ML, Bosse R, Vestweber D, Tedder TF, et al. Sequential contribution of L-and P-selectin to leukocyte rolling in vivo. Journal of Experimental Medicine. 1995;181(2):669-75.

258.   Laudanna C, Kim JY, Constantin G, Butcher EC. Rapid leukocyte integrin activation by chemokines. Immunological reviews. 2002;186(1):37-46.

259.   Lei X, Lawrence M, Dong C. Influence of cell deformation on leukocyte rolling adhesion in shear flow. Journal of biomechanical engineering. 1999;121(6):636-43.

260.   Li Z, Delaney MK, O'brien KA, Du X. Signaling during platelet adhesion and activation. Arteriosclerosis, thrombosis, and vascular biology. 2010;30(12):2341-9.

261.   Savage B, Saldívar E, Ruggeri ZM. Initiation of platelet adhesion by arrest onto fibrinogen or translocation on von Willebrand factor. Cell. 1996;84(2):289-97.

262.   Sakariassen K, Bolhuis P, Sixma J. Human blood platelet adhesion to artery subendothelium is mediated by factor VIII–von Willebrand factor bound to the subendothelium. Nature. 1979;279(5714):636.

263.   Savage B, Shattil SJ, Ruggeri ZM. Modulation of platelet function through adhesion receptors. A dual role for glycoprotein IIb-IIIa (integrin alpha IIb beta 3) mediated by fibrinogen and glycoprotein Ib-von Willebrand factor. Journal of Biological Chemistry. 1992;267(16):11300-6.

264.   Nuyttens BP, Thijs T, Deckmyn H, Broos K. Platelet adhesion to collagen. Thrombosis research. 2011;127:S26-S9.

265.   Ruggeri ZM. Platelets in atherothrombosis. Nature medicine. 2002;8(11):1227.

266.   Nieswandt B, Brakebusch C, Bergmeier W, Schulte V, Bouvard D, Mokhtari-Nejad R, et al. Glycoprotein VI but not α2β1 integrin is essential for platelet interaction with collagen. The EMBO journal. 2001;20(9):2120-30.

267.   Cheow ESH, Cheng WC, Lee CN, De Kleijn D, Sorokin V, Sze SK. Plasma-derived extracellular vesicles contain predictive biomarkers and potential therapeutic targets for myocardial ischemic (MI) injury. Molecular & Cellular Proteomics. 2016;15(8):2628-40.

268.   Vallabhaneni KC, Penfornis P, Dhule S, Guillonneau F, Adams KV, Mo YY, et al. Extracellular vesicles from bone marrow mesenchymal stem/stromal cells transport tumor regulatory microRNA, proteins, and metabolites. Oncotarget. 2015;6(7):4953.

269.   Hynes RO. Integrins: versatility, modulation, and signaling in cell adhesion. Cell. 1992;69(1):11-25.

270.   Heusermann W, Hean J, Trojer D, Steib E, Von Bueren S, Graff-Meyer A, et al. Exosomes surf on filopodia to enter cells at endocytic hot spots, traffic within endosomes, and are targeted to the ER. J Cell Biol. 2016;213(2):173-84.
271.   Peralta M, Steed E, Harlepp S, González-Rosa JM, Monduc F, Ariza-Cosano A, et al. Heartbeat-driven pericardiac fluid forces contribute to epicardium morphogenesis. Current Biology. 2013;23(18):1726-35.
272.   Ridder K, Sevko A, Heide J, Dams M, Rupp A-K, Macas J, et al. Extracellular vesicle-mediated transfer of functional RNA in the tumor microenvironment. Oncoimmunology. 2015;4(6):e1008371.
273.   Roh-Johnson M, Shah AN, Stonick JA, Poudel KR, Kargl J, Yang GH, et al. Macrophage-Dependent Cytoplasmic Transfer during Melanoma Invasion In Vivo. Developmental cell. 2017;43(5):549-62. e6.
274.   Carney TJ, Mosimann C. Switch and Trace: Recombinase Genetics in Zebrafish. Trends in Genetics. 2018.
275.   Nolan JP, Duggan E. Analysis of individual extracellular vesicles by flow cytometry. Flow Cytometry Protocols: Springer; 2018. p. 79-92.
276.   van der Pol E, de Rond L, Coumans FA, Gool EL, Böing AN, Sturk A, et al. Absolute sizing and label-free identification of extracellular vesicles by flow cytometry. Nanomedicine: Nanotechnology, Biology and Medicine. 2018.
277.   van der Pol E, Sturk A, van Leeuwen T, Nieuwland R, Coumans F, group ISVW, et al. Standardization of extracellular vesicle measurements by flow cytometry through vesicle diameter approximation. Journal of Thrombosis and Haemostasis. 2018;16(6):1236-45.
278.   González-Rosa JM, Mercader N. Cryoinjury as a myocardial infarction model for the study of cardiac regeneration in the zebrafish. Nature protocols. 2012;7(4):782-8.